ISTANBUL TECHNICAL UNIVERSITY ★ GRADUATE SCHOOL

HIGH INTERNAL PHASE EMULSION TEMPLATE METHOD FOR FAST AND SELECTIVE MERCURY ADSORPTION

M.Sc. THESIS

Melis Şeval YILDIRIM

Department of Polymer Science and Technology

Polymer Science and Technology Programme

JANUARY 2022

ISTANBUL TECHNICAL UNIVERSITY ★ GRADUATE SCHOOL

HIGH INTERNAL PHASE EMULSION TEMPLATE METHOD FOR FAST AND SELECTIVE MERCURY ADSORPTION

M.Sc. THESIS

Melis Şeval YILDIRIM
(515171009)

Department of Polymer Science and Technology

Polymer Science and Technology Programme

Thesis Advisor: Assoc. Prof. Dr. Erdem YAVUZ

JANUARY 2022

ISTANBUL TEKNİK ÜNİVERSİTESİ ★ LİSANSÜSTÜ EĞİTİM ENSTİTÜSÜ

HIZLI VE SEÇİCİ CİVA ADSORPSİYONU İÇİN YÜKSEK İÇ FAZ EMÜLSİYON ŞABLON YÖNTEMİ

YÜKSEK LİSANS TEZİ

Melis Şeval YILDIRIM
(515171009)

Polimer Bilimi ve Teknolojisi Anabilim Dalı

Polimer Bilimi ve Teknolojisi Programı

Tez Danışmanı: Doç. Dr. Erdem YAVUZ

OCAK 2022

Melis Şeval YILDIRIM, a M.Sc. student of İTU Graduate School of Science Engineering and Technology student ID 515171009, successfully defended the thesis entitled "HIGH INTERNAL PHASE EMULSION TEMPLATE METHOD FOR FAST AND SELECTIVE MERCURY ADSORPTION", which she prepared after fulfilling the requirements specified in the associated legislations, before the jury whose signatures are below.

Thesis Advisor :	**Assoc. Prof. Dr. Erdem YAVUZ** İstanbul Technical University	.....
Jury Members :	**Prof. Dr. Bahire Filiz ŞENKAL** Istanbul Technical University	.....
	Prof. Dr. Özlem CANKURTARAN Yıldız Technical University	.....

Date of Submission : 24 January 2022
Date of Defense : 6 January 2022

To my family,

FOREWORD

First of all, I would like to express my sincere appreciation and gratitude to my advisor, Assoc. Prof. Dr. Erdem YAVUZ , for his academic guidance and enthusiastic encouragement throughout the thesis. He always listened to me throughout my academic journey and did his best to help when there was a problem. His understanding of the other person, his ability to empathize, and his conversations have always made me comfortable and helped me to focus on my work. I would not be doing this work without his generosity in sharing his experiences and knowledge. I am grateful to him for all the support and help he has shown me.

I would like to thank Prof. Dr. Filiz Şenkal for giving her the opportunity to use her laboratory and for sharing her knowledge and helping. I am grateful for her helpful and motherly attitude towards me. At the same time, I would like to thank Burak Korkmaz and Büşra Akın Özmen who are research assistant in the laboratory for their support.

I would like to thank Kübra GÖRAL, Nida Nur BORA, Tuba BAL, Birsen KOÇAK, Gülenay ÜZÜM, Merve SÜSLÜKAYA and Eda KÜÇÜK, who are among the strong women in my life, for their support and encouraging attitude towards me. For this I want to specially thank them.

Finally, I would like to thank my family for encouraging me and leading me on this journey. I would like to thank you deeply for your financial and moral support during this process.

January 2022

Melis Şeval YILDIRIM
(Chemical Engineer)

TABLE OF CONTENTS

Page

FOREWARD ..... **ix**
TABLE OF CONTENTS ..... **xi**
ABBREVIATIONS ..... **xiii**
SYMBOLS ..... **xv**
LIST OF TABLES ..... **xvii**
LIST OF FIGURES ..... **xix**
SUMMARY ..... **xxiii**
ÖZET ..... **xxv**
1.INTRODUCTION **1**
2.THEORY **3**
2.1 Polymer 3
2.2 Emulsion 3
2.2.1. Emulsion stability 4
2.3 Emulsion Polymerization 6
2.4 Porous Polymer 7
2.4.1 Direct templating methodology 8
2.4.2 Block copolymer self-assembly methodology 9
2.4.3 Direct synthesis methodology 10
2.4.4 Polymers of instrinsic microporosity 11
2.4.5 High internal phase emulsion polymerization (HIPE) 12
2.5 Polymerization of HIPE (PolyHIPE) 13
2.5.1 PolyHIPE morphology 13
2.5.2 PolyHIPE surfactants 16
2.5.2.1 Hydrophhilic-lipophilic balance of surfactant 18
2.5.3 PolyHIPE mechanical properties 19
2.6 Hypercrosslinking 20
2.6.1 Preparation of hypercrosslinked polymer 21
2.6.2 Solvent effect 22
2.7 Characterization of Porous Polymers 22
2.7.1 Branauer-emmett-teller (BET) method 23
2.7.2 X-ray photoelectron spectroscopy (XPS) 24
2.7.3 Scanning electron microscopy (SEM) 25
2.7.4 Uv-vis spectroscopy 26
2.7.5 Fourier-transform infrared (FT-IR) spectroscopy 28
2.8 Adsorption 29
2.8.1 Factors affecting adsorption 30
2.8.1.2 Adsorption properties 31
2.8.1.3 Surface acidity 31
2.8.1.4 Temperature 31
2.8.2 Adsorption kinetics model 31
2.8.2.1 Pseudo-first-order (PFO) model 31

2.8.2.2 Pseudo-second-order (PSO) model 32
2.8.2.3 Intra-particle diffusion (IPD) rate model 33
2.8.3 Adsorption isotherm 34
2.8.3.1 Langmuir isotherm 34
2.8.3.2 Freudlich isotherm 35
2.8.3.3 Dubinin-radushkevich (D-R) isotherm 36
2.9 Heavy Metals 36
2.9.1 Mercury effect for human and environment 37
2.9.2 Mercury removal techniques 39
2.9.3 Adsorption study for removal mercury 40
3.EXPERIMENTAL 43
3.1 Materials and Instruments 43
3.1.1 Materials 43
3.1.2 Instruments 43
3.2 Preperation of the Amide Functional High-Surface Area Porous Polymers 44
3.2.1 Polymerized high internal phase emulsions (polyHIPE) 44
3.2.2 Preparation of the hypercrosslinked polyHIPE (HXL-PHP) 45
3.2.3 Formylation reaction of VBC polyHIPE (kornblum oxidation) 45
3.2.4 Preparation of carboxylic acid functional polyHIPE 46
3.2.5 Tailoring polyHIPE surfaces with various amide groups 46
3.3 Functional Group Content Determination 47
3.4 Adsorption Experiments 47
3.4.1 Adsorption performance of polyHIPE adsorbents in aqueous single metal solution 47
3.4.2 Adsorption performance of polyHIPE adsorbents in aqueous ternary metal solutions 48
3.4.3 The effect of solid/liquids ratio (optimum adsorbent amount) on mercury adsorption 49
3.4.4 The effect of pH on mercury adsorption 49
3.4.5 Determination of the max. adsorption capacity of the adsorbents 49
3.4.6 Mercury adsorption kinetics of the adsorbents 49
3.4.7 The recyclability of HXL-30min-PHP-$CONR_2$ 50
4.RESULTS AND DISCUSSION 51
4.1 Emulsion Templated High Internal Phase Emulsion and PolyHIPE 51
4.1.1 Preparation of high internal phase emulsion and polyHIPE 52
4.1.2 Synthesis of polymeric adsorbents 52
4.2 Physicochemical Properties of the Adsorbents 56
4.3 Adsorption Experiments 67
4.3.1 The selectivity measurements 69
4.3.2 Adsorption kinetics performance 69
4.3.3 The effect of solid/liquid ratio on mercury adsorption (determining the optimum absorbent) amount 71
4.3.4 The effect of pH on mercury adsorption 72
4.3.5 Evaluating mercury adsorption mechanism 73
4.3.6 Thermodynamic analysis 82
4.3.7 Adsorbent reuse 84
5.CONCLUSION 87
REFERENCES 89
APPENDICES 97
APPENDIX A 98
CURRICULUM VITAE 105

ABBREVIATIONS

DEA **:** Diethylamine
DCE **:** 1,2-dichloroethane
DMSO **:** Dimethyl Sulphoxyde
DVB **:** Divinylbenzene
EDTA **:** Ethylene Diamine Tetra Acetic Acid
HIPE **:** High Internal Phase Emulsion
HLB **:** Hydrophile-Lipophile Balance
HXL **:** Hypercrosslinking
HXL-PHP **:** Hypercrosslinked polyHIPE
HXL-30min-PHP **:** 30 minutes hypercrosslinked PolyHIPE
HXL-30min-PHP-COOH **:** 30 minutes hypercrosslinked carboxylic acid PolyHIPE
HXL-30min-PHP-CONR$_2$ **:** 30 minutes hypercrosslinked amide PolyHIPE
O/W **:** Oil-in-Water
PHP **:** PolyHIPE
SEM **:** Scanning Electron Microscope
UV **:** Ultra-violet
VBC **:** Vinylbenzyl Chloride
W/O **:** Water-in-Oil
XPS **:** X-ray Photoelectron Spectrometer

SYMBOLS

‹d›/‹D›	**:** Degree of interconnectivity
‹d›	**:** Average diameter of interconnecting windows
‹D›	**:** Average diameter of voids
n	**:** Adsorption intensity
nm	**:** Nanometer
ε	:Polanyi potential
Φ	**:** Volume ratio

LIST OF TABLES

Page

Table 2.1 : Some surfactant and HLB values.……...**19**
Table 2.2: Mercury removal techniques and their explains……..**39**
Table 4.1: Morphology Characterization of PHP, HXL-30min-PHP, and HXL-30min-PHP-CONR2 by a) Surface Area and Porosity Analysis and b) Surface Morphology Analysis……**60**
Table 4.2 : Functional group contents of polymeric adsorbents……...**65**
Table 4.3 : The comparison for adsorption capacities in single metal solutions…..**68**
Table 4.4 : Pseudo-first-order, Pseudo-second-order, and Intra-Particle Diffusion Model Parameters for HXL-30min-PHP-CONR2 (ethanolamine) and PHP-CONR2 (ethanolamine) ……**76**
Table 4.5 : Isotherm parameters and correlation coefficients for HXL-30min-PHP-CONR2 (ethanolamine)(A) and VBC-PHP-CONR2 (ethanol amine) (B) ……**81**
Table 4.6 : Thermodynamic parameters for mercury adsorption on HXL-30min-PHP-$CONR_2$ ……**84**

LIST OF FIGURES

Page

Figure 2. 1: Representation of instable emulsion type **5**
Figure 2. 2: Mechanism of emulsion polymerization **6**
Figure 2. 3: Illustration of pore geometry **7**
Figure 2.4: Schematic illustration of fabrication of (a) individual spherical porous polymers from solid spherical nanoparticle templates, (b) tubular porous polymers from tubular porous templates, such as AAO, and (c) ordered macroporous polymers from colloidal crystal templates **9**
Figure 2. 5: Equilibrium morphologies of AB diblock copolymers in the bulk. S: cubic spheres, C: hexagonally packed cylinders, G: bicontinuous gyroids, L: lamellae, G',C',S' : the copolymer composition is reversed. **9**
Figure 2. 6: Block copolymer self- assembly in solution. The self assembled structures are determined by the packing parameter (p). **10**
Figure 2.7: Self assembly block copolymers with removal of one component **10**
Figure 2. 8: Schematic representations of emulsion and high internal phase emulsion **12**
Figure 2. 9: Representation of synthesized porous polymer **12**
Figure 2. 10: Illustration of polyHIPE creation **13**
Figure 2. 11: PolyHipe morphology in SEM imaging **13**
Figure 2. 12: Sem images of PolyHipes with different internal phase ratios. These ratios can be summarized as a) 75% b) 80% c) 85% d) 90% **15**
Figure 2. 13: a) Open cell (Wu et al. 2021) [38] and b)closed cell (Krajnc et al. 2005) morphology of PolyHipe **15**
Figure 2. 14: Adsorption of surfactant at oil/water interface **17**
Figure 2. 15: Surfactants structure **17**
Figure 2. 16: Span 80 molecule structure **18**
Figure 2. 17: Representation of hypercrosslinked polystyrene network **21**
Figure 2. 18: A hypercrosslinked polymer prepared from gel poly(divinylbenzene-co-vinylbenzyl chloride) **21**
Figure 2. 19: a) Adsorption and desorption mechanism of BET b) BET instrument **23**
Figure 2. 20: Basic diagram of XPS spectroscopy **24**
Figure 2. 21: Electron beam interaction of SEM **25**
Figure 2. 22: Illustration of SEM low to very high magnifications (100,000x to 1,000,000x) of secondary electron **26**
Figure 2. 23: Measurement principle of UV **27**
Figure 2. 24: UV spectroscopy **27**

Figure 2. 25: FT-IR spectroscopy……....**28**
Figure 2. 26: Illustration of Mid Infrared Regions……...**29**
Figure 2. 27: Physical and chemical adsorption……...**30**
Figure 2. 28: Pseudo First Order and Pseudo Second Order model and their physical meanings……..**33**
Figure 2. 29: Sources of heavy metals and their harm to the human body……..**37**
Figure 2. 30: Mercury cycle in environment ……...**39**
Figure 4. 1: Schematic illustration of a typical polyHIPE preparation…..……..**52**
Figure 4. 2: Preparation of hypercrosslinked polyHIPE……..**53**
Figure 4. 3: Modification steps of amide functional polyHIPE…….....**54**
Figure 4. 4: The hypercrosslinking reaction mechanism……**55**
Figure 4. 5: The probable crosslinking formations during the hypercrosslinking reaction……**56**
Figure 4. 6: SEM images of powdered samples showing void diameter distributions of (a) VBC-PHP, (b) HXL-30min-PHP, and (c) HXL-30min-PHP-CONR2. Scale bares = 20μm……...**58**
Figure 4. 7: SEM images of powdered samples showing window diameter distributions of (a) VBC-PHP, (b) HXL-30min-PHP, and (c) HXL-30min-PHP-CONR2. Scale bars: a) 5 μm , b)10 μm, c) 10 ……...….....**59**
Figure 4. 8: FTIR spectra of PHP (a), aldehyde functional PHP (b), carboxylic acid functional PHP (c) and amide functional (ethanolamine)……**61**
Figure 4. 9: FTIR spectra of HXL-30min-PHP (a), aldehyde functional HXL-30min-PHP (b), carboxylic acid functional HXL-30min-PHP (c) and amide functional (ethanol amine) HXL-30min-PHP……...**62**
Figure 4. 10: FTIR spectra of a) HXL-30min-PHP-CONR2 (aniline), b) HXL-30min-PHP-CONR2 (diethylamine), c) HXL-30min-PHP-CONR2 (ethanolamine) HXL-30min-PHP-CONR2 (propylamin)……..……...**62**
Figure 4. 11: Increase in surface area and decrease in chlorine content with the progress of hypercrosslinking reaction……..….**63**
Figure 4. 12: XPS surveys of (a) HXL-30min-PHP, (b) HXL-30min-PHP-COOH and (c) HXL-30min-PHP-CONR2 (propylamine)…….....**64**
Figure 4. 13: Nitrogen adsorption-desorption isotherms…….....**66**
Figure 4. 14: Pore size distribution for VBC-PHP and HXL-30min-VBCPH…....**67**
Figure 4. 15: The calibrtion curve for Hg(II)-diphenylcarbazide method…….....**70**
Figure 4. 16: The comparision of mercury adsorption kinetic performances for VBC-PHP-CONR2 (ethanolamine), HXL-15min-PHP-CONR2 (ethanolamine) and HXL-30min-PHP-CONR2 (ethanolamine). The initial Hg(II) concentration = 5x10-4 M, 25 mg adsorbent, 10 mL metal solution, 250C……...**70**
Figure 4. 17: The effect of the solid-liquid ratio on mercury adsorption for HXL-30min-PHP-CONR2 (ethanolamine) adsorbent. Experimental conditions : 10 mL of mercury solution (0.005 M), 25Oc solution temperature……**71**
Figure 4. 18: The effect of pH on Hg(II) adsorption for HXL-30min-PHP-CONR2 (ethanolamine). Adsorption conditions : 25 mg polymer, the initial HgCl2 concentration = 0.05 M, the volume of metal solution = 10 mL……**73**
Figure 4. 19: a) UV spectrums of mercury adsorption kinetics on HXL-30min-PHP-CONR2 (ethanolamine) at 100 ppm initial HgCl2 concentration. b) The adsorption capacity comparision between unhypercrosslinked and hypercrosslinked (30 min hypercrosslinking reaction) amide functional (ethanolamine) polyHIPEs.

Experimental conditions : 25 mg adsorbent. 10 ml adsorption medium. at 25oC, 400 rpm stirring rate.....**74**
Figure 4. 20: Pseudo first order kinetic plot for Hg(II) adsorption on HXL-30min-PHP-CONR2 (ethanolamine) and VBC-PHP-CONR2 (ethanolamine). Adsorption conditions: 25 mg polymer, the initial HgCl2 concentration = 100 ppm, the volume of metal solution = 10 mL……...……**75**
Figure 4. 21: Pseudo second order kinetic plot for Hg(II) adsorption on HXL-30min-PHP-CONR2 (ethanolamine) and VBC-PHP-CONR2 (ethanol amine). Adsorption conditions: 25 mg polymer, the initial HgCl2 concentration = 100 ppm, the volume of metal solution = 10 mL…….....**75**
Figure 4. 22: Intra-particle diffusion plot for Hg(II) adsorption on HXL-30min-PHP-CONR2 (ethanolamine) and VBC-PHP-CONR2 (ethanolamine). Adsorption conditions: 25 mg polymer, the initial HgCl2 concentration = 100 ppm, the volume of metal solution = 10 mL……...……**77**
Figure 4. 23: Adsorption capacity – HgCl2 concentration plot…….....**78**
Figure 4.24: Langmuir isotherms HXL-30min-PHP-CONR2 (ethanolamine) and VBC-PHP-CONR2 (ethanolamine)…….....**79**
Figure 4. 25: The Freundlich isotherms for mercury adsorption on HXL-30min-PHP-CONR2 (ethanolamine) and PHP-CONR2 (ethanolamine)……..……..**80**
Figure 4. 26: Dubinin–Radushkevich (D–R) isotherms….....**81**
Figure 4. 27: van't Hoff (a) and Arhenius (b) plots for mercury adsorption on HXL-30min-PHP-CONR2 (ethanolamine)……. ……...**83**
Figure 4. 28: Mercury adsorption kinetics on HXL-30min-PHP-CONR2 (ethanolamine) at various temperatures…….....**83**
Figure 4. 29: Adsorbent Reuse.....**85**

HIGH INTERNAL PHASE EMULSION TEMPLATE METHOD FOR FAST AND SELECTIVE MERCURY ADSORPTION

SUMMARY

There are many template methods for designing porous polymers. Porous polymers have become highly preferred in the industry due to their easy processability and properties. In this study, it was polymerized using a high internal phase emulsion template (HIPE). HIPE is named by looking at the ratio of the external phase volume to the total volume. If this ratio is greater than 0.74, it can be called HIPE.Macroporous polymers prepared by the HIPE method were used. The main disadvantage of PolyHIPE polymers is that they have a low high area (S_{BET} ~9 m^2g^{-1}). To overcome this disadvantage, a hypercrosslinking reaction was performed. High surface area polymers were obtained with the Fiedel Crafts reaction (S_{BET} ~ 594 m^2g^{-1}). After the hypercrosslinked polymer was obtained, three different functionalization steps were applied. These are respectively; aldehyde, carboxylic acid and amide functionalization. The main purpose of this study is to obtain a selective, fast adsorbent on mercury. It is amide groups that provide selectivity to mercury. The -$CONR_2$ group was obtained from the -Cl groups. In this study, amide group was obtained from carboxylic acid by using four different amides as propylamine, ethanolamine, aniline, diethylamine and DIC/NHS.

With the emulsion templating strategy, hypercrosslinking polymers with different hyper-crosslinking times (15 minutes, 30 minutes, 60 minutes, 22 hours) were obtained, increased to amide groups and adsorption studies were carried out. While the main product, HXL-30min-PHP-$CONR_2$, adsorbs 28 mg/g mercury in the first 2 minutes, it is 40.5 mg/g in the 180th minute when it reaches equilibrium. For these studies, different pH ranges were tried (pH 3, pH 4, pH 5, pH 6, pH 7) and the optimum pH was found to be 7.Isotherm (Langmuir, Freundlich, Dubinin- Radushkevich) and kinetic (pseudo-first order, pseudo-second order, intra-particle diffusion) models were made for HXL-30min-PHP-$CONR_2$. Window and void diameter were calculated by using SEM images with Imagej program. Reuse studies were performed for HXL-PHP-$CONR_2$ using 0.1 M HNO3, and 90% capacity was observed up to the 5th cycle.

HIZLI VE SEÇİCİ CIVA ADSORPSİYONU İÇİN YÜKSEK İÇ FAZ EMÜLSİYON ŞABLON YÖNTEMİ

ÖZET

Gözenekli polimerler tasarlamak için birçom şablon yöntemi bulunmaktadır. Gözenekli polimerler endüstride kolay işlenebilirliği ve özellikleri sayesinde çok fazla tercih edilir hale gelmiştir. Bu çalışmada yüksek iç fazlı emülsiyon şablonu kullanılarak(HIPE) polimerleştirilmiştir. Dış faz hacminin toplam hacme oranına bakılarak HIPE olarak adlandırma gerçekleştirilir. Bu oran 0.74'ten büyükse HIPE olarak isimlendirilebilir. Emülsiyon sistemleri suda yağ (oil-in-water; o/w) emülsiyonu ya da yağda su (water-in-oil; w/o) emülsiyonu olarak sınıflandırılabilir. Bu ayrım organik fazın su içerisine mi yoksa yağ içerisine mi damladığı ile ilgilidir. Yani organik faz su içerisine damlıyorsa suda-yağ emülsiyonu, yağ içerisine damlıyorsa yağda-su emülsiyonu olarak adlandırılır. Yağda su emülsiyonu ters emülsiyon olarak da geçmektedir. HIPE şablonu ile hazırlanılan gözenekli polimerlerde yüksek oranda ters emülsiyon kullanılmaktadır. Burada damlacıklar başlatıcı monomer ve yüzey aktif madde ile yoğun bir şekilde bir araya gelir ve viskoz olarak nitelendirebileceğimiz macun kıvamında bir malzeme oluşur. Bu monomer fazının polimerleştirilmesi ile PolyHIPE(PHP) olarak adlandırılan gözenekli polimerler oluşur. PolyHIPE'lar makro boyutlu büyük ve buna nispeten daha küçük gözeneklerden oluşur. PolyHIPE'larda çok çeşitli monomerler kullanılabilmesine karşın, en fazla kullanılan monomerler, Divinilbenzen(DVB), stiren ve vinilbenzil klorürdür (VBC).

HIPE metoduyla elde edilen gözenekli polimerlerin yüzey alanı BET ile yaklaşık 9 m^2g^{-1} ölçülmüştür. Bu durum yapısında mezo ve makro boyutlu gözeneklerin eksikliğinden kaynaklanmaktadır. Düşük yüzey alanlı polimer eldesi bu metodun en önemli dezavantajlarından biridir. Düşük yüzey alanı adsorpsiyon hızını da etkilemektedir. Düşük yüzey alanlı polimerlerin yüksek verim hedeflenen çalışmalarda kullanımı alınacak sonucu düşürmektedir. Bu dezavantajı ortadan kaldırmak için yüzey alanı arttırılması bu çalışmanın ilk hedefidir. Bunun için hiper çapraz bağlama(hypercrosslinking) metodu kullanılmıştır. Kısaca bu metod düşük çağraz bağlı kopolimerlerin yüksek çapraz bağlanması olarak açıklanabilir. Friedel Craft alkilasyon reaksiyonu ile yüzey alanı yaklaşık 50 kat arttırılmıştır. (S_{BET} ~ 594 m^2g^{-1}) Bu reaksiyonun temel amacı aromatik halkada yer alan fenil halkalarının yüksek oranda metilen blokları oluşturmaktır. En temel haliyle aromatik halkaya açil grubunun bağlanması fikrine dayanmaktadır.

Hiper çapraz bağlanma reaksiyonu(HXL) çok hızlı gerçekleşir ve kısa bir sürede yüzey alanını yaklaşık 50 kat arttırabilir. Bu reaksiyon 15 dakikada PolyHIPE'ın yüzey alanını yüksek oranda arttırarak zincir içerisindeki çapraz bağlanmaların hızlıca gerçekleşmesine olanak sağlamaktadır. Farklı sürelerde yapılan hiper çağraz bağlama reaksiyonu (15 dakika, 30 dakika, 60 dakika, 120 dakika ve 22 saat) ile yüzey alanları incelendiğinde ilk 15 dakikada yaklaşık 45 kat arttığı , 30.dakikada en yüksek yüzey alanına sahip olup; 60 dakika, 120 dakika ve 22 saatte değişiklik gözlemlenmemiştir. Böylece çalışma için optimum hiper çapraz bağlanma süresi 30 dakika olarak belirlenmiştir. Elde edilen ana malzeme HXL-30min-PHP olarak kodlanmıştır.

Hiper çapraz bağlanma reaksiyonu ile elde edilen yüksek yüzey alanlı polimer fonksiyonlandırılmıştır. –Cl grupları fonksiyonlandırmada rol almıştır. Hiper çapraz bağlı polimer sırasıyla aldehit, karboksilik asit ve amid gruplarına yükseltgendirilmiştir. Karboksilik asitten amid fonksiyonuna dönüştürmede diizopropilkarbodiimid (DIC) ve N-Hidroksi süksinimit (NHS) kullanılmıştır. Bu reaksiyon iki aşamada gerçekleştirilmiştir. İlk aşamada polimer yüzeyinde NHS/DIC ile ester oluşturulur. İkinci aşamasında ise aktive edilmiş esterli polimer, amin ile eşleşme reaksiyonu ile amid grubu elde edilmiştir. Bu çalışmada, eşleşme reaksiyonu (coupling agent) için farklı aminler kullanılıp amid dönüşümüne etkisi incelenmiştir. 4 farklı amin ile yapılan bu çalışmada kullanılan her farklı amin, farklı bir dönüşüm yüzdesine sahip olmuştur. Etanolamin, dietilamin, propilamin ve anilin gibi farklı aminler denenerek, en yüksek dönüşüm elde edilen etanolamin ile çalışmaya devam edilmiştir. Etanolamin ile sentezlenen asıl madde HXL-30min-PHP-$CONR_2$ olarak kodlanmıştır. Amid grubu civaya selektifliği yüksek olan bir grup olduğundan dolayı, yapılan malzeme amide yükseltgenmiştir. Bu çalışmanın esas amacı olan civaya selektif bir polimer sentezlemektir.

Civa, sağlığa ciddi zararları olan ağır bir metaldir. Civanın solunması yüksek oranda akciğer tahribatına, üst solunum yolu rahatsızlıklarına neden olabilmektedir. Cıvanın zararı sadece üst solunum yollarıyla sınırlı değildir ve merkezi sinir sistemine de ciddi etkileri olabilmektedir. Civa çok farklı alanlarda kullanılabilmektedir. Bu alanlar; tarım alanları, termometre, elektrik sektörü, ayna yapımı, dişçilik olarak sıralanabilmektedir. Ağır bir metal olan civanın kullanım alanları ve sağlığa zararları düşünüldüğünde giderilmesi üzerine yapılan çalışmalar da mevcuttur. Civanın en ekonomik giderimi adsorpsiyon ile sağlanabilmektedir. Adsorpsiyon temel olarak fiziksel ve kimyasal adsorpsiyon olarak ikiye ayrılmaktadır. Fiziksel adsorpsiyon van-der Waals kuvvetleri gibi zayıf kuvvetlerle gerçekleşirken, kimyasal adsorpsiyonda adsorplanan madde ile katı yüzey arasındaki fonksiyonel grupların kimyasal etkileşmesi söz konusudur. Fiziksel adsorpsiyonda katı yüzey ile adsorplanan madde molekülleri arasındaki çekim kuvvetleri söz konusudur. Burada kimyasal adsorpsiyon söz konusu iken fiziksel adsorpsiyonda söz konusu olabilir. Yapılan reaksiyonlar sonucu adsorban olarak kullanılan madde HXL-30min-PHP-$CONR_2$ (etanolamin) ile en iyi adsorpsiyon sonuçları elde edilmiştir. Hiper çapraz bağlı olmayan polyHIPE(VBC-PHP), 30 dakikalık hiper çapraz bağlı polyHIPE (HXL-30min-PHP), ve 30 dakikalık hiper çapraz bağlı, farklı aminlerle amid fonksiyonuna dönüştürülmüş polyHIPE'lar (HXL-30min-PHP-$CONR_2$) farklı adsorbanlar olarak kullanılmıştır. İlk aşamada HXL-30min-PHP, VBC-PHP' a göre daha hızlı ve yüksek kapasitede adsorplama gerçekleştirmiştir.Böylece yüzey alanının arttırılması (50 kat) adsorpsiyon hızını ve adsorpsiyon kapasitesini arttırmıştır. Amid gruplarının devreye girmesi ile de en yüksek civa kapasitesine ulaşılmıştır.

Farklı aminler sadece amid dönüşümüne etki etmemiş, aynı zamanda da adsorpsiyon kapasitesini de etkilemiştir. Burada da en iyi sonuç etanolamin ile alınmıştır. Adsorpsiyon ölçümleri Uv-vis spektrofotometresi ile gerçekleştirilmiştir. Difenilkarbazid ile civa reaksiyona sokulup, pembe-mor arası renk aldıktan sonra Uv-vis spektrofotometresi ile absorbanslar ölçülmüştür. Ölçümden önce farklı konsantrasyonlarda(0.0005 M, 0.001 M, 0.0025 M, 0.005 M, 0.01 M, 0.025 M, 0.05 M) civa hazırlanıp, en yüksek kapasitedeki civa adsorpsiyonu ile devam edilmiştir. Optimim civa konsantrasyonu $5x10^{-4}$ M olarak bulunmuştur. Adsorpsiyon kapasitesini etkileyen bir diğer faktör olan çözeltinin optimum pH'ının bulunması için farklı pH tampon çözeltileri denenmiştir. Deneysel sonuçlara dayanarak optimum pH 7 olarak bulunmuştur. Adsorpsiyon için optimum koşullar, pH 7 , $5x10^{-4}$ M civa çözeltisi içerisinde gerçekleştirilmiştir.

HXL-30min-PHP-$CONR_2$ (etanolamin) adsorbanı ile civa için elde edilen maksimum adsorpsiyon kapasitesi sonrasında civaya selektiflik çalışmalarına başlanmıştır. Selektiflik için iki farklı yönteme başvurulmuştur; titrasyon ve XPS. Titrasyon için kadmiyum, çinko ve civa olmak üzere üç farklı metal kullanılmıştır. Bu üç metal ile hazırlanan çözelti, EDTA ile kompleksleştirilip, kurşun nitratla titrasyona tâbi tutulmuştur. 2-tiazolin 2 tiyol ile civayı tutan EDTA salınmıştır ve kurşun nitratla yapılan titrasyon sonucunda civa miktarı bulunmuştur. XPS ile de selektiflik desteklenmiştir. Yapılan çalışmalar sonucunda HXL-30min-PHP-$CONR_2$ (etanolamin) adsorbanının civaya selektifliği yüksek bulunmuştur. HXL-30min-PHP-$CONR_2$ (etanolamin) ve HXL-30min-PHP-COOH ile yapılan bu titrasyon çalışmasında, karboksilik asit grupları olan HXL-30min-PHP-COOH adsorbanının civanın yanında kadmiyum ve çinkoyu da tuttuğu gözlemlenmiştir. HXL-30min-PHP-$CONR_2$ (etanolamin) adsorbanını ise kadmiyum ve çinkoyu eser miktarda tutmuştur.

Adsorpsiyon düşük maliyeti sebebiyle civa gideriminde en fazla kullanılan yöntemdir. Avantajı uygun fiyatı ve hızlı olabilmesi sayılırken, dezavantajı ise yeniden kullanımının sıkıntılı olması sayılabilmektedir. Bu çalışmada en önemli kısım elde edilen HXL-30min-PHP-$CONR_2$'nin (etanolamin) 5 döngüye kadar %90 oranında kapasite ile kullanılabilmesi sayılabilmektedir. Yeniden kullanım, 0.1 M HNO_3 ile yapılmıştır. Amid grupları asitte bozunabileceği için karboksilik asitten amid dönüşüm yüzdesi yaklaşık %50-%60 arasında tutulmuştur. Karboksilik asit grupları sebebiyle yapıda bozunma gerçekleşmeden, yeniden kullanıma olanak sağlanmıştır. Fiziksel adsorpsiyon etkisini ortadan kaldırabilmek için kinetikten sonra adsorban su ile yıkanmıştır.

HXL-30min-PHP-$CONR_2$ için izoterm (Langmuir, Freundlich, Dubinin-Radushkevich) ve kinetik (pseudo-first order, pseudo-second order, intra-particle diffusion) modelleri yapılmıştır. Imagej programı ile SEM görüntülerinden yararlanılarak pencere (window) ve boşluk (void) yarıçapları hesaplanmıştır.

Çalışmanın ana maddesi olan HXL-30min-PHP-$CONR_2$ (etanolamin) ile yapılan çalışmalar ve deneyler sonucu bu adsorbanın adsorpsiyon kapasitesi ve adsorpsiyon hızı oldukça yüksek bulunmuştur. Dolayısıyla bu yaklaşım ile yüksek kapasite, hız ve verim elde etmek mümkündür.

1. INTRODUCTION

Mercury is one of the heavy metals that can cause serious harm to the environment and human being. In this study, our aim was to remove the heavy metal –mercury (II)- quickly and effectively. Once synthesizing VBC PolyHIPE, it was aimed to increase the surface area and adsorption kinetic performance through hypercrosslinking. VBC PolyHIPE and hypercrosslinked PolyHIPE comparisons were made in this study and it was observed that surface area and adsorption kinetics were enhanced which were comfired by BET and adsorption kinetics measurements. Our work was carried out by using the material (HXL-30min-PHP) prepared by 30-min-hypercrosslinking reaction and the other hypercrosslinked PolyHIPE's also were prepared (15min, 60min, 120min, 22h). It was possible to obtain mercury selectivity (Hg(II)) with amide groups. Therefore, we functionalized the polHIPE's with aldehyde, carboxylic acid and amide, respectively. Four different amines, namely propylamine, diethylamine, aniline and ethanolamine, were tested for amide functionalization. Our goal was to keep the conversion of carboxylic acid to amide between 50-65%. The study was focused on the polyHIPE prepared with ethanolamine, which had the highest affinity towards mercury (II). Mercury (II) adsorption studies were carried out with HXL-30min-PHP-$CONR_2$, which became our main polymer after amide conversion. To observe the selectivity, a triple heavy metal mixture (Cd, Zn, Hg) was prepared and the results were found based on the titration method. Titration results are also in good agreement with XPS surface area mesurement results. As a result of the experiments, the selectivity of our HXL-30min-PHP-$CONR_2$ (ethanolamine) polymer for mercury was found out to be very high. Reuse studies, which can be considered as an advantage of adsorbents, were carried out in 0.1 M aqueous HNO_3 solutions. The reason we do not want to convert all of the carboxylic acid to the amide was that the amide groups can be hydrolysed in acidic medium. The remaining carboxylic acid groups on the polymer surface both contribute to the adsorption process and also prevent the hydrolysis of amide groups during the desorption process. Thus, 90% efficiency was achieved in reuse up to 5 cycles. Based on the results obtained, the synthesized and functionalized

HXL-30min-PHP-$CONR_2$ showed fast adsorption kinetics and selectivity for mercury (II).

2. THEORY

2.1 Polymer

Polymers are a material with a high molecular weight formed by the merging of the of a small molecules that are called monomer. Natural polymers, deoxyribonucleic acid (DNA) and ribonucleic acid (RNA), which are necessary for life , have been in place since early on, and lifes depends on polymers. In addition, cellulose, lignin, starch , natural rubber are examples of natural polymer. Synthetic polymers are relatively more modern than natural polymers, since they entered in the early twentieth century. Since synthetic polymers are made as a result of chemical reactions called polymerization, polymers with different properties can be obtained. Polymers can create the content of different products in the sectors such as coating, automotive, furniture, cosmetics, food, pharmaceuticals, etc. It has an important place in every aspect of our lives. [1]

2.2 Emulsion

Emulsions are systems that are obtained by dispersing one of two immiscible liquids as droplets in the other. The phase dispersed in droplets is called "internal phase", "dispersed phase", "discontinuous phase", while the phase into which the drops are dispersed is called "external phase" or "continuous phase". [2]

A number of theories have been proposed for the emulsification to occur. These theories;

Surface tension theory: This theory explains that the surface tension between two immiscible phases (oil and water phase) decreases and emulsion is formed.

Repulsion theory: It assumes that emulsifiers form a film containing spheres in one of two heterogeneous phases that repel each other. These spheres remain suspended due to repulsive forces.

Viscosity theory: This theory also assumes that emulsifiers increase the viscosity of the environment and form the viscous suspension. [3]

Emulsions can generally be divided into three;

1. Water in oil emulsion (w / o)
2. Oil in water emulsion (o / w)
3. Multiple emulsion
    - Oil-in-water-in-oil emulsion (o / w / o)
    - Water-in-oil-in-water emulsion (w / o / w) [4]

Water-in-oil emulsions are formed by dispersing the water phase into an emulsion whose continuous phase is oil. Oil-in-water emulsions are the opposite of water-in-oil emulsions. Water is created by dispersing the oil phase into a continuous phase. Multiple emulsions contain both emulsions. In w/o/w emulsions, oil drops are dispersed in the water phase and envelop the water drops in itself. In o/w/o emulsions, the water phase disperses in the oil droplets and surrounds the oil droplets within itself. In other words, the continuous phase varies according to the emulsion type. [5]

2.2.1 Emulsion stability

Some changes in the external environment may occur over time. Emulsion stability can be expressed as the resistance to this change. However, in some cases, emulsion stability may deteriorate. In this case, flocculation, creaming, coalescence, phase separation, Oswald ripening and sedimentation may occur. [6]

Creaming: It is a kind of emulsion instability situation. If the dispersed phase is less dense than the continuous phase, the droplets collect on top. The difference in size is in question here. The motion of the droplets of different sizes affect each other and cause collapse by disrupting the stability.

Sedimentation: Sedimentation is similar to sedimentation. Since the density of the dispersed phase is greater than the density of the continuous phase, these droplets tend to settle. [7]

Flocculation: While the pulling force in the emulsion depends on the London van der Waals force, the repulsive force is due to the surfactant at the interface. Here the dispersed phase begins to aggregate together. As the distance between the droplets decreases, the Van der Waals attractive force increases. This situation causes the

droplets to come together. This occurs when there is not enough repulsive force to reduce the attractiveness (to keep the droplets apart). [8,9]

Coalescence: This refers that the dispersed phase comes together and forms a larger droplet. As with flocculation, this can increase the probability of creaming and sedimentation occurring.

Phase inversion: This refers to the phase displacement situation. A water-in-oil emulsion can be transformed into an oil-in-water emulsion or opposite situation actualize. This can mostly happen in multiple emulsions.[7]

Ostwald ripening: Ostwald ripening is based on the fact that small droplets expand and form larger droplets. This is due to the limited solubility of the liquid phase according to Figure 2.1.[7]

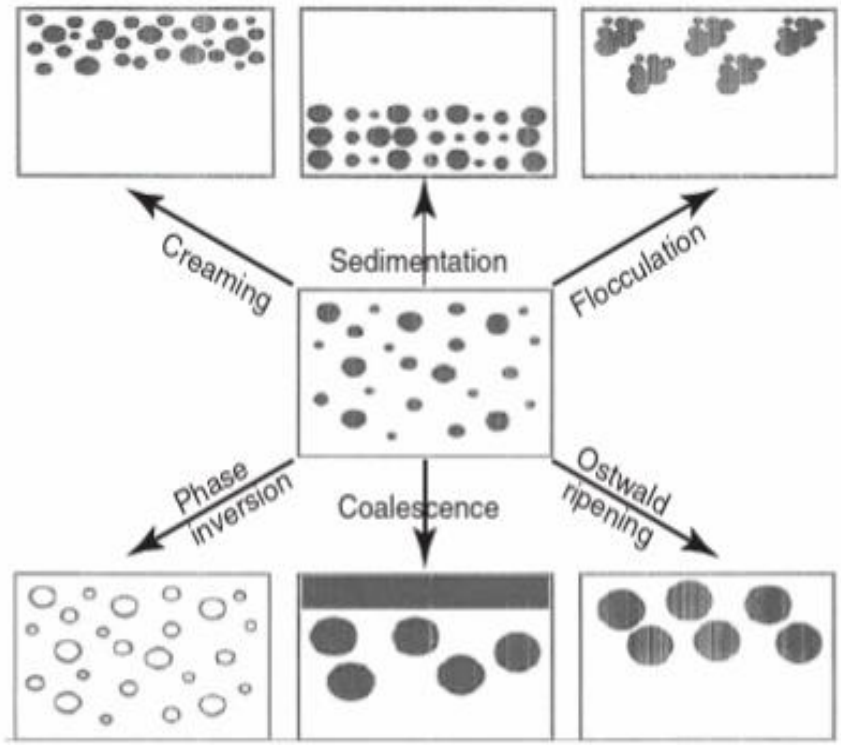

Figure 2. 1: Representation of instable emulsion type[10].

Emulsion fragmentation(instability) are affected by environmental conditions such as temperature and pH. Emulsifiers play an important role in stability. Emulsifiers reduce the interfacial tension between water and oil phases. At the same time, by forming an interface film around the droplets, they prevent these droplets from coming together and destabilizing. [9]

2.3 Emulsion Polymerization

It is possible to categorize polymerization under different headings. It can be divided into subheadings such as step growth polymerization, emulsion polymerization, radical polymerization and examined.[11]

An emulsion in general; contains initiator, hydrophobic monomer, water and oil phase, surfactant. Emulsion polymerization is a type of radical polymerization and has a complex process. The end product is artificial latex containing very small sized polymer particles. Here, surfactants called emulsifying agents are used to provide the emulsion. Surfactants consist of two ends, hydrophilic and hydrophobic. Hydrophobic parts tend towards hydrophobic ends (monomers) while hydrophilic ends tend towards water. Thus, surfactants settle on the interfaces between the monomer and water and prevent the deterioration of the emulsion stability by combining with each other.[12]

[13]Since emulsion polymerization is a kind of free radical addition polymerization, it consists of three steps. These steps; (i) initiation, (ii) propagation, and (iii) termination.

Initiation step: Initiator causes the formation of free radicals by activating monomers containing unsaturated carbon-carbon bonds.

Growth step: Radicals that react with the monomer create a larger free radical, which reacts with another monomer causing growth.

Termination step: In the previous step, the ever-growing polymer chains are terminated by another free radical or another factor. [14,15] The basic mechanism of emulsion polymerization is shown in Figure 2.2.

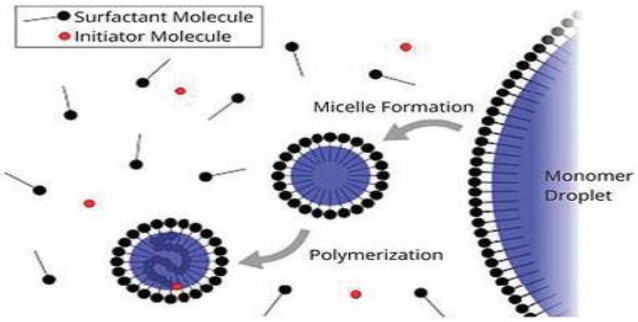

Figure 2. 2: Mechanism of emulsion polymerization[16].

Most of the emulsifiers (surfactants) combine to form micelles. A small part can be dissolved in water as molecules. The number of micelles to be formed depends on the

emulsifier and monomer type. In emulsion systems, polymerization takes place inside micelles. The formed free radicals enter the micelles and initiate polymerization. Here, if the critical micelle concentration falls below the critical value, the micelles become unstable and dissolve in water. [17]

2.4 Porous Polymer

Porous polymers have become important recently. The reason for its increased importance is the combination of the properties of polymers with porous structures. The advantages of porous polymers can be mentioned as follows;

- They have high surface area and well defined porosity.

- They can be easily processed (made as monolith or film and can be easily used in many different industries.)

- It is easy to create porous structure, shape the structure of polymers and design the polymer in polymers with many synthetic production methods.

- Light elements are formed due to their organic structure and their weight provides advantages in many industries.

Figure 2.3 shows the structure of porous polymers.

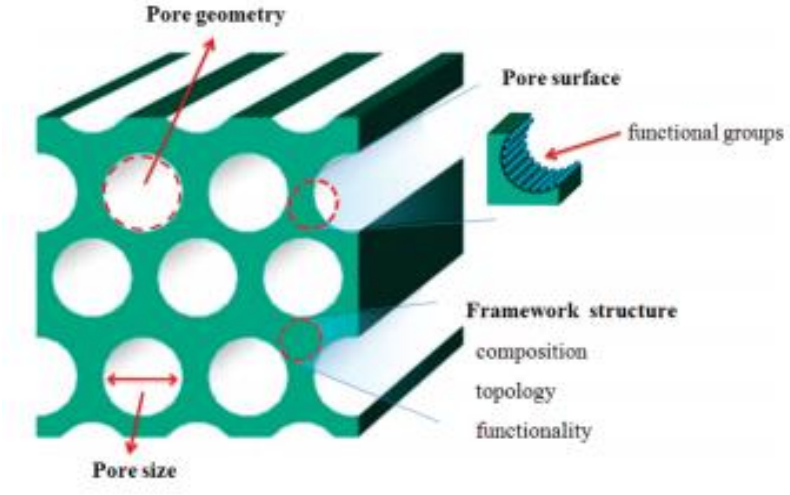

Figure 2. 3: Illustration of pore geometry

According to IUPAC, microporous polymers are divided into three considering the pore size. Micropore polymers smaller than 2 nm, mesoporous polymers between 2-50 nm, and macropore polymers larger than 50 nm.

There are different template methods for synthesizing porous polymers like direct templating, block copolymer templating, colloidal templating, high internal phase emulsion,etc. [18]

In general, the continuous phase is polymerized from two-phase systems consisting of an internal and an external phase (continuous phase) to form a colloidal templating. [19]

There are multiple synthetic methods to produce porous polymer network with different structures. Some of these are given below;

- Hypercrosslinked polymers (HCPs)
- Covalent organic framework (COFs)
- Conjugated microporous polymers (CMPs)
- Porous aromatic frameworks (PAFs)
- Polymers of intrinsic microporosity (PIM)
- Covalent triazine frameworks (CTFs) etc. [20]

2.4.1 Direct templating methodology

The direct templating technique generally includes three parts. First, the basic processing of the raw materials required for the preparation of polymeric framework (adsorption or filtration). The other step is in situ polymerization or solidification of dispersed materials, Finally, removal of templates. Figure 2.4 shows this mechanism more clearly.

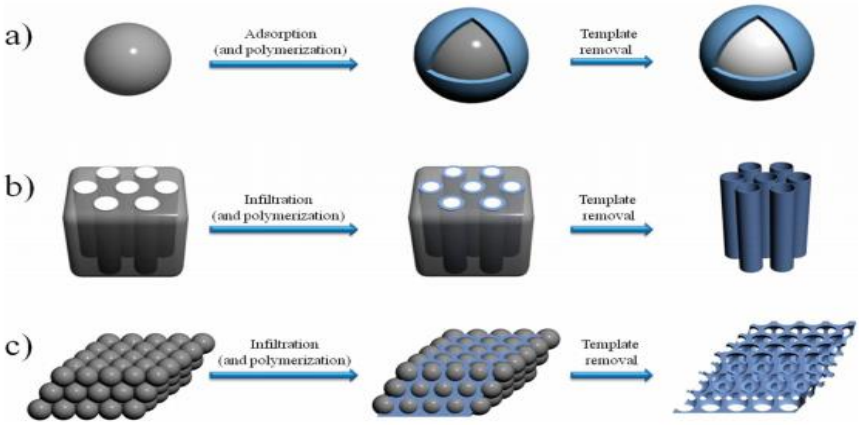

Figure 2. 4: Schematic illustration of fabrication of (a) individual spherical porous polymers from solid spherical nanoparticle templates, (b) tubular porous polymers from tubular porous templates, such as AAO, and (c) ordered macroporous polymers from colloidal crystal templates[18].

2.4.2 Block copolymer self-assembly methodology

Self-assembly of block copolymers (BCPs) allows controlled preparation of materials with different structures in a wide framework. This method provides a strategy for generating two- and three-dimensional morphologies between 5 and 50 nm. The field of use of block copolymers is to provide self-adhesion of nano-sized particles or additives to organic-organic, organic-inorganic hybrid materials as an agent. This methodology is shown in Figure 2.5.

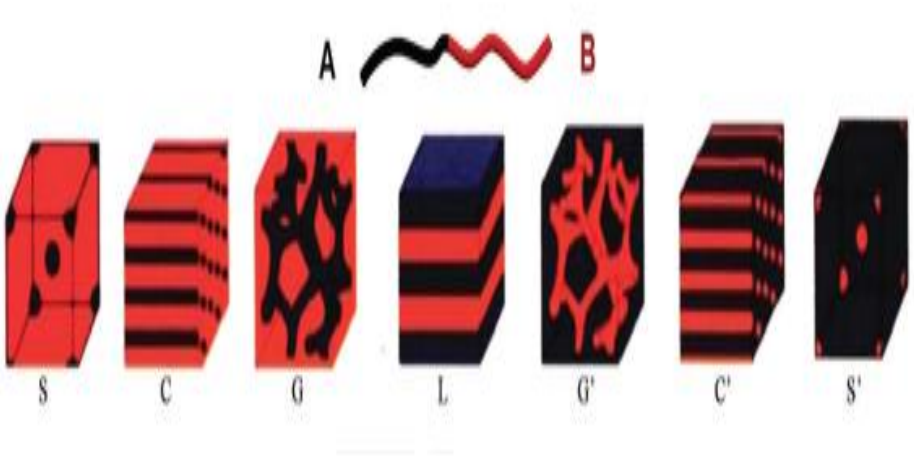

Figure 2. 5: Equilibrium morphologies of AB diblock copolymers in the bulk. S: cubic spheres, C: hexagonally packed cylinders, G: bicontinuous gyroids, L: lamellae, G',C',S' : the copolymer composition is reversed.

According to Figure 2.6:
$p < 1/3$: spherical micelles or spheres

$1/3 < p < 1/2$: cylindrical micelles or hexagonally packed cylinders

$1/2 < p < 1$: vesicles or modulated lamellae

$p = 1$: planar bilayers or multi-layered lamellae

$p > 1$, minimal surfaces (G, D, and P surfaces) or inverse Hex (fcc and bcc)

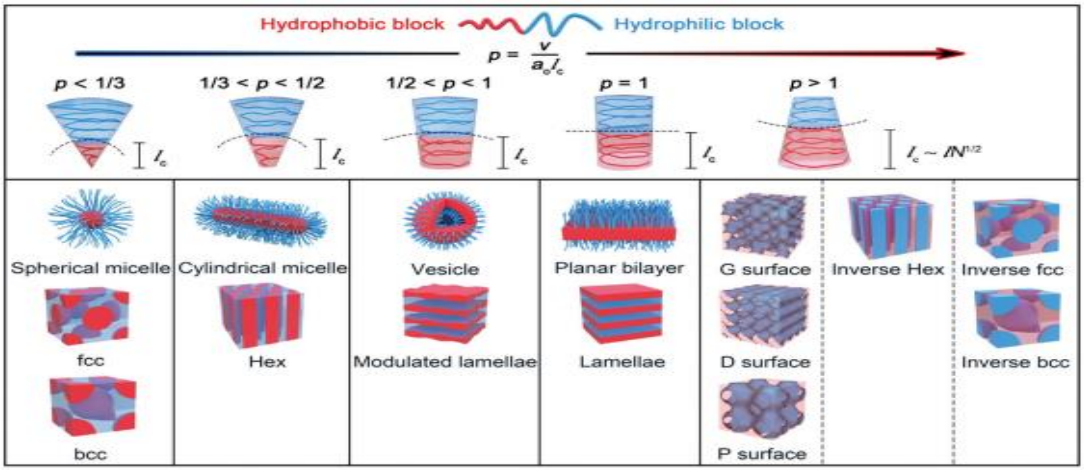

Figure 2.6: Block copolymer self- assembly in solution. The self assembled structures are determined by the packing parameter (p). [21]

Vertical cylinders in block copolymer structures are in the focus of attention as they obtain nanoporous structures. Porous structures can be formed by dissolving a polymer block with the appropriate solvent or by removing a block by abrasion, as shown in Figure 2.7. [22]

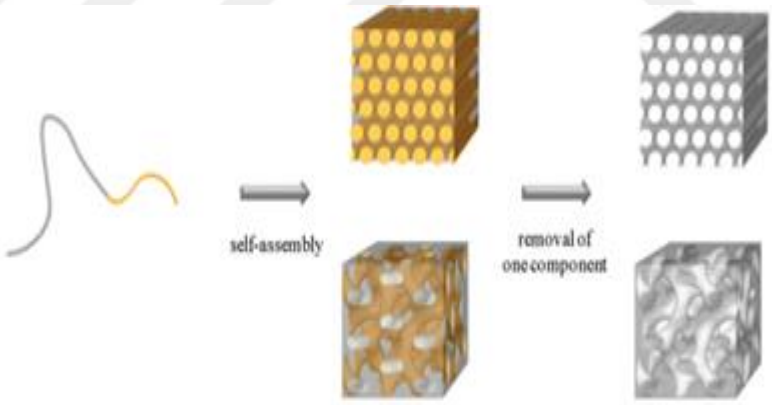

Figure 2. 7: Self assembly block copolymers with removal of one component [18].

2.4.3 Direct synthesis methodology

This method is based on the direct formation of porous polymers. First of all, a suitable polymerization reaction is selected for polymerization and direct porous polymers are formed by removing the reaction solvent trapped in the pores.

For the formation of meso and macroporous structures;

- Initiator, reagent, solvent, etc. researching and selecting the necessary reaction elements for the reaction to occur.

- This selected reaction system creates phase separation.

- Choosing the appropriate monomer to prevent the collapse of pores during drying and having the appropriate rheology of the network structures.

Radical polymerization or polycondensation is used to form nano or nano-porous networks. [18]

2.4.4 Polymers of instrinsic microporosity

Polymers named in this way were mentioned by McKeown and Budal and developed for the first time. Expanded aromatic components are added to the structure, the polymer network, to mimic graphene structures (consisting of activated carbon). Polymers are synthesized by irreversible condensation reactions. The compounds included in the structure are hard, therefore they force polymers to bend to fill gaps.[23]

2.4.5 High internal phase emulsion polymerization (HIPE)

High internal phase emulsions are a common method used to synthesize porous polymers. High internal phase emulsions consist of two phases as internal and external phase. The internal phase volume is more than 74% of the total emulsion volume. This allows for the formation of pores. HIPE's can be polymerized and used in many industries such as medicine, cosmetics, food and construction [24]

Porous polymers obtained with high internal phase emulsions that have become the center of attention in recent years, because of their pores are dense and these pores are highly interconnected.[25]

In high internal phase emulsions, the dispersed (internal) phase and the continuous (external) phase are mentioned. During its polymerization, the external phase shrinks to form an open cell with polyhipe morphology.[26]

As can be seen in Figure 2.8, HIPE has a volume fraction greater than 74%..

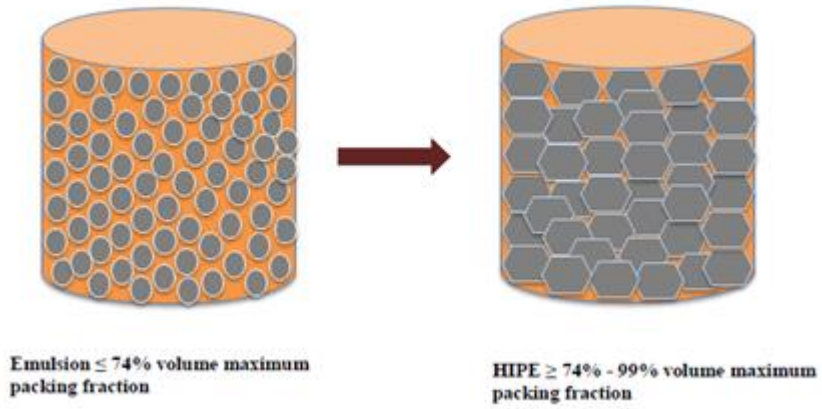

Figure 2.8: Schematic representations of emulsion and high internal phase emulsion [27].

As it is known, the presence of two immiscible liquids, one of which is an aqueous solution, is important for the formation of Hipes. As can be seen in Figure 2.9., the higher internal phase emulsions, which consist of two basic structures: aqueous phase and organic (oil) phase, are more stable due to the use of more hydrophobic liquids.

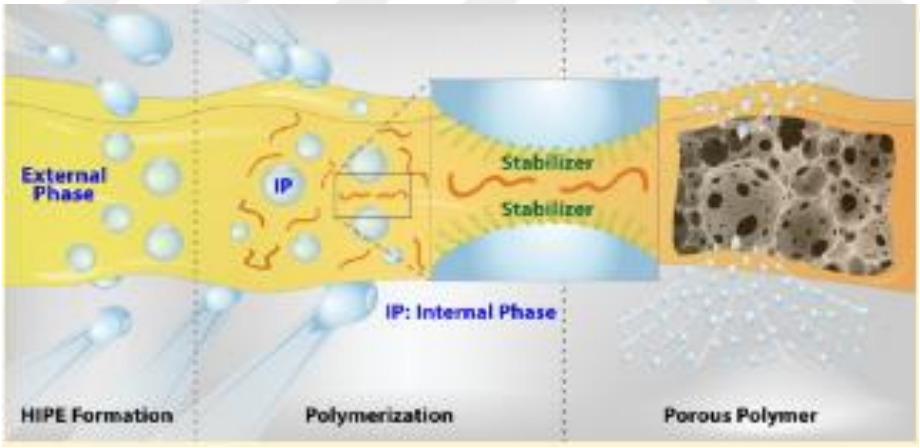

Figure 2.9: Representation of synthesized porous polymer.

High internal phase emulsions are generally formed with the help of surfactant by mixing the external phase into the internal phase. It is possible for HIPE to occur in other situations. Poihedras can be formed by deformation in an emulsion. It occurs when a centrifugal field is applied to the emulsion, causing the droplets to interact with each other. Excess outer phase is removed from the emulsion by creating a separate phase. This is called cream. [28]

2.5 Polymerization of HIPE (PolyHIPE)

The first names that come to mind when talking about PolyHipe are Barby and Haq, who patented in 1982. Although the usage areas of PolyHipes are very common now, they were first synthesized for use in areas such as chemical synthesis, ion exchange, and chromatography. PolyHipes contain approximately 90% water phase and 10% organic phase. It is usually synthesized using hydrophobic monomers and is known as a water / oil emulsion.[29]

Although the usage area of high internal phase emulsions is very wide, they also serve as a template to create porous structures. The structures obtained by hardening the outer (continuous) phase are called PoyHipe. With this solidification, emulsion droplets penetrate into the material, forming small and interconnecting frames, allowing these droplets to be removed. Thus, highly porous materials are produced.[30] PolyHipe formation can be easily seen in Figure 2.10 below.

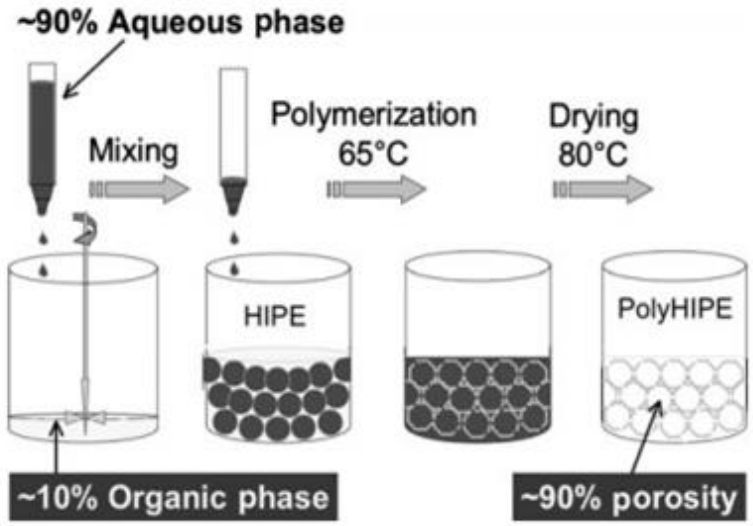

Figure 2.10: Illustration of PolyHipe creation [31].

2.5.1 PolyHIPE morphology

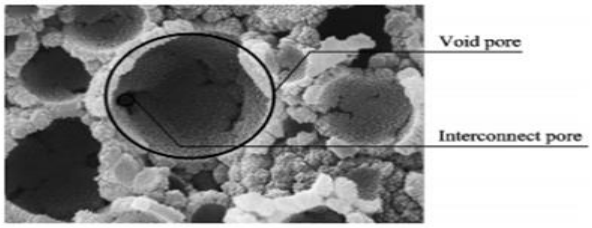

Figure 2. 11: PolyHipe morphology in SEM imaging.

Figure 2.11 shows the SEM image of the PolyHipe morphology. Accordingly, the morphology basically consists of void and interconnect pore.

As it is known, PolyHipes have become the favorite of many industries thanks to their low density, low weight and more pore structures. The characteristic properties of PolyHipes are generally determined by their pores, also called voids, holes and windows. This is achieved by emulsion polymerization. PolyHipes show two types of morphology. These;

- Open cell (interconnected)
- Closed cell [32,33]

Windows or holes are formed by the freezing of the outer phase. There are some factors that affect the formation of open cells and closed cells. Some of those;

- The proportion of surfactant (most important)
- Type of surfactant
- Stabilizer type
- Place of initiation [34]

The open cell structure consists of holes instead of the dispersed phase. Although the diameters of the pore vary between the open cell structure is interconnected and this happens through the holes. The width of the holes affects the bonding to each other as well as the permeability and usage areas of PolyHipes. Structures without interconnection can be defined as closed cell structures. [35]

One of the factors affecting the size of the pores is the dispersed phase ratio. In the following study (Zhang et al.) Observed the change by keeping the surfactant and nanoparticle ratio constant and changing the paraffin fraction. (Increased from 75% to 85%). As the ratio of dispersed phase increased, the droplets combined and enlarged the diameters of the voids. SEM images of this study are given in Figure 2.12.

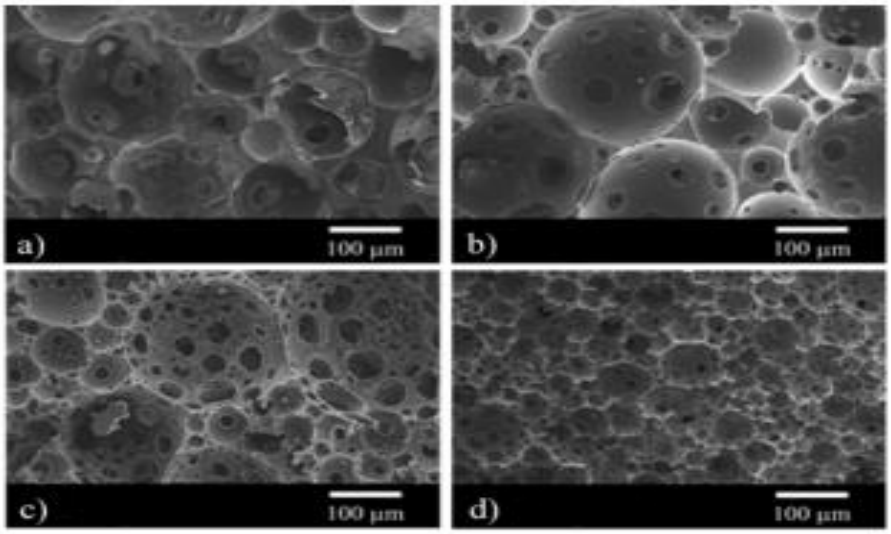

Figure 2.12: Sem images of PolyHipes with different internal phase ratios. These ratios can be summarized as a) 75% b) 80% c) 85% d) 90% [36]

According to the study of Williams and Wrobleski (Williams; Wrobleski, 1988), the rate of surfactant is the most important factor that creates the open cell and closed cell structure. If the surfactant content ratio is below 5%, closed cells, that is, non-interconnected structures occur. [37] Open cell and closed cell morphology SEM images are given in Figure 2.13.

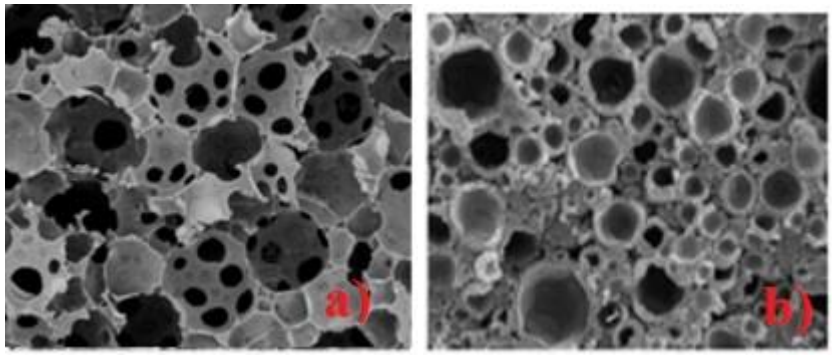

Figure 2.13: a) Open cell (Wu et al. 2021) [38] and b)closed cell (Krajnc et al. 2005) morphology of PolyHipe [39].

In the study of Wu et al, Polyhipe was synthesized and its morphology was investigated. Here, they showed that the closed cell structure is derived from hydrophobic chains. The increase in the monomeric external(outer) phase also increased the emulsion viscosity and formed a closed cell by preventing the open cell structure. In fact, if less surfactant is used, Polyhipe morphology tends to closed cell. This study also included other factors affecting the morphology of polyHipes. It has

been found that by varying the shear rate (from 6000rpm to 3000rpm) the pore diameters are approximately doubled. As the mixing speed increases, the water droplets convert to the smaller droplets at this speed. This is an acceptable finding. The increase in the aqueous phase is directly proportional to the improvement in the pores. However, when the aqueous phase is rised, the increase of pores depends on the type of surfactant. [38]

2.5.2 PolyHIPE surfactants

It has already been mentioned that surfactants are an important factor affecting the morphology of PolyHipes. The processes provided by emulsifications can be summarized as follows;

- First, the droplets are damaged and rupture to break up into smaller pieces.
- Surfactant penetrates these separated droplets.
- Droplets see each other and come together.

These processes can be followed over and over again during emulsion formation. As this continues, smaller droplets are possible.

During emulsification, the amount of surfactant decreases. If the interfacial tension is low, the droplets break up easily. The surfactant takes on this task here. It also prevents droplets from reuniting. [40]

Span 80, also known as sorbitan monooleata, is the most commonly used surfactant in the synthesis of Hipe. (to ensure stability) The morphology of PolyHipes is not solely dependent on the proportion of surfactant. It also depends on the nature of the surfactant. PolyHipe synthesized using only Span 80 has larger pores than PolyHipe synthesized using a Span 80 and Span 85 mixture. This means that the mixture of Span 80 and Span 85 reduces the pore diameter.[41]

Figure 2.14. shows the adsorption of the surfactant on the surface, while Figure 2.15. shows the structure of the surfactant. Surfactants consist of two parts, the hydrophilic head group and the hydrophobic tail.

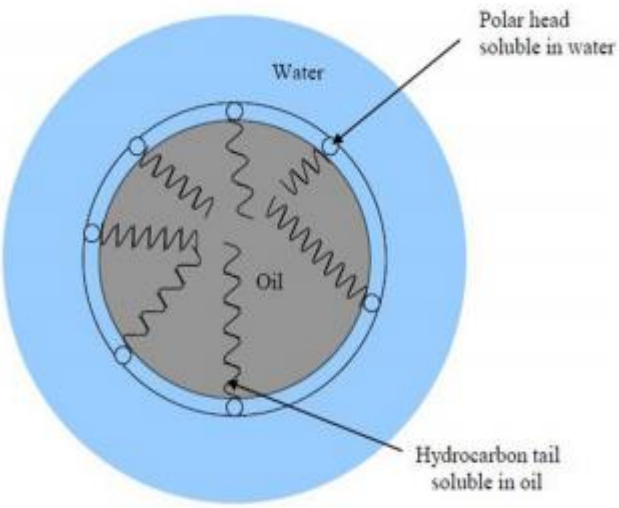

Figure 2.14: Adsorption of surfactant at oil/water interface [42].

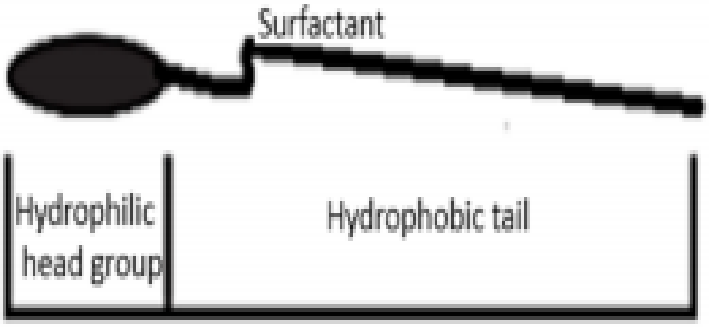

Figure 2. 15: Surfactants structure [43].

Generally, a surfactant consists of two different parts. It is divided into two parts with hydrophobic and hydrophilic properties.

Hydrophilic group: -NH_2, -OH, -COOH, -SO_3H, -OSO_3H, -N (CH_3) 3Cl, -CH_2CH_2O etc.

Hydrophobic group: It can consist of hydrocarbon or oleophilic chains with very long chains. [44]

Figure 2.16. shows the structure of Span80, the surfactant used in the study.

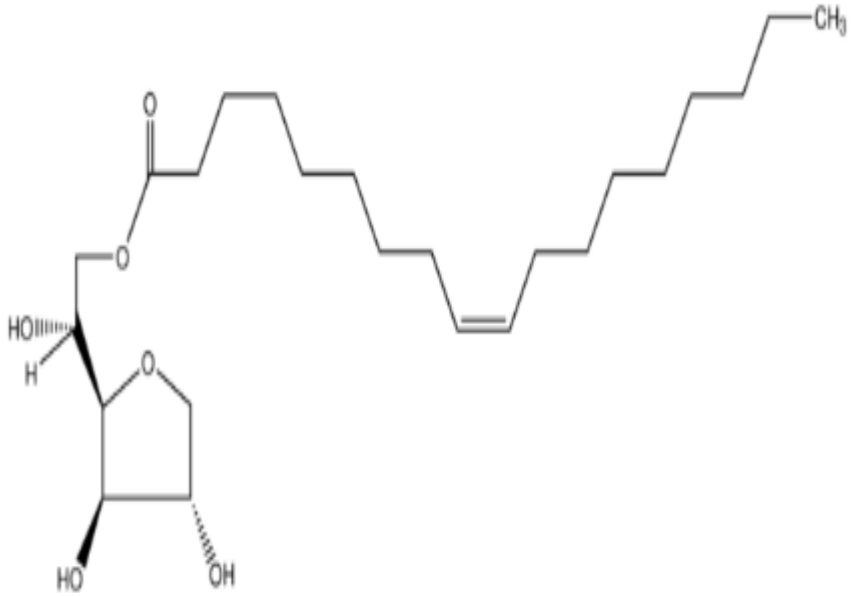

Figure 2. 16: Span 80 molecule structure.

2.5.2.1 Hydrophilic- lipophilic balance of surfactant

Hydrophilic-lipophilic balance was first taken by Griffin with the HLB scale. According to Griffin, the HLB value is calculated by ethylene oxide groups and refers to the balance between the hydrophilic and lipophilic parts of the amphiphilic molecules. In fact, the surfactant is defined as lipophilic surfactant if the HLB value is low, and as hydrophilic surfactant if the HLB value is high. The number given for the average HLB value is 10.

When preparing emulsions (w / o) the HLB value of the surfactant used should be between 4 and 6, that is, a lipophilic surfactant should be preferred. Optimum conditions in an emulsion process are not determined solely by the type of surfactant. The HLB value of the organic phase also has a significant effect. In order to achieve the best emulsification, the HLB value of the surfactant to be used is selected equal to the HLB value of the oil phase. [44] HLB values of some surfactants are given in Table 2.1.

Table 2. 1: Some surfactant and HLB values [44,45].

Surfactant	HLB Value
Span 20	8,6
Span 40	6,7
Span 60	4,7
Span 80	4,3
Span 85	1,8
Brij-30	9,5-9,7
PEG-200	9,1
PEG-300	11,3
PEG-400	12,9-13,1
PEG-600	14,5
Renex-648	10,0
Renex-688	12,5
Renex-690	13,0
Tween 20	16,7
Tween 40	15,6
Tween 60	14,9
Tween 80	15,0
Tween 81	10,0
Tween 85	11,0

2.5.3 PolyHIPE mechanical properties

The low mechanical properties of PolyHipes can be considered as a disadvantage. Various ways can be tried to increase its mechanical properties.

In the study of Haibach et al., They chose two ways to increase the mechanical properties of PolyHipe. The first method is to increase the organic phase, the second method is to add nanosilica particles to the structure. With the increasing volume of organic phase, there is an increase in density, which has increased the elastic modulus. There was also a noticeable increase in elastic modulus with the addition of SiO_2. [46]

In their study, Livshin et al. Synthesized the crystalline polyHipe by copolymerization using stearyl acrylate and stearyl methacrylate monomer and divinylbenzene (DVB)

to crystalline PolyHipe. They synthesized 13 different PolyHipes with different initiators using stearyl acrylate and stearyl methacrylate as monomers, crosslinking comonomer DVB, non-crosslinking comonomer styrene. It has been observed that PolyHipes with the lowest DVB ratio have a high density and a low surface area compared to others. PolyHipes with low DVB content are more prone to crash. DVB polymer both crosslinks and adds rigid units to the polymer backbone. For this reason, the low rate of this ratio decreases the resistance against capillary forces during drying and causes it to collapse. This situation directly affects its mechanical properties.

They observed that increasing the amount of DVB led to three interrelated effects. These; (i) Increasing polymer backbone stiffness, (ii) increasing the degree of crosslinking and this affecting the direct modulus, (iii) decreasing crystallinity and modulus. Since not all double bonds will react in polyHipes with high DVB content, not all of them are used as crosslinkers.

In their study, they showed that the rate of DVB affects the mechanical properties of PolyHipes. As can be understood from here, there are many factors that affect the mechanical properties and it is not possible to explain with a single factor [47].

Kovacic et al. Stated that the mechanical properties of PolyHipes are low due to their low density and fragile structure, and they have worked to strengthen their mechanical properties in this study. Different ways such as decreasing the porosity by increasing the organic phase, including additional particles in the structure, changing the content of the monomer phase have been tried and an important way has been taken to increase the mechanical properties.

In this study, PolyHipe was synthesized by ring opening metathesis polymerization using dicyclopentane as monomer. The mechanical properties of this synthesized polyHipe were found to be quite strong. [48]

2.6 Hypercrosslinking

Davankov and Tsyurupa synthesized hypercrosslinked polystyrene in the 1970s and added hypercrosslinked polymers to the literature. Hypercrosslinked polymers obtained by the Friedel Crafts reaction have a very high surface area and absorption capacity. [49]

It is possible by synthesizing very high area polymers with hypercrosslinking method. It is possible to increase the surface areas up to approximately 2000 m^2 / g. This gives the polymer extremely good properties. They have a much higher adsorption property compared to a conventional crosslinked polymer. [50]

2.6.1 Preparation of hypercrosslinked polymer

According to this procedure, a suitable solvent is selected to obtain the polystyrene hypercrosslinked polymer. Usually, the polymer mixed with 1,2 dichloroethane is expected to open and swell the pores. Lewis acids such as $FeCl_3$, $SnCl_4$ are added to the solvent and polymer mixture to form crosslinks and fix the polymer in swollen state. By removing the solvent, microporous hypercrosslinked polystyrene is obtained. With the removal of the solvent, it causes the formation of pores with the discharge of the area covered by it. Thus, interconnected porous structures are formed. A schematic representation of this is available in Figure 2.17 below [49,51].

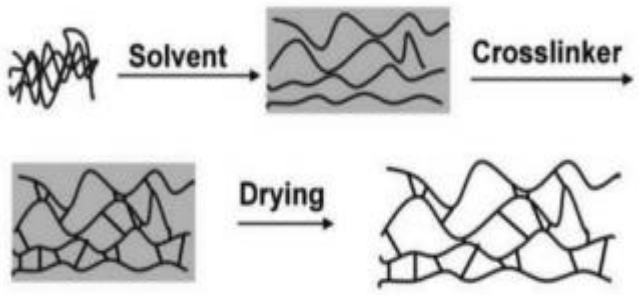

Figure 2.17: Representation of hypercrosslinked polystyrene network [52].

Poly (divylbenzene co vinylbenzyl chloride) has been one of the well-known processes in hyper-crosslinked polymer synthesis. The high surface area and high efficiency it provides is possible by giving the internal electrophile of the -CH_2Cl substituent and causing the formation of crosslinking. The reaction representation of VBC PolyHIPE to hypercrosslinked PolyHIPE is shown in Figure 2.18 below.

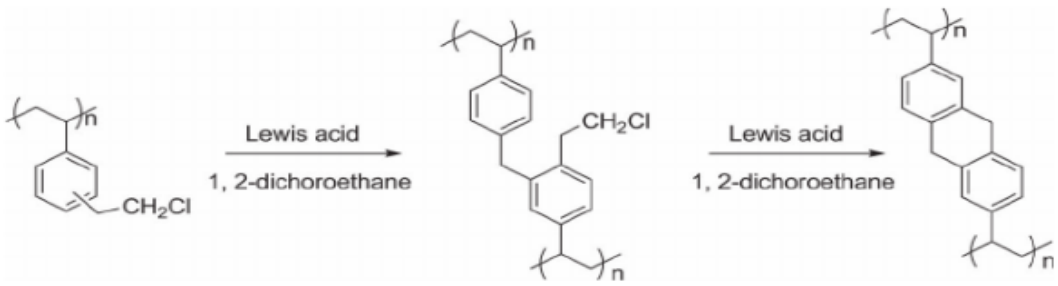

Figure 2. 18: A hypercrosslinked polymer prepared from gel poly(divinylbenzene-co-vinylbenzyl chloride) [53].

In the study of Ahn et al., The surface areas of hyper-crosslinked poly (divinylbenzene co vinylbenzyl chloride) resin were measured by BET with the effect of different parameters. In this study where three different Lewis acids ($FeCl_3$, $AlCl_3$, $SnCl_4$) were tested, the best was found to be $FeCl_3$. At the same time, different proportions of monomer were added and its surface area effect was investigated. Hypercrosslinked polymers synthesized by using 2 mol% DVB-VBC monomers, formed dense crosslinking and dense porosity in 15 minutes, and the surface area (with BET) was found to be approximately 1200 m^2g^{-1}. The maximum value was reached at the end of 18 hours with 2000 m^2g^{-1}. In this study, the surface areas were measured between 300-2000 m^2g^{-1}. [54]

PolyHipes have approximately 20 m^2 / g surface area. This is an indication that it does not have a very high surface area. Factors such as the addition of porogenic solvent, addition of crosslinking agents have been used to increase the surface area. With these factors, the surface area has been increased up to 700 m^2 / g. [55]

2.6.2 Solvent effect

As mentioned before, a thermodynamically good solvent is chosen and the polymer is mixed in the solvent. With this mixing, the polymer chain is expected to swell. The polymer chains are locked by cross-linking, so that the structure does not deteriorate with the removal of the solvent. Here, the solvent plays an important role in the swelling of the polymer. Many studies have been done for the selection of suitable solvent.

Sherrington tried different solvents such as chlorobenzene, hexane, dichloroethane (DCE), dichloroethane / hexane. (It was worked with 80% VBC, 20% DVB.) With the experiments, it was found that the best solvent was dichloroethane. The surface area of the hypercrosslinked polymer made with DCE blown polymer measured ~ 1200 m2 / g, while this area was measured at 600 m^2 / g with hexane and chlorobenzene. Although hexane and dichlorobenzene are relatively poor solvents for polystyrene, the surface area was measured at 600 m2 / g. [56]

2.7 Characterization of Porous Polymers

It is extremely important to characterize porous materials after synthesis. Although the characterization of porous structures has been researched from past to present, there are studies on this subject. Characterization has also become important for the determination of the additives of substances such as clay and nanoparticles added to porous materials. In 1922, Paneth's radioactive monitoring and dye studies were followed by Brunauer and Emmett's physisorption (gas adsorption) studies between 1935-1937. With the publication of the multimolecular theory of adsorption by Brunauer, Emmett and Teller (BET) in 1938, this theory assumed a universal role in determining the surface area. Afterwards, with the ongoing studies, it became possible to use many methods for the characterization of these porous substances. These methods are briefly described below [57].

2.7.1 Brunauer–emmett–teller (BET) Method

The Brunauer-Emmett-Teller (BET) method is used to measure the surface area of porous materials. With this technique, the surface area is determined by measuring the amount of physically adsorbed gas in general terms. A gas (usually nitrogen gas) is adsorbed onto the surface of porous materials. Since nitrogen is below the critical temperature at boiling point, they tend towards the surface of the material. Since the size of the gas molecules is known, the amount of gas adsorbed determines the total surface area [58,59]. Figure 2.19a shows the BET mechanism, while Figure 2.19b shows the BET device.

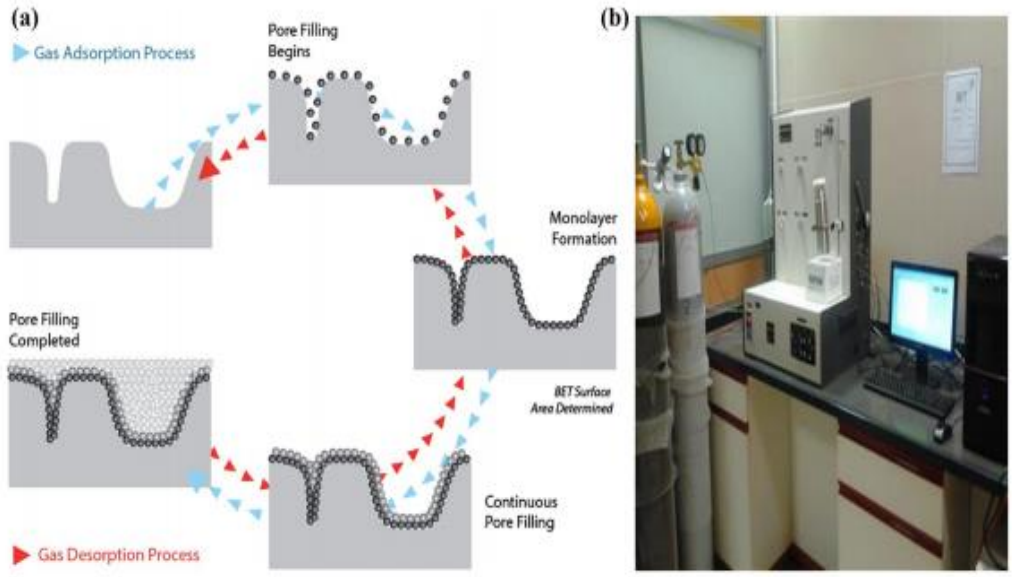

Figure 2.19: a) Adsorption and desorption mechanism of BET b) BET instrument [60].

Even the smallest operation changes the surface area of the material. Processes such as grinding into smaller pieces, dissolving, increasing the pores increase the surface area.

Basically, BET is gas adsorption of porous polymer or solid. This adsorption takes place by Van der Waals forces. Adsorption; divided into physical and chemical. While physical adsorption is by Van der Waals forces, chemical adsorption is caused by the chemical reaction between the material and the gas (adsorbate). This theory, which assumes that gas molecules form a monolayer adsorption, is linked to the Langmuir theory. Gas molecules held on the surface of the material are adsorbed to the surface due to Van der Waals forces and form a single gas layer. Thus, it is possible to measure the surface area in m^2 / g [58].

2.7.2 X-ray photoelectron spectroscopy (XPS)

Another method used to analyze porous materials is X-ray photoelectron spectroscopy (XPS). XPS is also known as electron spectroscopy for chemical analysis(ESCA). The mechanical strength and surface properties of the material affect its usage areas. The point where these materials come into contact with the atmosphere is their outer surface. The physical and chemical changes that occur affect the entire material. Surface analyzes are needed to understand the surface chemistry of the material. XPS is a method used to examine these changes that occur on the surfaces of materials. It was first developed in Switzerland in 1940-1950 by Kai Siegbahn and his coworkers. The operating principle of the XPS device in its most general form is given in Figure 2.20.

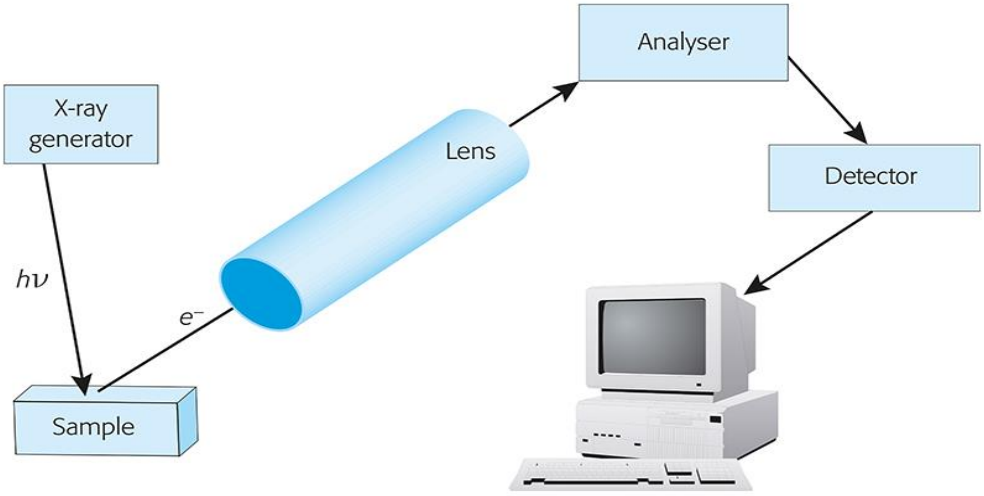

Figure 2. 20: Basic diagram of XPS spectroscopy [61].

By emitting photoelectrons, the device excites electrons in the energy level in the inner shell of atoms as a result of photoelectricity. X-rays hit the surface of the sample. The number of electrons ejected from the material and the kinetic energy of the surface are determined by these beams sent in XPS, which is based on the photoelectric principle. Knowing the kinetic energies of the electrons allows the binding energies to be found. Thus, it is possible to have information about the atoms on the surface, the properties and structure of the atom. [62]

Low energy and high energy resolution XPS gives various information about the elements. While qualitative and quantitative information is provided for elements with low energy resolution, information about the bond structure and chemical structure of elements with high energy resolution is provided. At the same time, it is possible to understand whether the reaction has taken place with high resolution XPS by tracking atoms. [63,64]

2.7.3 Scanning electron microscopy(SEM)

Hugo Stintzing is known as the scientist who patented the scanning electron microscope. However, the first study on this subject was done by M. von Ardenne as scanning transmission electron microscope (STEM). In the following years, studies that will contribute to the scanning electron microscope have been increased. Studies with electron sample interactions led to the development of this device. Scanning electron microscopy, which enables the imaging of surfaces, is used for characterization in many different areas. [65]

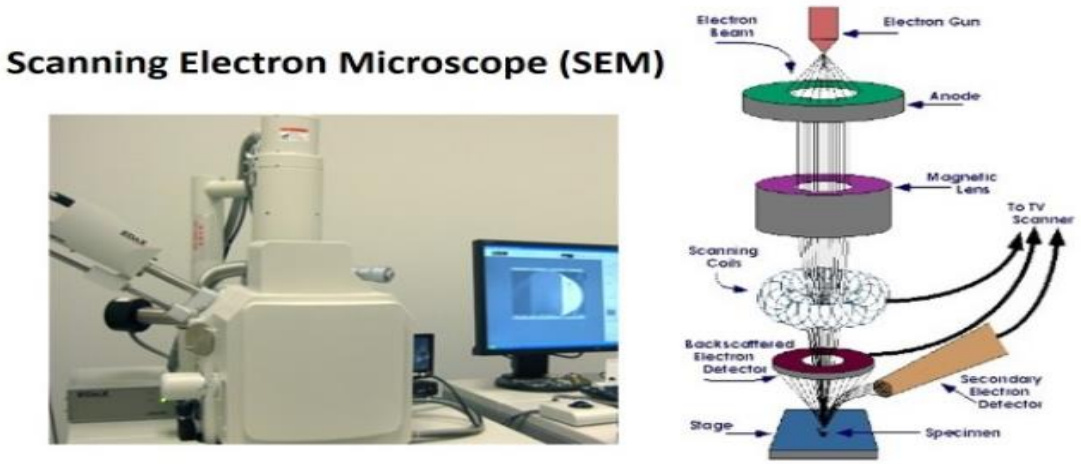

Figure 2.21: Electron beam interaction of SEM [66].

SEM device image and working mechanism are given in Figure 2.21. The sample must undergo preparatory procedures before measuring with SEM. The preparation step is necessary for them to react when electrons are sent to the sample. No preparatory step is necessary for substances that conduct electricity. Conductivity is achieved after the sample is coated with a surface -usually gold- that will scatter electrons. The gold plating process is usually done with argon gas. However, it is possible to take images without coating process in new SEM devices. This allows many samples to be imaged.

The electron beam sent from the SEM to the sample creates an electric field, causing the electrons to be detached from the atom. The resulting signals are measured by detectors. By sending a high-energy electron beam to the sample, secondary electrons, backscattered electrons, and X-ray signals are produced. SEM images at different magnifications are given in figure 2.22 below.

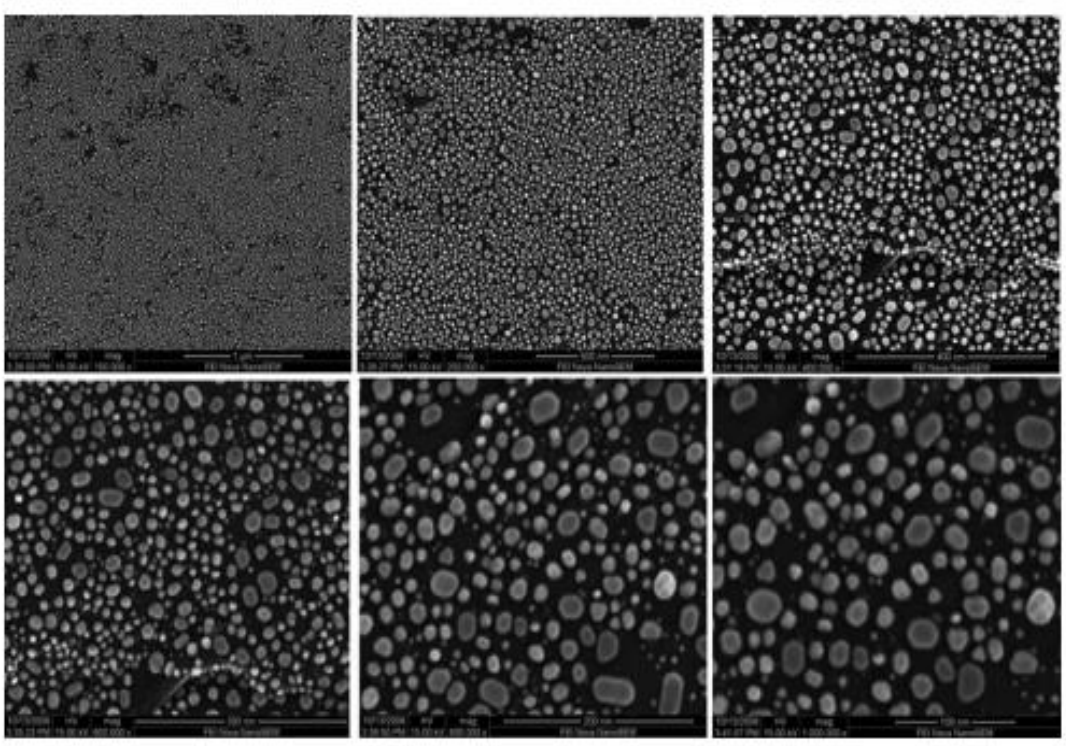

Figure 2.22: Illustration of SEM low to very high magnifications (100,000x to 1,000,000x) of secondary electron [67].

2.7.4 Uv-vis spectroscopy

The UV device, consisting of a monochromator, light source, UV tub, detector and recorder, is used for the analysis of inorganic and organic substances. It is a

quantitative analysis method that can determine functional groups. This spectroscopy operates in the UV visible region (390-780 nm) wavelength. UV-visible spectroscopy is based on the absorption of light (Figure 2.23.). The image of the UV device is given in Figure 2.24.

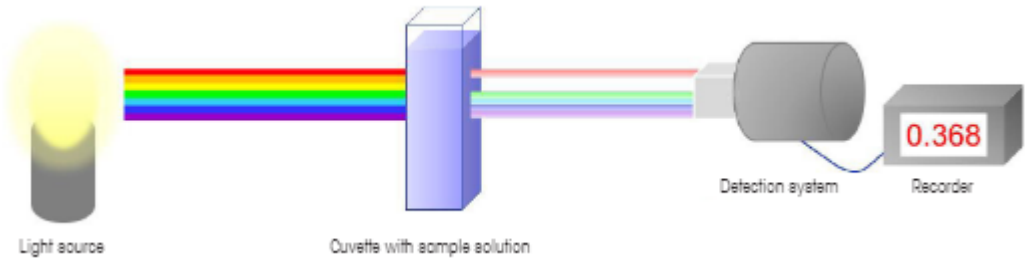

Figure 2.23: Measurement principle of UV [68].

Figure 2. 24: UV spectroscopy [69].

It is first placed in an blank cuvette to measure the intensity of the incident light. This is necessary for measuring the sample. Water or alcohol solvent is placed in the cuvette and exposed to a beam of light. Some of these rays, which are sent at different wavelengths, are absorbed by the solvent. These absorbed beams are determined with the help of a detector. After emptying, the sample is put into the cuvette in liquid form. One of the two cuvettes is left empty and the other as a sample.

The sample placed in the UV cuvette is placed in the chamber of the device. The transmitted beam of light is passed through this sample. The emitted light intensity

decreases as the sample absorbs the light. The intensity and wavelength of light absorbed by each substance is different. The amount of light absorbed by the sample is found by measuring in terms of absorbance [68].

2.7.5 Fourier-transform infrared(FT-IR) spectroscopy

Infrared (IR) spectroscopy is a method used in the analysis of organic and inorganic substances. FT-IR spectroscopy provides the determination of functional groups in the structure of solid or liquid samples, the number of bonds in the structure of the sample, its condition, and the determination of aromatic or aliphatic groups. [70]

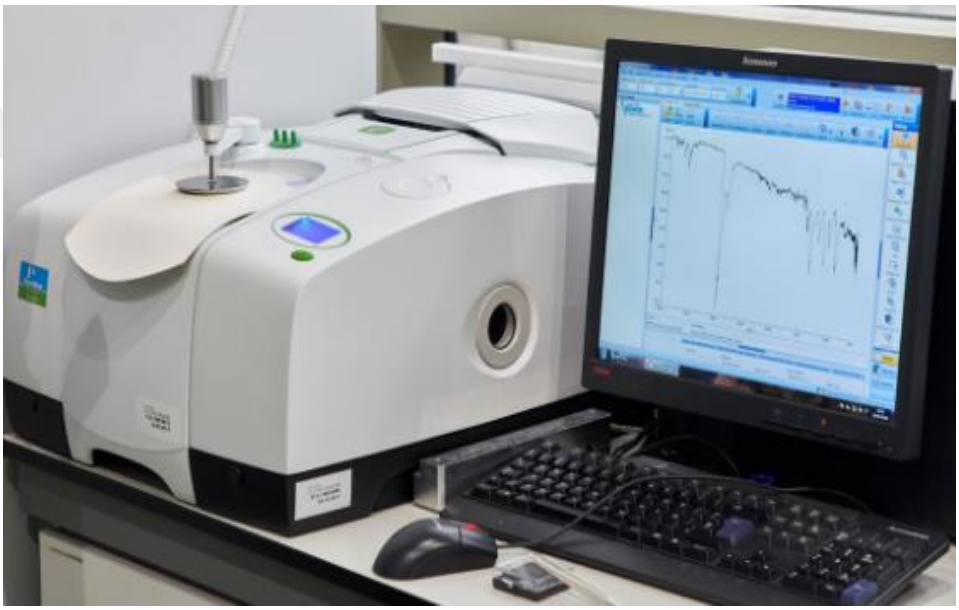

Figure 2. 25: FT-IR spectroscopy [71].

The FT-IR spectrometer (Figure 2.25) measures the infrared intensity of the light versus the wave number. In this method, which is based on the vibration of molecular bonds, the results are found by the Fourier mathematical transform method. Solid, liquid, fiber, polymer etc. is measured by FT-IR spectrometer.The working principle of the FT-IR device is based on the principle of measuring the rotational and vibrational energies formed in the molecules by sending the infrared light to the material and absorbing it by the material. By interpreting the spectra (peaks) obtained, the unknown substance is determined from the bond structure. Here, the so-called fingerprint region (in the range of 1200 cm^{-1}-700 cm^{-1} wave number) is used(Figure 2.26). The infrared region is divided into three as near, mid and far. The mid-infrared region is generally preferred for measurements. Basically, two types of vibrations are

observed in the mid-infrared region; bending and stretching. Stretching vibrations are vibrations that occur along the chemical bond, while bending vibrations result from the change between bond angles. [72]

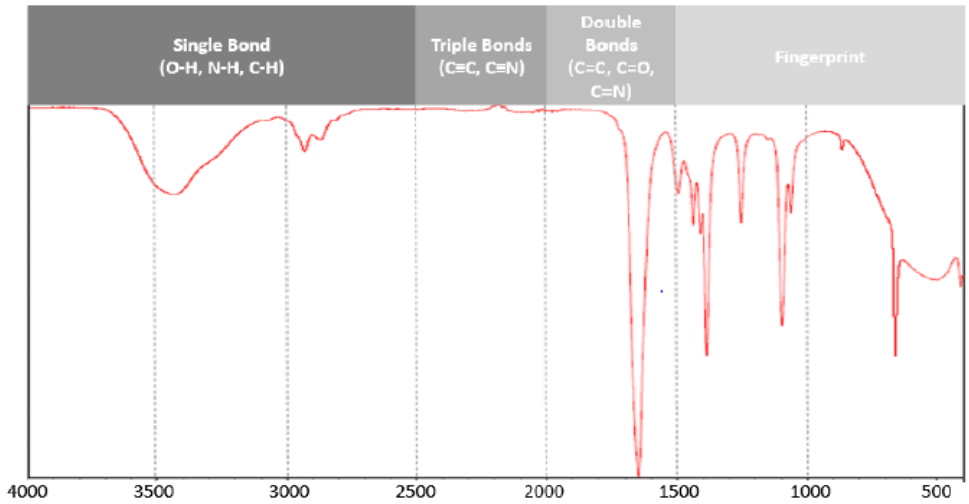

Figure 2.26: Illustration of Mid Infrared Regions [73].

2.8 Adsorption

The bonding of a substance to a solid surface by physical or chemical interactions is called adsorption. Adsorption is based on mass transfer. The solid is called adsorbent, the substance attached to the solid surface is called adsorbate, the separation of these substances attached to the solid surface is called desorption [74].

Adsorption is divided into physical and chemical adsorption. In physical adsorption, adsorbate are held on the surface of the adsorbent by physical forces such as Van der Waals forces, hydrogen bonds, and dipole-dipole interactions. The strong binding of the adsorbate to the adsorbent surface due to electron exchange is called chemical adsorption. Chemical adsorption is also known as chemisorption.

Adsorption is widely used to remove heavy metals and dyes from water. The adsorption process has become the choice of these areas due to the reasons such as low cost and high efficiency. It is preferred that the adsorbents to be used are not expensive and do not require pre-treatment [75].

Adsorption has proven to be the most energy efficient and efficient at low concentration of mercury ions compared to other methods. Polymeric materials have proven to be successful in removing mercury. These polymers (polyvinyl alcohol,

polyaniline, polypyrrole, polyacrylonitrile etc.) are repeatedly used to remove mercury in second, third or even multiple cycles [76].

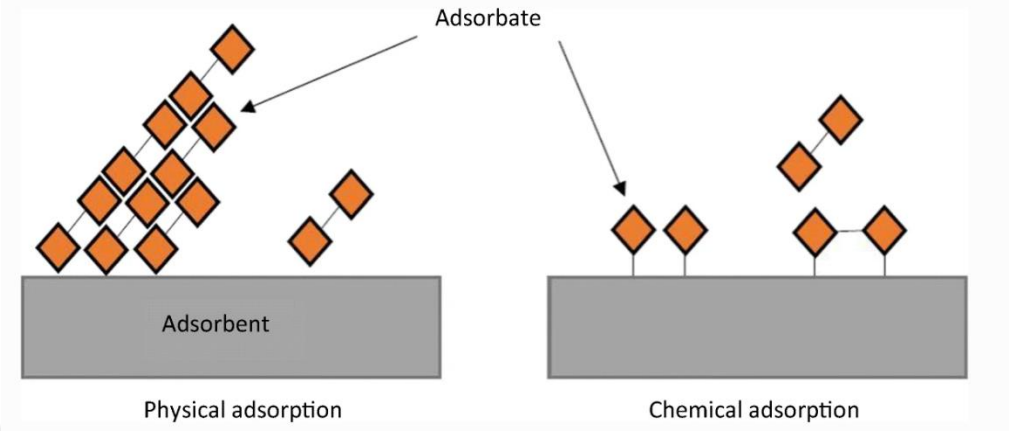

Figure 2.27: Physical and chemical adsorption [77].

Since physical adsorption is caused by weak attraction such as Van der Waals, the adsorption energy does not exceed 80 kJ/mol. In this type of adsorption, the adsorbate and adsorbent are easily reversible because they are weakly bonded. In chemical adsorption, the bond between the adsorbent and the adsorbate is strong because it results from electron exchange, so it is difficult to reverse. While chemical adsorption is highly selective, physical adsorption takes place on the entire surface at appropriate temperature and pressure parameters. In physical adsorption, it is possible for adsorbents to form multiple layers, while chemical adsorption is single-layered (Figure 2.27) [78].

2.8.1 Factors affecting adsorption

Many factors such as the chemical structure of the adsorbent and the adsorbate, temperature, surface acidity affect the adsorption. These factors will be discussed one by one below.

2.8.1.1 Chemical structure of absorbent

Since adsorption is an event occurring on the surface, the surface area of the adsorbent directly affects the adsorption mechanism. The surface area of the adsorbent, the electric field on the surface, the size of this area and its density are among the factors affecting the adsorption.

2.8.1.2 Absorbant properties

There are four important factors that determine the chemical character of the adsorbate. (i) the structure of the functional group or groups (ii) the substituent group structure (iii) the location of the substituent group (according to the functional group) (iv) the presence and amount of unsaturated structures in the molecule. At the same time, the hydrophilicity and concentration of the adsorbate directly affect the adsorption mechanism.

2.8.1.3 Surface acidity

Surface acidity refers to the acidity at the colloidal surface and refers to the action of the process as both Lewis acid and Bronsted acid. Surface acidity is one of the important features of soil and colloidal system in determining the mechanism of adsorption of basic organic substances. This concept is very important for metal adsorption. Groups such as phenol groups and carboxyl groups are effective in increasing the total surface acidity.

2.8.1.4 Temperature

Adsorption is an exothermic mechanism while desorption is an endothermic process. Therefore, increasing the temperature of the system is expected to increase desorption while decreasing adsorption. With increasing temperature, the amount of solute in the solvent increases, but the attraction force between the solute and the solid decreases [79].

2.8.2 Adsorption kinetics model

2.8.2.1 Pseudo – first-order (PFO) model

The pseudo-first order equation, introduced by Lagergren in 1898, is proportional to the rate of adsorption by the number of accessible regions on the adsorbent. İntegrated form of this equality as Equation 2.1 below;

$$q_t = q_e\left[1 - \exp\left(-k_f t\right)\right] \tag{2.1}$$

Where q_e(mg/g) is the amount of substance adsorbed by the adsorbent at equilibrium, q_t (mg/g) is the amount of substance adsorbed by the adsorbent at any time. K_f is the rate constant for Pseudo-first order model, t is time [80].

The differential form of this equation is as Equation 2.2 follows;

$$\frac{dq_t}{dt} = k_1(q_e - q_t) \tag{2.2}$$

k_1 = constant of pseudo-first-order

The linearized form of the pseudo-first-order model as Equation 2.3 follows;

$$\ln(q_e - q_t) = \ln q_e - k_1 t \tag{2.3}$$

In equation 2.3, $\ln(q_e-q_t)$ is plotted against t and the pseudo first order constant k_1 is found.

PFO rate is calculated as Equation 2.4 follows;

$$\text{PFO rate} = k_1(q_e - q_t) \tag{2.4}$$ [81]

2.8.2.2 Pseudo-second-order (PSO) model

The pseudo-second-order model was used for the first time for lead adsorption on peat. In the following periods, the equation was applied to adsorption studies in general. The equations used to have information about the experimental data and to calculate the adsorption rate constants are given Equation 2.5 belows.

$$\frac{dq_t}{dt} = k_2(q_e - q_t)^2 \tag{2.5}$$

The integrated form of this equation is as Equation 2.6 follows;

$$q_t = \frac{q_e^2 k_2 t}{1 + q_e k^2 t} \tag{2.6}$$

Conversion of nonlinear pseudo-second-order model to linear form of this equation is as Equation 2.7 and Equation 2.8 follows ;

$$\frac{t}{q_t} = \frac{1}{k_2 q_e^2} + \frac{t}{q_e} \tag{2.7}$$

$$\text{PSO rate} = k_2(q_e - q_t)^2 \tag{2.8}$$

Where q_e(mg/g) is the amount of substance adsorbed by the adsorbent at equilibrium, q_t (mg/g) is the amount of substance adsorbed by the adsorbent at any time. K_2 is the rate constant for Pseudo-second-order model, t is time.

The equilibrium capacity q_e and the rate constant k_2 can be found by plotting the graph of t/qt versus t and taking the slope and intersection. Summary information of pseudo first order and pseudo second order models are given in Figure 2.28.

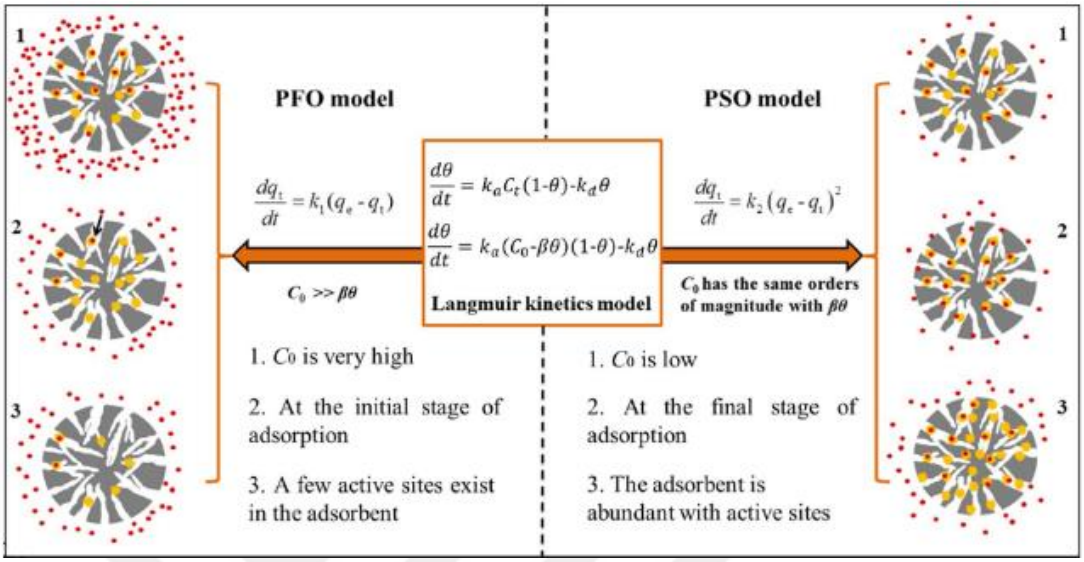

Figure 2.28: Pseudo First Order and Pseudo Second Order model and their physical meanings [81].

2.8.2.3 Intra-particle diffusion(IPD) rate model

The intraparticle diffusion model was first introduced by Weber and Morris in 1962. Equality is expressed as Equation 2.9 follows;

$$q_t = k_p t^{1/2} + C \tag{2.9}$$

q_t (mg/g) = adsorption capacity at any time

kp (mg/(g $min^{1/2}$)) = Intraparticle diffusion rate constant

t (min) = adsorption time

C (mg/g) = constant for any experiment [82]

If the mechanism obeys intraparticle diffusion, an solute sorbed graph plotted against the square root of the contact time should be a linear curve through the origin. Biosorption systems are systems that comply with the intraparticle diffusion mechanism [83].

2.8.3 Adsorption isotherm

Appropriate correlation must be found in order to construct equilibrium curves under optimal conditions of the adsorption mechanism. The isotherms show the interaction of adsorbates with adsorbents. The x-axis of the drawn graph is Ce(mg/l), and the y-axis is qe(mg/g). Qe is the amount of adsorption at equilibrium, while Ce is the equilibrium concentration of adsorbate in solution. Various isotherms have been proposed for optimal conditions; There are many isotherms such as Freundlich, Sips, Redlich-Peterson, BET, Sigmoid [84,85].

2.8.3.1 Langmuir isotherm

The Langmuir isotherm(1918) is one of the simplest and most widely used isotherms. Langmuir isotherm is derived due to equalization of adsorption and desorption rates on a flat surface. The assumptions on which the Langmuir equation is based are summarized in Equation 2.10 belows;

(i) Adsorption is held in a single layer on the adsorbent.

(ii) The adsorption energy is equal in all adsorption sites, these indicates the homogeneity of the surface.

(iii) The adsorbent surface is exactly the same [86].

$$\frac{1}{q_e} = \frac{1}{q_m K_L C_e} + \frac{1}{q_m} \tag{2.10}$$

q_e (mg/g) : The amount of adsorbed adsorbate per unit weight of adsorbent at equilibrium

C_e (mg/L) : Concentration of unadsorbed adsorbate in the solvent at equilibrium

K_L (L/g) : Langmuir equilibrium constant

q_m (mg/g) : Monolayer saturation capacity (theoretical)

Expression of the Langmuir isotherm can also be as seen below. These formula is expressed by R_L (Equation 2.11) , which is called the separation factor or equilibrium parameter.

$$R_L = \frac{1}{1+K_L C_0} \tag{2.11}$$

C_0 (mg/l)= Concentration of initial adsorbate

The R_L value represents the shape of the isotherm. The values and definitions of the R_L factor are given below.

$R_L > 1$ → unfavorable

$R_L = 1$ → linear

$0 < R_L < 1$ → favorable

$R_L = 0$ → irreversible [87]

2.8.3.2 Freudlich isotherm

The Freundlich isotherm(1906) is a mathematical expression that expresses the equilibrium adsorption between solid and liquid (or gas). The Freundlich isotherm can be expressed as Equation 2.12 belows;

$$q_e = K_f C_e^{1/n} \tag{2.12}$$

q_e (mg/g)= Amount of adsorbate adsorbed per unit mass (solid mass)

C_e (mg/L)= Unadsorbed adsorbate concentration at equilibrium

K_f (L/g) = Costant of Freudlich adsorption

n = Empirical constant [88]

Freundlich isotherm is an important isotherm used for heterogeneous surfaces and multisite adsorption isotherm. Its linear form can be expressed as follows(Equation 2.12).

$$\log q_e = \log K_F + \frac{1}{n} \log C_e \tag{2.13}$$

Kf (L/g) = Costant of Freudlich adsorption

n (g/L) = Freundlich exponent [87].

2.8.3.3 Dubinin–radushkevich (D–R) isotherm

The D-R isotherm model is used to express adsorbents with porous structure. Here, the adsorption mechanism was thought to be related to the filling of the micropore volume. This formula is expressed as:

$q_e = q_{max} \exp(-\beta \varepsilon^2)$

q_e (mg/g) = The amount of adsorbate adsorbed by the adsorbent per unit mass (at equilibrium)

q_{max} = Maximum capacity of adsorption

β (mol^2/kj^2) = Constant (connected with adsorption energy)

ε (kj/mol) = Potential of adsorption

The adsorption potential is calculated as follows(Equation 2.14);

$$\varepsilon = RT \ln \left(\frac{C_s}{C_e}\right) \tag{2.14}$$

Where C_s is the solubility concentration of adsorbate, C_e equilibrium concentration of adsorbate. R is universal gas constant and its unit 8.314 $J.mol^{-1}.K^{-1}$, T(K) is absolute temperature [89].

2.9 Heavy Metals

Heavy metals, consisting of elements with high relative density, adversely affect human health. Heavy metals such as mercury, lead, cadmium, arsenic and zinc cause acute or chronic poisoning. These metals, which can enter the human body through the skin, mucous membrane, by ingestion or inhalation, can be stored in the soft tissues of the body. These metals entering the body bind to proteins and impair enzymatic activity (Figure 2.29) [90].

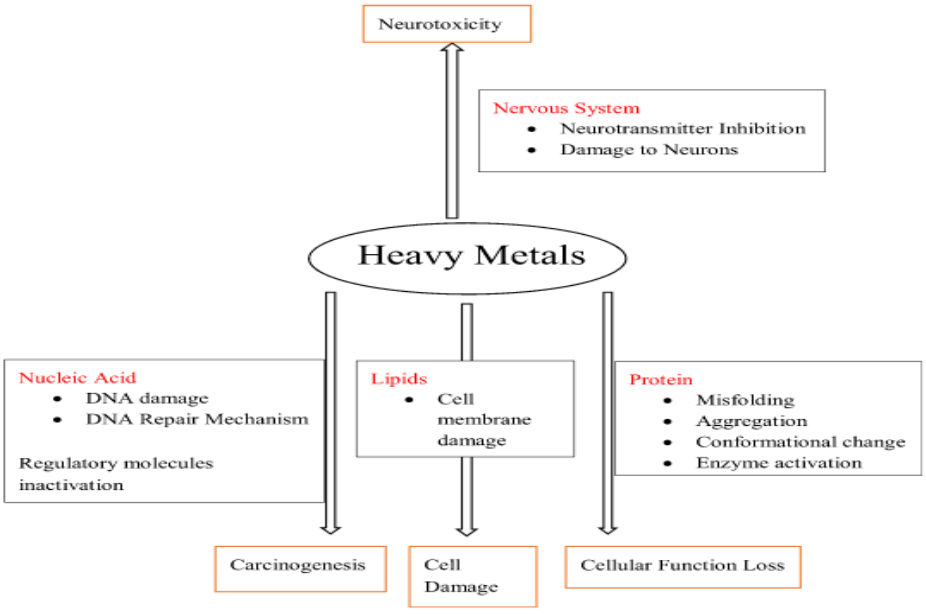

Figure 2.29: Sources of heavy metals and their harm to the human body [91].

Heavy metals, which are found in nature as reserves, can be mixed with the environment through human activities. It can come into contact with the environment and people in ways such as the extraction of reserves, metal smelting, fuel burning. China is an important country where there are reserves of heavy metals such as mercury, nickel, lead, and zinc, especially coal, and where these metals are processed. Problems such as heavy metals, soil erosion, and metal emissions have been encountered with the processing of the reserves. It also negatively affects the health of people living in nearby residential areas with metal emissions.

According to the list published by the Agency for Toxic Substances and Diseases Registry (ATSDR), "The World's 20 Most Dangerous Substances" has been determined. According to this list, Arsenic (As) is in the first place, Lead (Pb) is in the second place, and Mercury (Hg) is in the third place. While some heavy metals (such as Cu, Ni) should be present in trace amounts of biota, increasing the dose brings about a toxic effect [92].

2.9.1 Mercury effect for human and environment

Mercury, which is in the heavy metal class, has very serious effects on human health and the environment. Mercury can be released into the environment in many ways and cause adverse effects on human health. In terms of human health, factors such as the duration of exposure to mercury, the type of mercury, the age and general health of the exposed person, and the mercury dose exposed cause different reactions in the body.

According to the World Health Organization, mercury, which is one of the ten most dangerous substances that can cause negative results in terms of public health, is the third most toxic element for humans.

Mercury, which is in the form of reserves, can be mixed with nature in different forms due to human influence. Mercury is exposed in the forms of elemental mercury, inorganic mercury, and methyl mercury.

Elemental (metallic) mercury is found in products such as thermometers, barometers, thermostats (usually it can be passed through by workers in factories during production) and can be mixed with the environment as these products deform. Since these pieces of mercury can evaporate very quickly, inhalation of these vapors can cause serious effects on the respiratory and nervous system. At the same time, since it is a strong neurotoxin, it causes speech, hearing and gait disorders.

Inorganic mercury can often be exposed through manufactured products such as latex paint. However, exposure is limited due to legal use limitations.

Methyl mercury passes to humans and animals mostly through food. Ingestion of cereals medicated with drugs containing methyl mercury can be exposed to animals by animals, and to humans by ingestion of sea and fishery products (especially fish) [93].

The mercury mixes with the environment in three basic ways. It can be mixed into the air from the soil in ways such as forest side, volcanoes, erosion of rocks. Secondly, they can be released into the environment by burning fossil fuels and wastes. Finally, they can easily spread to the environment by natural means, such as the evaporation of ocean waters. According to the National Emissions Inventory report published by the USA in 2014, mercury emissions occur mostly with power plants that burn coal to produce electricity. This situation constitutes 42% of the pollution [94].

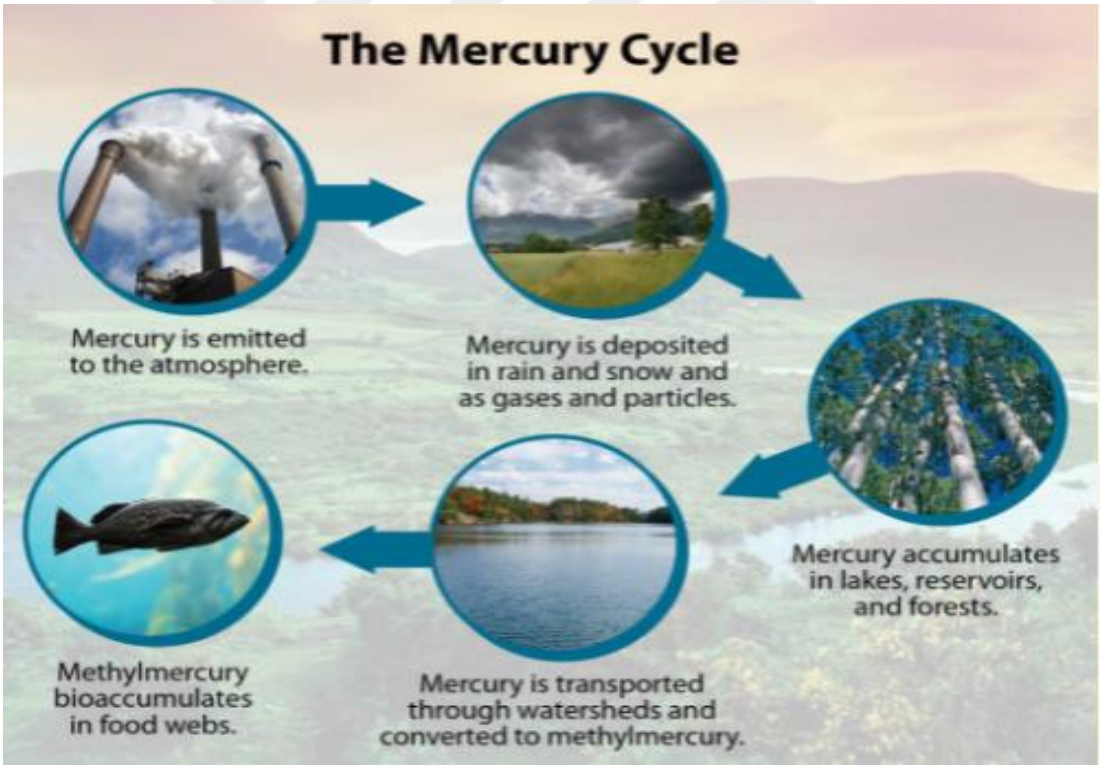

Figure 2.30: Mercury cycle in environment [95].

2.9.2 Mercury removal techniques

The following Table 2.2 describes some mercury removal techniques with their advantages and disadvantages.

Table 2. 2: Mercury removal techniques and their explains [96].

Mercury Removal Techniques	Advantages	Disadvantages
Adsorption	Can be used in a wide pH range The cost is quite low Metal retention rate (capacity) is quite good The process is easy	Waste problem of adsorbent Very low selectivity
Chemical precipitation	The process is quite easy The cost is low	The cost of sludge formed after processing is high
Membrane filtration	High selectivity in adsorption Does not require high pressure and large space	The process is very complex It is quite an expensive method. In this method, the permeability flux is low.
Flotation	Metal selectivity is high Highly concentrated sludge is obtained	Capital, maintenance and operating costs are high
Ion exchange	Kinetics is pretty fast High capacity and high removal efficiency	Selectivity is low Secondary waste may occur Waste is a serious problem in this process Synthetic resins are expensive

Adsorption is a widely used method for the removal of mercury and heavy metals due to its low cost. The cost is directly proportional to the production or purchasing cost of the adsorbent to be used. The selectivity of the adsorbent against mercury, its

environmental friendliness, high capacity and reusability are important in adsorption [97].

2.9.3 Adsorption study for removal mercury

Polymeric materials are highly preferred in the adsorption process, especially in the adsorption of mercury. Xiong et al.(2013) synthesized polyacrylonitrile -2 aminothiazole (PAN-AT) to remove mercury in their study and evaluated its performance. They found the maximum adsorption capacity of mercury to be 454.9 mg/g at 308 K. (According to Langmuir isotherm) For the selectivity test, solutions were prepared from Ni(II), Cu(II), Zn(II), Pb(II) and Hg(II) metal ions, and adsorption tests were carried out at room temperature in the pH range of 2.5-6.5. Except for Hg(II), PAN-AT, the synthesized and functionalized polymer, is quite low capacity in the mentioned pH ranges. The reason for choosing the highest pH range of 6.5 is the degradation of metal ions at high pH's. The highest mercury holding capacity was found to be 6.5 in this study. Different temperature tests were made for this pH and it was found that the best mercury holding capacity was at 308K [98].

In the study of Bozkaya et al., (2012) poly (ethylene terephthalate) briefly PET fibers were grafted with 4-vinyl pyridine monomer. The adsorption of mercury with this obtained polymeric material was investigated. The effects of different parameters such as pH, graft yield, adsorption time and temperature on adsorption were observed. The maximum capacity for mercury adsorption was found to be 137.18 mg/g. In the selectivity test, the grafted fiber was tested in different solvents in which Hg(II)- Ni(II), Hg (II) - Zn(II) and Hg(II)- Ni(II)- Zn(II) solutions and it has proven to be more selective for mercury. The selectivity for mercury in binary and ternary metal mixtures exceeds 94% at pH 3 [99].

In another study(Saad et al., 2013), they tried to develop crosslinked polyethyleneimine with a thiol-based functional group for Hg(II) adsorption. Even in the presence of other metals, a high selectivity of 97% was observed in this synthesized polymer. Tests were made for the reuse of this synthesized polymeric material and the yield was found to be high up to 5 cycles.

This polymeric material showed the highest efficiency for mercury in the selectivity test among the multi-metal mixtures containing Co(II), Cu(II), Pb(II), Zn(II), Ni(II),

Fe(III) and Hg(II). The metal is considered a Lewis acid, while the sulfur on the thiolated polymer acts as a Lewis base. This bonding is explained by Lewis acid-base theory. Soft acids such as Hg(II), Co(II) and Cu(II) tend to bond more with sulfur, a soft base. Thiol has a higher affinity for mercury than Co(II) and Cu(II).Ni(II), Zn(II) and Pb(II) are moderate acids and their adsorption is high because these metals can be bonded with soft and hard acids. Since Fe(II) is a hard acid, it has the lowest removal rate.

In these adsorption studies carried out in different pH experiments, measurement could not be made because most of the metals hydrolyzed and precipitated at pH 8 [100].

In the study of Ma et al., (2009) chitosan functional amino-terminated hyperbranched polyamidoamine polymers (CTS-1.0 , CTS-2.0 , CTS 3.0) were synthesized and the adsorption of mercury was tested. In this study performed at different pH ranges, the mercury adsorption capacity of all three adsorbents was found at pH 5 the best. (pH in the range of 2-6) The capacity was measured for three different adsorbents at different temperatures up to 5-35 ˚C. The capacity increased with increasing temperature and the highest capacity was found to be 397.60 mg/g at 35˚C [101].

3. EXPERIMENTAL

3.1 Materials and Instruments

3.1.1 Materials

4-Vinyl Benzyl Chloride (VBC; 90%, Sigma-Aldrich) was passed through alumina column to remove inhibitors. Divinyl Benzene (55%, Aldrich) was distilled with 5% $NaOH_{(aq)}$ solution. $FeCl_3$ (anhydrous, Sigma-Aldrich), $CaCl_2$ (anhydrous, 97%, Fluka) and $K_2S_2O_8$ (Fluka) were used as received. Nitric acid (65%, Merck), Hydrochloric acid , Isopropyl alcohol (IPA; technical grade), Acetone (technical grade), Ethanol (95 %, Carlo Elba), Dimethyl sulfoxide (DMSO; Merck), Sodium bicarbonate (Merck), Calcium chloride dehydrate (Fluka), nonionic surfactant Span®80 (Aldrich), 1,2-dichloromethane (DCE; Lab-Scan Analytical Sciences), Nitric Acid (65%, Merck), Dichloromethane (DCM; Merck), $KMnO_4$ (Merck), K_2HPO_4 (J.T.Baker), N-Hydroxysuccinimide (NHS; Fluka), N-N'-Diisopropylcarbodiimide (DIC; Sigma-Aldrich), $CaSO_4.2H_2O$ (Merck), KOH (99.99% Sigma-Aldrich), Mercury(II) sulfate (Fluka), Cadmium nitrate (Sigma-Aldrich), Zinc sulfate (Merck), Hexamine (Sigma-Aldrich), Lead(II) Nitrate (Sigma-Aldrich), EDTA (Merck), 2-Thiozoline 2-thiol (Merck), Xylenol orange (Merck), were all used as received without any purification . Ethanolamine (Fluka) and aniline (Merck) were purified by vacuum distillation in calcium sulfate. Propylamine (Fluka) and diethylamine (DEA;Fluka) were purified by distillation with potassium hydroxide.

3.1.2 Instruments

The surface morphologies of all polymers were examined by SEM (FEI-Philips XL30 Environmental Scanning Electron Microscope with Field Emission Gun (Equipped with EDAX-Energy Dispersive X-ray Analysis Unit) operating at 10.0 kV. The samples were prepared by dispersing the powder onto a double-sided adhesive surface. Nitrogen adsorption isotherms were measured at -196°C using a Micromeritics TriStar II 3020 Surface Area and Pore Size Analyser. Prior to measurement, the samples were degassed for 12 h at 100°C. The average pore size was determined using the Barrett−Joyner−Halenda (BJH) method. Functional groups of the polymers were confirmed by Fourier Transform Infrared (FTIR) spectroscopy (Thermo Scientific, Nicolet iS20) in the range between 4000-450 cm^{-1}. Dye concentrations in the

adsorption experiments were determined by a double beam ultraviolet–visible (UV−vis) spectrophotometer (Perkin Elmer, Lambda 25). Thermo Scientific K-Alpha X-ray Photoelectron Spectrometer (XPS) was used to identify the elemental composition of the polymer surfaces operation in the range between 100-4000 eV.

3.2 Preparation of the Amide Functional High-Surface-Area Porous Polymers

In this thesis First, emulsion templated polymers (polyHIPE) were prepared and then through Friedel Craft reaction using $FeCl_3$ as catalyst hypercrosslinked. Through a 3-step-reaction amide functional high-surface-area polymers were prepared, characterized and used for mercury adsorption in aqueous solutions.

3.2.1 Polymerized high internal phase emulsions (PolyHIPE)

First, high internal phase emulsions were prepared. For this purpose 90% pore volume was choosen. The initial emulsion was composed of 10 ml organic or continuous phase and 90ml water or internal phase. A 250 ml round-bottomed flask was charged with vinyl benzyl chloride (8 ml), DVB (2 ml) as crosslinker and surfactant Span 80 (200 mg) with an overhead stirrer fitted with a D-shaped PTFE paddle. And then this mixture was purged with nitrogen gas approximetely for 15 min. The aqueous phase was prepared as follows separately: 0.2 g. potassium persulfate and 1 g. calcium chloride were dissolved in 90 mL de-ionised water and the resulting solution was purged with nitrogen for 15 min. While the organic solution was stirred under nitrogen at 300 rpm the aqueous phase was added for 30 min under constant mechanical stirring in a dropwise manner. Once the addition of the aqueous phase was completed mechanical stirring was continued for 1 h at 300 rpm to produce a homogeneous emulsion and at 50 rpm to remove any entrapped air bubbles. At the end of the process very viscous emulsion (HIPE) was obtained and it was then transferred to the mold (PET container) and cured at 60^{o}C for 48 h. To remove surfactant and polymerization impruties polyHIPE in the shape of monolith was extracted by Soxhlet extraction with distilled water and isopropyl alcohol, both for 24 h, then dried in vacum for 24 h.

3.2.2 Preparation of the hypercrosslinked polyHIPE (HXL-PHP)

PolyHIPE’s with 90% pore volume were were hypercrosslinked to obtain high-surface-area polymers: Initially the monolith polyHIPE’s were powdered using a

mortar and pestle for a uniform reaction mixture. 1 g powdered VBC polyHIPE was placed in a 250 mL 3 necked round bottom flask and 50 mL DCE was added to the flask. One of the necks was fitted with rubber septum and the other two were fitted with glass stopper, and a reflux condenser was attached to one of them. The mixture was degassed through a needle under a stream of nitrogen for 15 min with 300 rpm stirring rate. When then nitrogen flow was removed the flask was left with stirring for a further 45 min to let the polymer swelled. Then the flask was placed in an ice bath and anhydrous 1.09 g $FeCl_3$ was added to the flask through the neck of the flask quickly. The flask was then degassed again for a period of 15 min. Once the nitrogen supply was removed the flask was left stirring for a further 45 min in the ice bath to make sure that a uniform dispersion of $FeCl_3$ was achieved. The sealed flask was allowed to reach a room temperature. Next, the flask was placed in an oil bath at 80°C to start Friedel Crafts reaction which was repeated for the reaction times: 15 min and 60 min. To control the reaction, the excess ethanol was added at the end of the given set time and then filtered under vacuum. The resultant 15min/60min HXLPHPs were washed with ethanol (3x40 mL) and 0.1 M $HNO_{3(aq)}$ (3x40 mL). A further soxhlet extraction in acetone for 10 h (15 cycle) was performed and the HXL-polymers were left in oven for drying at 60°C.

3.2.3 Formylation reaction of VBC polyHIPE (kornblum oxidation)

Benzyl chloride groups were converted to aldehyde function through kornblum oxidaiton in DMSO. 2.8 g. $NaHCO_3$ was dissolved in 50 mL DMSO (partially dissolved) and 2 g. powdered VBC polyHIPE (11 mmol functional group) was added to this 250 mL erlenmeyer flask fitted with reflux condenser. The mixture was heated to 155 °C for 24h under reflux. At the end of the reaction the mixture was filtered under vacuum and washed with DMSO (2x20 mL), hot water (3x30 mL, 60°C), acetone (2x20 mL). A further soxhlet extraction in water for 24 h (15 cycle) was performed to remove remaining $NaHCO_3$ and the polymer were left in a conventional oven for drying at 60°C. The procedure was repeated for the hypercrosslinked polyHIPE prepared by hypercrosslinking reaction for 15 min (HXL-15min-PHP) and 30 min (HXL-15min-PHP).

3.2.4 Preparation of carboxylic acid functional polyHIPE

To obtain carboxylic acid groups on polyHIPE surface 1g. powdered polyHIPE with

aldehyde groups was placed in a 100 mL 1-necked round bottom flask and 24 mL methanol was added. 1.89 g. (12 mmol) $KMnO_4$ and 2.09 g (12 mmol) Na_2HPO_4 were dissolved in distilled water (50 mL) in another flask and this solution was added to the polymer-methanol mixture. The mixture was stirred for 24 hours at room temperature. At the end of the reaction the mixture was filtered and washed with 1 M HCl (3x50 mL), distilled water (3x50 mL) ethanol (2x50 mL) under vacuum and dried for 24 hours at 60^oC in a conventional oven. The procedure was repeated for the aldehyde functional hypercrosslinked polyHIPEs prepared in 3.2.3.

3.2.5 Tailoring polyHIPE surfaces with various amide groups

The polymer surfaces were tailored with amide groups by using various amines through DIC/NHS coupling chemistry. This method involves 2 steps : The first step is to prepare NHS ester on the polymer surface and then in the second step the coupling reaction takes place between the polymer with activated ester and an amine. 0.581 mL Diisopropylcarbodiimide (DIC) (3.75 mmol) and 433 mg (3.75 mmol) N-hydroxy succinimide (NHS) were dissolved in 60 mL dry DCM in a 100 mL round-bottom flask fitted with a rubber septum in an ice-bath. The solution was degassed through a needle under a stream of nitrogen for 15 min. And then, the flask was unsealed to insert 500 mg (around 3 mmol functional group) carboxylic acid functional polyHIPE and quickly sealed again. The flask was then degassed for 15 min. and stirred at room temperature for 48 hours. The polymer with the activated acid group (NHS ester) was then filtered under vacuum and washed with DCM (4x40 mL). In a separate flask 15 mmol freshly distelled amine (and 50 mL dry DCM was mixed and 500 mg activated polymer was added to this flask. The flask was degassed for 15 min. and stirred for 24 hours at room temperature. The resulting polymer was filtered under vacuum and washed with DCM (2x30 mL), ethanol (2x30 mL), water-ethanol (30 mL), 0.1 M HNO_3-ethanol (30 mL), 0.1 M HNO_3 (3x30 mL), water (3x30 mL), ethanol (3x30 mL) and extracted by Soxhlet extraction with distilled water, then dried in for 24 h at 60^oC in a conventional oven. The procedure was repeated for the carboxylic acid functional hypercrosslinked polyHIPEs prepared in 3.2.4.

3.3 Functional Group Content Determination

The carboxylic acid contents of carboxylic acid functional polyHIPEs were

determined by acid-base back titration. For this purpose, 50 mg of the polymer sample was left in contact with 10 mL 0.1 M NaOH(aq) with constant stirring for 24 h at room temperature. After filtration, 1 mL of each filtrate was transferred into 10 mL flask and the carboxylic acid contents of the polymers were determined by titration with 0.01 M HCl solution in the presence of phenolphthalein indicator. Acid to amide conversion was also calculated by acid-base back titration from the unreacted carboxylic acid groups of the amide functional polymers.

3.4 Adsorption Experiments

Adsorption experiments were carried out using acid and amide functional polyHIPEs. We had two main purpose to perform the adsorption experiments: Firstly, the selectivity of polyHIPE's carrying different type of amide groups towards mercury and secondly, the faster reaction kinetics for mercury adsorption. On the basis of these purposes four different type of amide functional polyHIPE with various hypercrosslinking extent were prepared and used in metal ion adsorption experiments.

3.4.1 Adsorption performance of polyHIPE adsorbents in aqueous single metal solution

0.05 M $HgCl_2$, 0.05 M $CdNO_3$, 0.1 M $ZnSO_4$, 0.1 M $MgSO_4$ and 0.0025 M $PbNO_3$ aqueous solutions were prepared. The polymeric adsorbents (25 mg) were placed in a 15 mL conical bottom centrifuge tube with 10 mL aqueous metal ion solutions to find the uptake capacities of the adsorbents. Metal ion solutions were mixed with the polymer samples and stirred at 400 rpm in the centrifuge bottles using magnetic stirring bar for 3 hours and then were centrifuged at 5000 rpm for 5 min. to separate solid and soulution phases. The amount of mercury adsorbed onto polyHIPE adsorbents was found by the absorbance at 542 nm after and before adsorption using UV–vis spectrophotometer using diphenylcarbazide [102]. The pH's of the samples were adjusted to pH=7 because the method is very pH sensitive. The adsorption capacities for the other metal ions were found by EDTA titration.

For Pb : Initial and final (after adsorption) $PbNO_3$ solutions were diluted to $2.5x10^{-3}$ M, pH of the solution was adjusted to 5 by hexamine and titrated with $2.5x10^{-3}$ M EDTA solution in the presence of xylenol orange indicator. The adsorption capacity of the adsorbent was calculated from the difference in concentration before and after

adsorption.

For Zn and Cd: Initial and final (after adsorption) metal solutions were diluted to $2.5x10^{-3}$ M, pH of the solution was adjusted to 9 by NH_3/NH_4Cl and titrated with $2.5x10^{-3}$ M EDTA solution in the presence of eriochrome black T indicator. The adsorption capacity of the adsorbent was calculated from the difference in concentration before and after adsorption.

For Mg*:* Initial and final (after adsorption) $MgSO_4$ solutions were undilute to 0.1 M, pH of the solution was adjusted to 10 by NH_3/NH_4Cl and titrated with 0.1 M EDTA solution in the presence of eriochrome black T indicator. The adsorption capacity of the adsorbent was calculated from the difference in concentration before and after adsorption.

For Hg: Initial and final (after adsorption) $HgCl_2$ solutions were diluted to $2.5x10^{-3}$ M, pH of the solution was adjusted to 6 by hexamine and titrated with $2.5x10^{-3}$ M EDTA solution in the presence of xylenol orange indicator. The adsorption capacity of the adsorbent was calculated from the difference in concentration before and after adsorption.

3.4.2. Adsorption performance of polyHIPE adsorbents in aqueous ternary metal solutions

The selectivity of polyHIPE adsorbents (carboxylic acid and amide functional) towards mercury were tested. For this purpose, an aqueous ternary metal solution composed of 0.02 M $HgCl_2$, $ZnSO_4$ and $CdNO_3$ was prepared. The polymeric adsorbent (25 mg) was placed in a 15 mL conical bottom centrifuge tube with 10 mL ternary metal solution and stirred at 400 rpm using a magnetic stirring bar for 3 hours and then centrifuged at 5000 rpm for 5 min to separate solid and soulution phases. 5 mL of this solution was placed in a flask and 15 mL 0.03 M EDTA solution was added. The amount of EDTA was calculated with respect to 1.5 fold total amount of metals in the solutions. The solution was diluted to 25 mL and pH of the solution was measured to be 2.25. pH of this solution was adjusted to 5.4 by hexamine and the indicator xylenol orange was added. The color of the solution turned to yellow and was titrated with 0.02 M $PbNO_3$ solution resulting red color. And then, 10 mL 2-thiozoline thiol solution (0.2 %, w/v) was added to the solution resulting yellow color

again and waited for 10 minutes for mercury to release. Finally, the solution was titrated with 0.02 M $PbNO_3$ solution.

3.4.3 The Effect of solid/liquid ratio (optimum adsorbent amount) on mercury adsorption

To obtain the optimum amount of adsorbent the effect of solid/liquid ratio on mercury adsorption capacity was studied by varying the amount of PolyHIPE adsorbents from 10 to 100 mg in the adsorption medium (10 mL). The parameters such as pH, stirring speed, mercury concentration (100 ppm), contact time were kept constant during adsorption experiments.

3.4.4 The effect of pH on mercury adsorption

The polymeric adsorbents (25 mg, optimum amount) were placed in a 15 mL conical bottom centrifuge tube with 10 mL aqueous mercury solutions (100 ppm) to find mercury adsorption capacities of the adsorbents. Aqueous $HgCl_2$ solutions with various pH's (4-7) were mixed with the polymer samples and stirred at 400 rpm in the centrifuge bottles using magnetic stirring bar for 3 hours and then were centrifuged at 5000 rpm for 5 min. to separate solid and soulution phases. The amount of mercury adsorbed onto polyHIPE adsorbents was found as explained before.

3.4.5 Determination of the max. adsorption capacity of the adsorbents

To find the max. amount of mercury adsorbed on the polymeric adsorbents the adsorption experiments were carried out with various $HgCl_2$ concentrations from 10 to 300 ppm. Adsorption experiments were performed as explained in 3.4.1 and the results were used to fit four adsorption isotherms namely Langmuir, Freundlich, Dubinin Radushkevich and Tempkin.

3.4.6 Mercury adsorption kinetics of the adsorbents

To investigate the effect of surface area on mercury adsorption on polyHIPE adsorbents, the batch adsorption kinetics expeiments were performed. The adsorption kinetic results of unhypercronslinked amide functional polyHIPE (PHP-$CONR_2$), hypercrosslinked amide polyHIPE prepared by 15 minutes-hypercrosslinking reaction (HXL-15min-PHP-$CONR_2$) and hypercrosslinked amide functional polyHIPE prepared by 30 minutes-hypercrosslinking reaction (HXL-30-min-PHP-$CONR_2$) were

compared. It was obseved that the further hypercrosslinking reaction (60 minutes, 120 minutes and 22h) did not enhance the surface area of the porous polymer so hypercrosslinked polyHIPEs with the higher hypercrosslinking extent were not used for mercury adsorption. The kinetic experiments were also carried out at various solution temperatures to to obtain the thermodynamic functions.

3.4.7 The recyclability of HXL-30min-PHP-CONR$_2$

The desorption capacity and the recyclability of HXL-30-min-PHP-CONR$_2$ was studied by using 100 ppm mercury(II) chloride solution 25 mg of polymeric adsorbent loaded with mercury was placed in a 15 mL conical bottom centrifuge tube. After mixing for 3 hours in a magnetic stirring bar, it was centrifuged at 5000 rpm for 3 min. to separate and solution phases. The adsorbed polymeric adsorbent was washed with distilled water (3x30 mL). Polymeric adsorbent was placed in 10 mL of 0.1M HNO_3(aq) solution. This mixture was stirred at 400 rpm in the centrifuge bottles using magnetic stirring bar for 3 hours and then were centrifuged at 5000 rpm for 5 min. to separate solid and solution phases. The amount of mercury released from the adsorbent surface was found by the absorbance after and before adsorption using UV–vis spectrophotometer. The desorbed polymeric adsorbent was washed with distilled water (3x30 mL) before charging the adsorbent with $HgCl_2$ to remove any non-bonded mercury from the polymer surface.

4. RESULTS AND DISCUSSION

In this thesis porous polymers were prepared on the basis of two main requirments for a adsorption process : Fast kinetics and selectivity. We chose mercury ions to adsorp from aqueous solutions because it is charged from industrial and municipal wastes to water sources and extremly dangerous to humans and environment. For real applications the adsorption process requires fast kinetics, high adsorption capacity and selectivity towards the target adsorbate. Mercury ions are found in waste stream together with other ions resulting a decrease in adsorption capacity if the adsorbent can not show selectivity for the target. Therefore, it is necessary to prepare the adsorbents with high capacity, kinetics performance and selectivity. These requirements led us to the functional porous polymers. Porous polymers are versatile materials which have been widely used as adsorbents. PolyHIPEs are porous polymers having open-porous cellular structure with interconnected pores. They are hierarchically porous with large pores allowing adsorbates to the functional groups located inside the pores by mass transfer rather than diffusion.

4.1 Emulsion Templated High-Surface-Area Amide Functional Porous Polymers

High-surface-area polymeric adsorbents with amide groups were preparared using emulsion templated method. First, a high internal phase emulsion was prepared using vinyl benzyl chloride (VBC), divinyl benzene (DVB) and span80 as organic phase and water including $K_2S_2O_8$ and $CaCl_2.2H_2O$ as water phase. Here, VBC monomer was choosen for two reasons : First, it has an alkyl chloride group which acts as an internal crosslinker in Friedel Crafts reaction to obtain high surface area polymers. Second, through hypercrosslinking reaction which is a controlled reaction, it is possible to remain unreacted alkyl chloride groups which can be converted to amide groups. By this strategy, we could obtain both high surface area and functional porous polymers. Divinylbenzene is a crossinker and it was used as 10% (mol%) of the total monomer phase. It is necessary to use a crosslinker to obtain a polyHIPE scaffold through enhancing the emulsion stability. It is a fact that polyHIPE's possess mainly macro pores (pores larger than 50nm), their surface areas are originally low (6-10 m^2/g) which causes slow adsorption kinetics. To overcome this drawback polyHIPE's were hypercrosslinked through Friedel-Crafts alkylation reaction catalyzed by a lewis acid

$FeCl_3$ and high-surface-area porous polyHIPEs can be prepared.

4.1.1 Preparation of high internal phase emulsion and polyHIPE

To prepare high internal phase emulsion (HIPE), the continuos phase (monomer phase : vinyl benzyl chloride, divinybenzene, and surfactant span 80) and water phase (distilled water, initiator $K_2S_2O_8$ and electrolyte $CaCl_2.2H_2O$) were prepared separately. The water phase was added to the organic phase slowly and by the polymerization of monomer phase a low density, permeable, highly porous material namely polyHIPE was obtained (Figure 4.1). The surfactant span80 stabilizes the emulsion and also it is necassary to obtain an open-porous, interconnected network. During the curing the polymer walls in droplets becomes thinner and eventually pores form between droplets (windows). Therefore it is very crucial to use a proper amount of surfactant to make sure that the resuted polymer has an intrconnected porous structure. After removing the droplet phase by drying, the large pores (voids) and the interconnecting pores (windows) are formed. Porosity is typically 80% and 90% and can be as high as 99%; pore diameter is controlled through variation of HIPE droplet diameter, and the surface can be functionalised chemically either during or postcure.

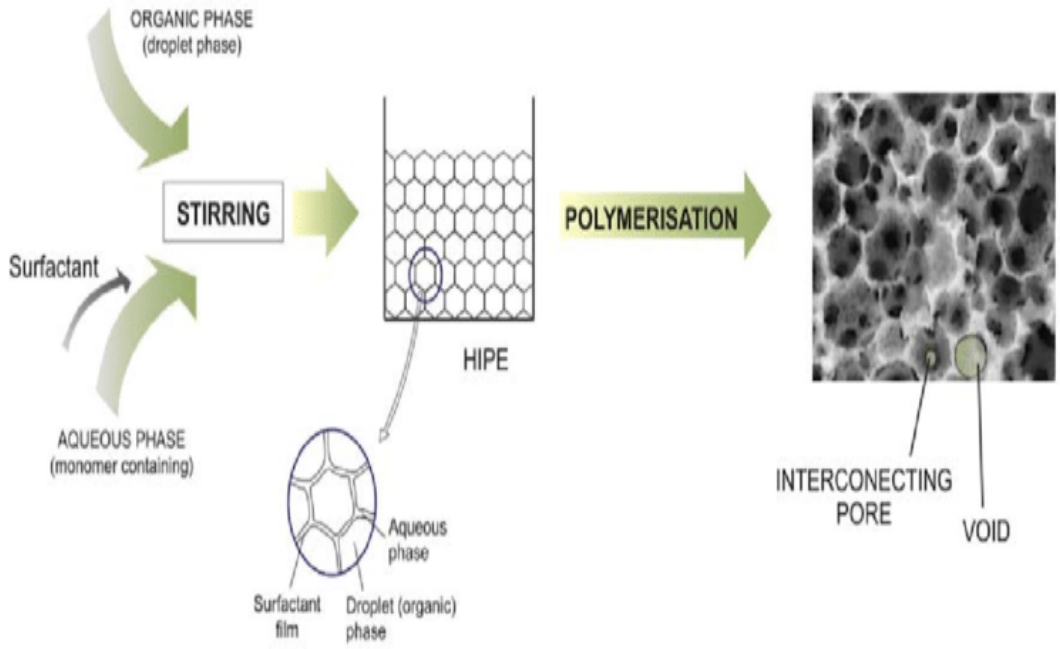

Figure 4. 1: Schematic illustration of a typical polyHIPE preparation. [103]

4.1.2 Synthesis of polymeric adsorbents

A five-step procedure was used to prepare a high-surface-area amide functional

polymeric adsorbent : 1) The preparation of High Internal Phase Emulsion composing VBC and DVB followed by curing the external phase to obtain polyHIPE material as a polymer support. 2) The controlled hypercrosslinking reaction through benzyl chloride groups to increase the surface area of polyHIPE. 3) The creating aldehyde groups on the surface of polyHIPE through the kornblum reaction using the unreacted alkyl chloride groups. 4) The conversion of aldehyde groups to carboyxlic acid groups. 5) The coupling reaction of surface carboxylic acid groups with various amines to create amide groups (Figure 4.2 and 4.3). By this procedure, polyHIPE surface could be tailored with different amide groups covalently bounded to test the effect of amide-side groups on selectivity towards mercury. The amines used in this study were diethylamine, propylamine, aniline and diethanolamine. Therefore, we could be able to test the secondary amide, tertiary amide and side group effect on mercury adsorption.

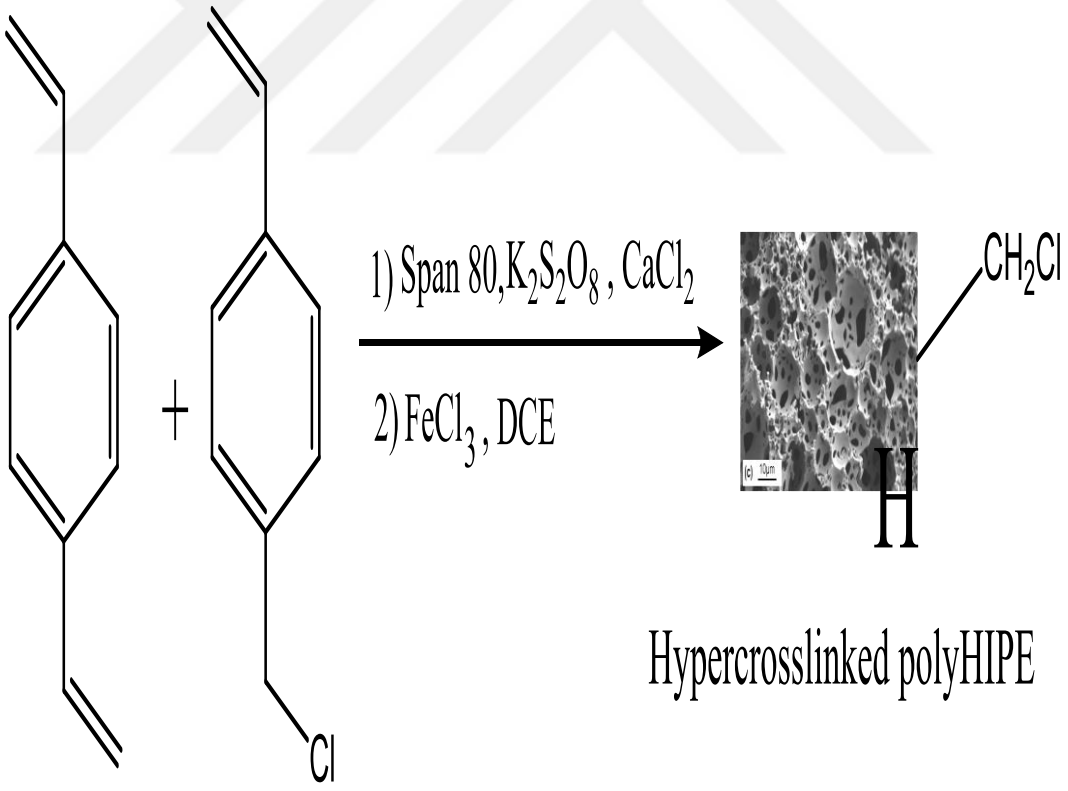

Figure 4. 2: Preparation of hypercrosslinked polyHIPE.

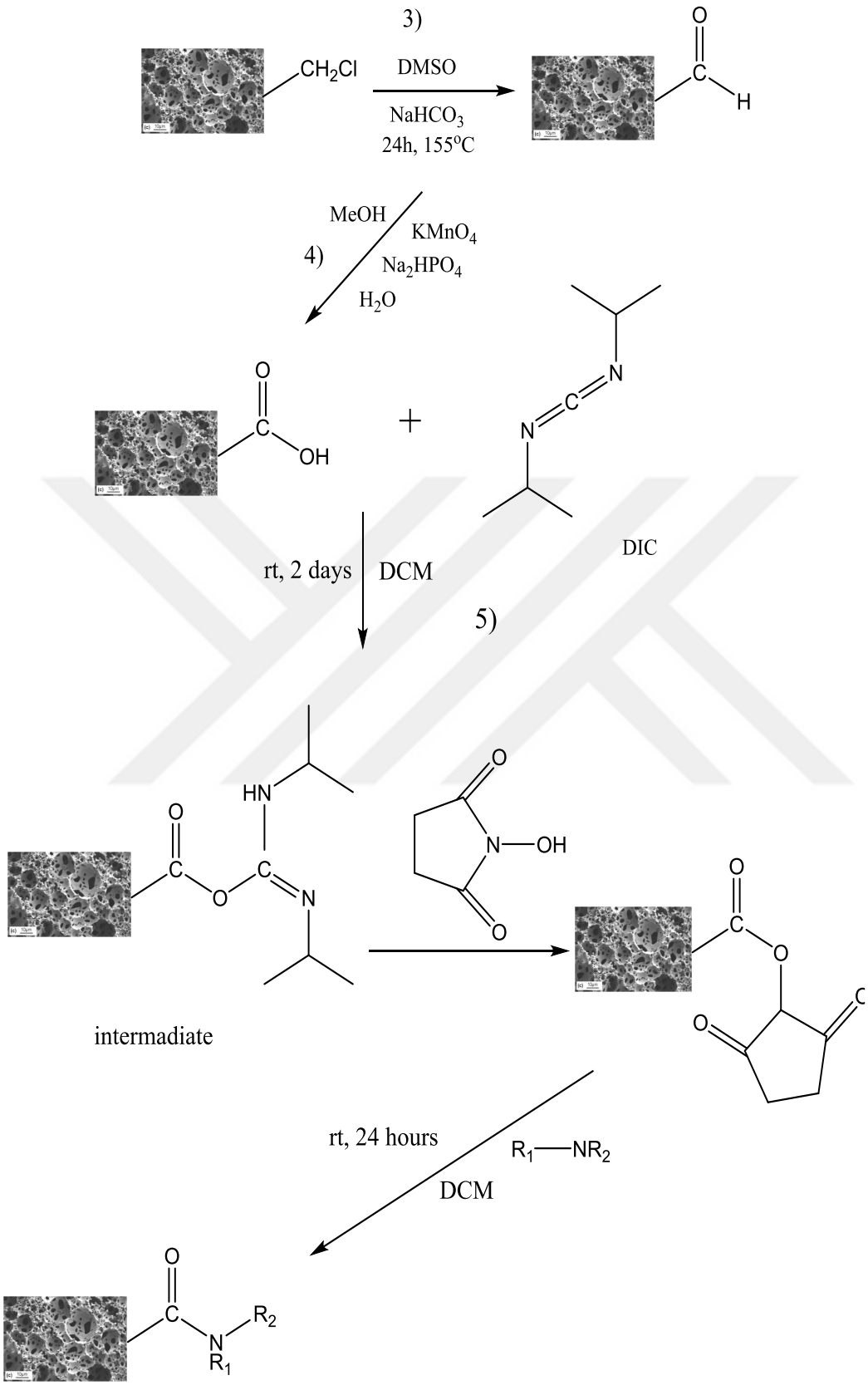

Figure 4. 3: Modification steps of amide functional polyHIPE.

As can be seen in Figure 4.2 and 4.3, VBC as monomer and DVB as crosslinker were used to prepare polyHIPE followed by the hypercrosslinking reaction to prepare high-surface-area polymers. To obtain a high-surface-area polymer, the hypercrosslinking reaction was applied through Friedel-Crafts alkylation reaction catalyzed by a Lewis acid $FeCl_3$ where chloromethyl group acts as an internal electrophile, and dichloroetane (DCE) as solvent and external crosslinker (Figure 4.4). DCE has a boiling point of 80^0C so this solvent both allows the reaction take place at high temperatures and also acts as a external crosslinker for the hypercrosslinking reaction. This reaction produces micro/meso pores and high specific surface area within the framework of polyHIPE precursor. During the reaction, methylene bridges form between the monomer units of VBC-VBC, also DCE as a external crosslinker involves in the bridge forming as well. Furthermore, formation of a six membered ring between two benzyl chloride is seen as a characteristic of the hypercrosslinking of VBC based polymeric precursors (Figure 4.5). The hypercrosslinking reaction is a controlled reaction that allows an increase of the surface area in a controlled way remaining unreacted pendant groups. The unreacted pendant groups allow for further functionalization to create aldehyde, carboxylic acid and finally amide groups with different side groups using various amines.

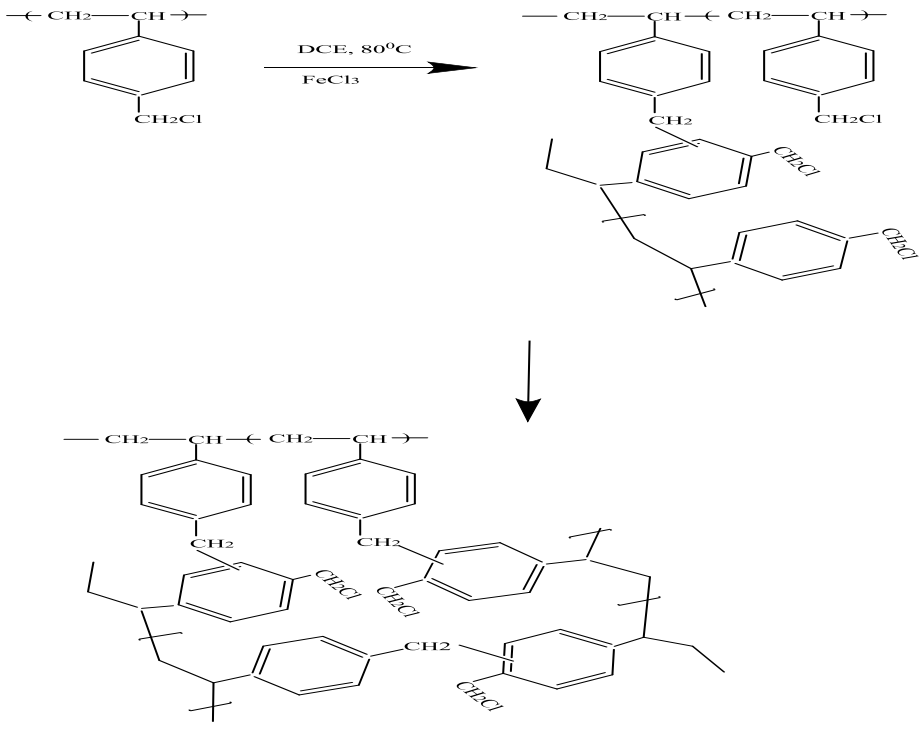

Figure 4. 4: The hypercrosslinking reaction mechanism.

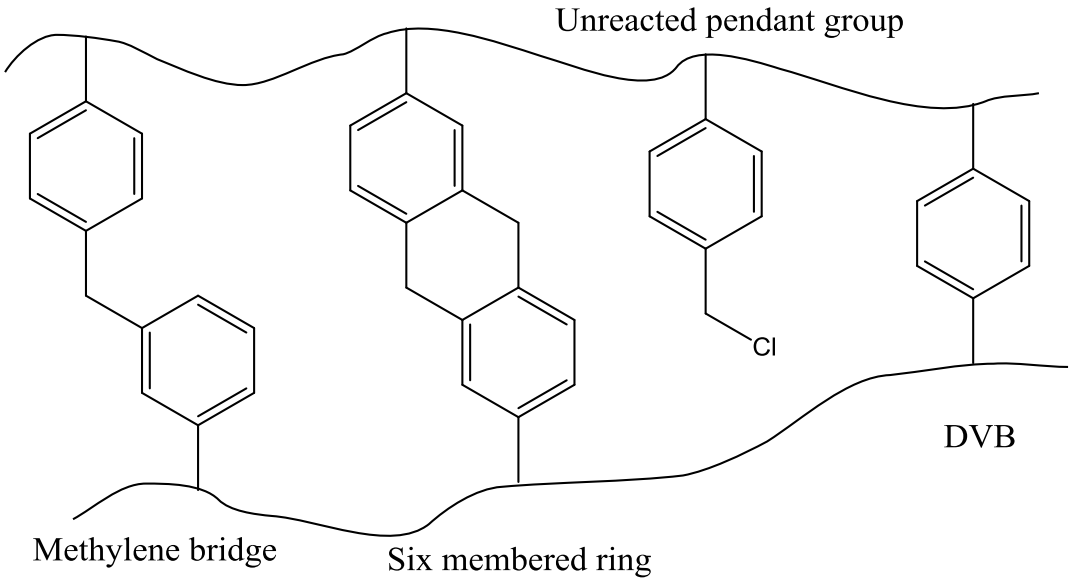

Figure 4. 5: The probable crosslinking formations during the hypercrosslinking reaction.

As can be seen from Figure 4.5 the hypercrosslinking reaction introduces the additional cronslinks together with DVB. It is a controlled reaction so some VBC groups can remain unreacted. To study the effect of hypercrosslinking on mercury adsorption, we prepared HXL-PHPs for 15 min and 30 min, and it was observed that the best results were obtained from the adsorbent named HXL-30min-PHP-$CONR_2$.

4.2 Physicochemical Properties of the Adsorbents

PolyHIPE's prepared in this thesis were characterized by Scanning Electron Microscopy (SEM), Brunauer–Emmett–Teller (BET), Fourier Transform Infrared (FTIR), X-ray photoelectron spectroscopy (XPS). PolyHIPE morphology is complex so the terminology created by Cameron and Barbetta was used [104]. They defined the large spherical pores as voids which form during the vaporization of water internal phase and the smaller pores which interconnects voids as windows. Interconnected pores are formed where monomer films between droplets walls become thinner and eventually windows are produced on polymerization at a critical level of surfactant. In Fig 4.6 the hierarchical pore structure of polyHIPE material can be clearly seen. It shows a typical polyHIPE morphology which contains macropores, voids and windows. In this study the porous polymers were prepared with 90 % porosity with voids and windows having a narrow diameter distribution. The void and interconnected pore distribution were studied by image analysis since the surface

porosity and the pore density can only be obtained by a visual analysis of micrographs [105] The surface porosity analysis, based on an average void and average interconnecting window diameters as seen in Figures 4.6 and 4.7, was analyzed by ImageJ software statistically [106] using a number of SEM images (Figures apendix) taken from the each sample. As can be seen from Figures 4.6 and 4.7, the individual morphology characteristics of each sample was sustained all over the frameworks. To obtain inferential results that quantitatively represents the surface morphologies of the samples, an average diameter analysis was performed with the datasets of 300−500 windows, while this dataset was limited with 50−100 counts for voids. The ratio of the average window diameter to average void diameter (⟨d⟩/⟨D⟩) is an indicator for the interconnectivity of open-porous network of polyHIPEs. Here, the average window and void diameters of polyHIPE precursor were found to be 7.55 ± 2.65 μm and 0.53 ± 0.10 μm, respectively. It can be seen in Figure 4.6 that hypercrosslinking reaction for 30 minutes caused a decrease in the void size; however, the average interconnecting window size of PolyHIPE precursor dropped from 0.53± 0.10 μm to 0.33 ± 0.14 μm. Introducing amide function to the surface of HXL-PHP did not have a signaficant difference on surface morphology. The average window and void diameters of amide functional HXL-PHP were found as 0.32 ± 0.11 μm and 3.86 ± 1.95 μm. As we expected the hypercrosslinking reaction and surface functionalization did not have a significant effect on surface morphology in terms of ⟨d⟩/⟨D⟩ indicating the similiar interconnectivity. The average diameter of interconnecting windows (⟨d⟩) and voids (⟨D⟩) as well as the degree of interconnections (⟨d⟩/⟨D⟩) of VBC polyHIPE (PHP), the hypercrosslinked polyHIPE prepared by the hypercrosslinking reaction for 30 minutes (HXL-30min-PHP), and the amide functional hypercrosslined polyHIPE prepared by the hypercrosslinking reaction for 30 minutes (HXL-30min-PHP-$CONR_2$) are summarized in Table 4.1.

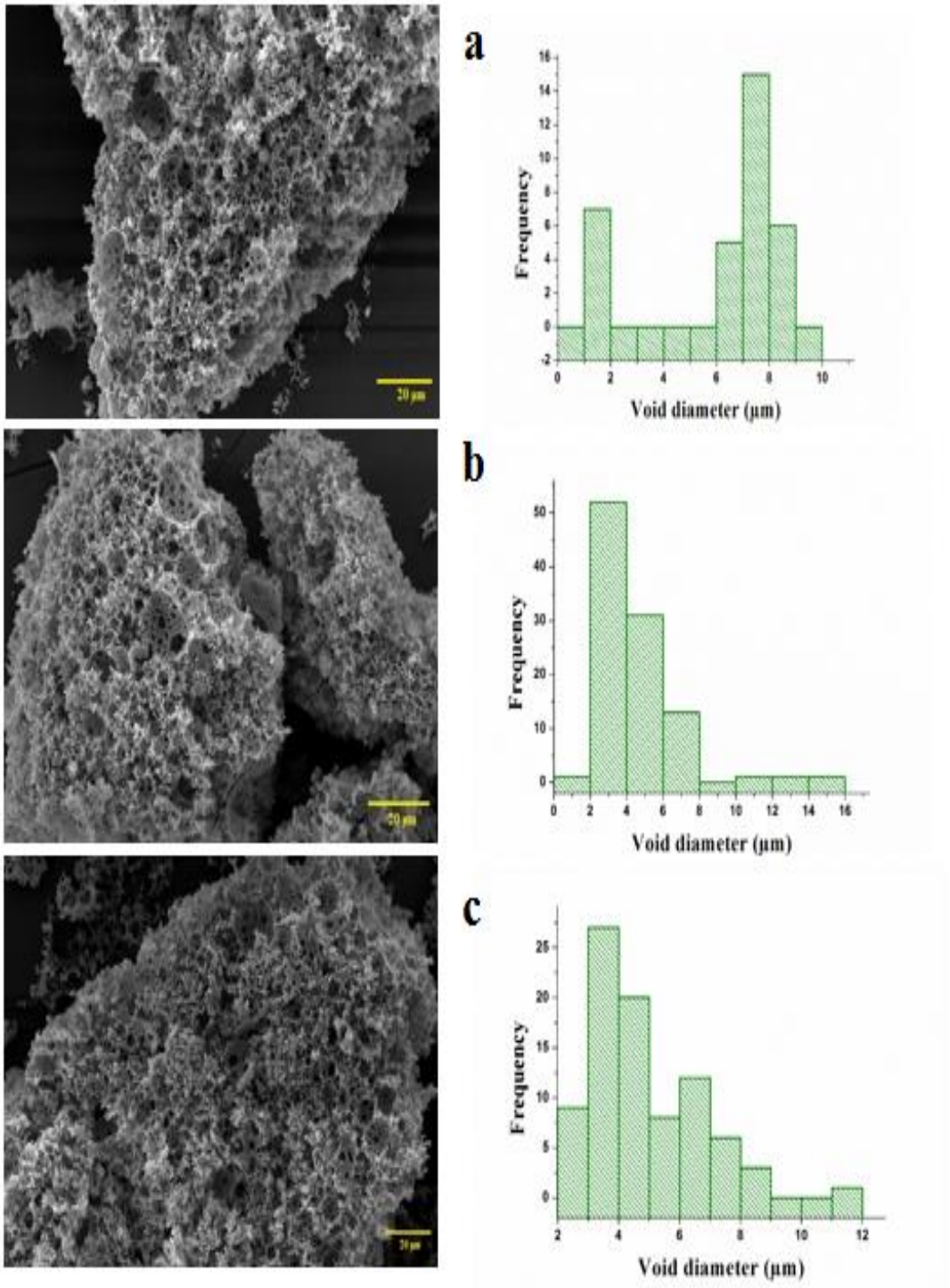

Figure 4. 6: SEM images of powdered samples showing void diameter distributions of (a) VBC-PHP, (b) HXL-30min-PHP, and (c) HXL-30min-PHP-$CONR_2$. Scale bares = 20μm.

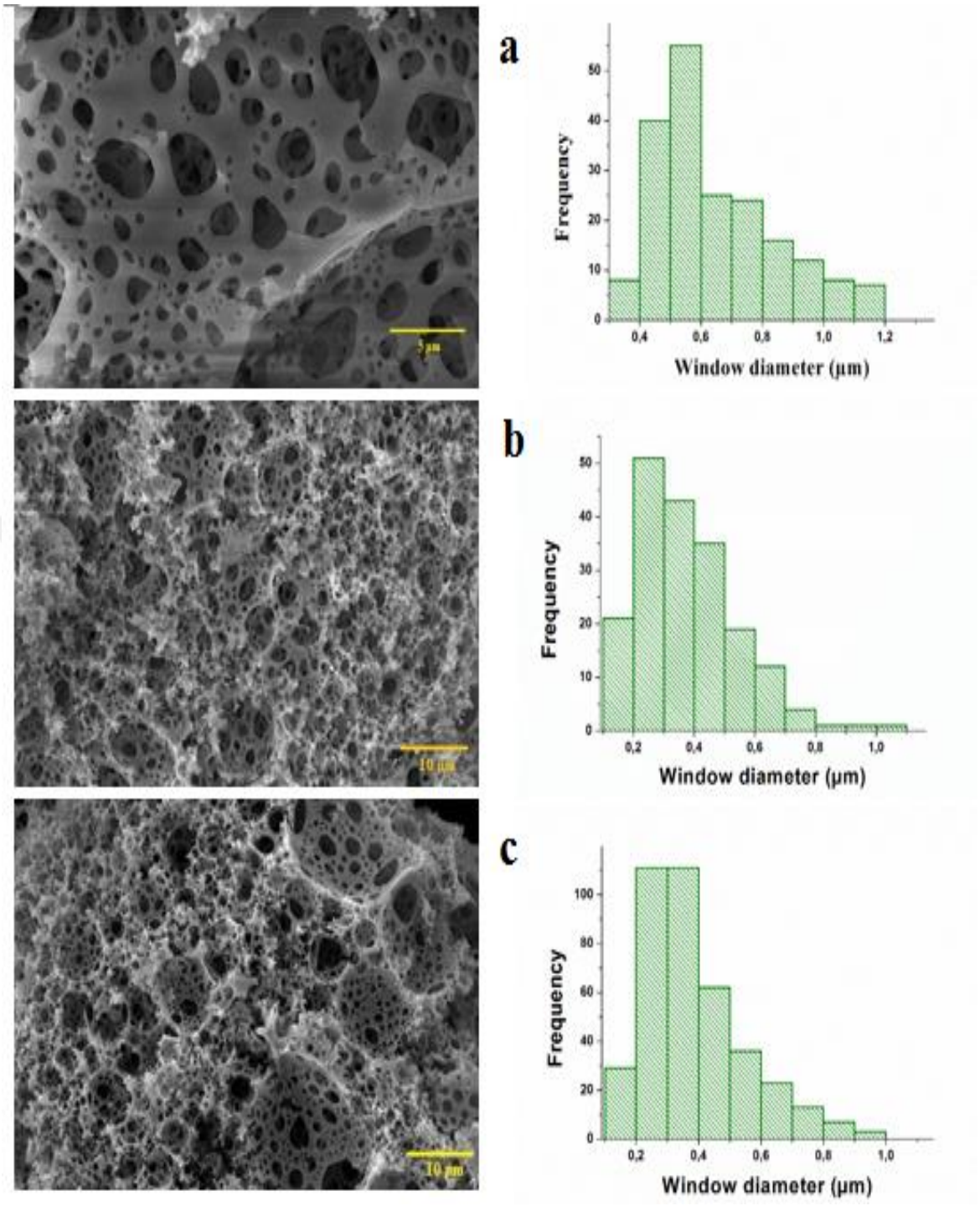

Figure 4. 7: SEM images of powdered samples showing window diameter distributions of (a) VBC-PHP, (b) HXL-30min-PHP, and (c) HXL-30min-PHP-$CONR_2$. Scale bars: a) 5 μm , b)10 μm, c) 10 μm.

Table 4. 1: Morphological Characterization of PHP, HXL-30min-PHP, and HXL-30min-PHP-$CONR_2$ by (a) Surface Area and Porosity Analysis and (b) Surface Morphology Analysis.

Sample ID	From BET measurements[a]					From SEM Images[b]		
	S_{BET} (m^2/g)	V_p (cm^3/g)	Avarage pore size[c] (nm)	Micropore volume (cm^3/g)	Micropore area	<d> µm	<D> µm	<d>/<D>
PolyHIPE	8.96	0.0336	5.13	*	*	0.53± 0.10	7.55 ± 2.65	0,07
HXL-30min-PHP	594	0.389	3.31	0.215	425	0.33 ± 0.14	3.84 ± 0.55	0,09
HXL-30min-PHP-$CONR_2$ (Ethanol amine)	460	0.511	5.12	0.123	245	0.32 ± 0.11	3.86 ± 1.95	0,08
HXL-15min-PHP	549	-	3.26	0.194	383	-	-	-
HXL-60min-PHP	617	0.396	2.99	0.194	385	-	-	-
HXL-120min-PHP	627	0.427	3.14	0.195	375	-	-	-
HXL-22h-PHP	631	0.415	3.21	0.223	443	-	-	-

Vp: pore volume
[c] Based on BJH Adsorption
‹d›: average window diameter, ‹D›: average void diameter, ‹d›/‹D›: the degree of interconnections
*The micropore area and micrpore volume are not reported because either the micropore volume is negative or the calculated external surface area is larger than the total surface area.

The selective removal of mercury ions from aqueous solutions is based on mainly specific interaction between mercury and amide groups located in pores of polyHIPE. Therefore it is crucial to identify the functional groups in detail. Here we identified the surface functional groups of polyHIPEs qualitatively by FT-IR and quantitatively by acid-base back titration and XPS. In Fig 4.8 the FTIR spectra of PHP (a), aldehyde functional PHP (b), carboxylic acid functional PHP (c) and amide functional (ethanol amine) PHP (d) can be seen.

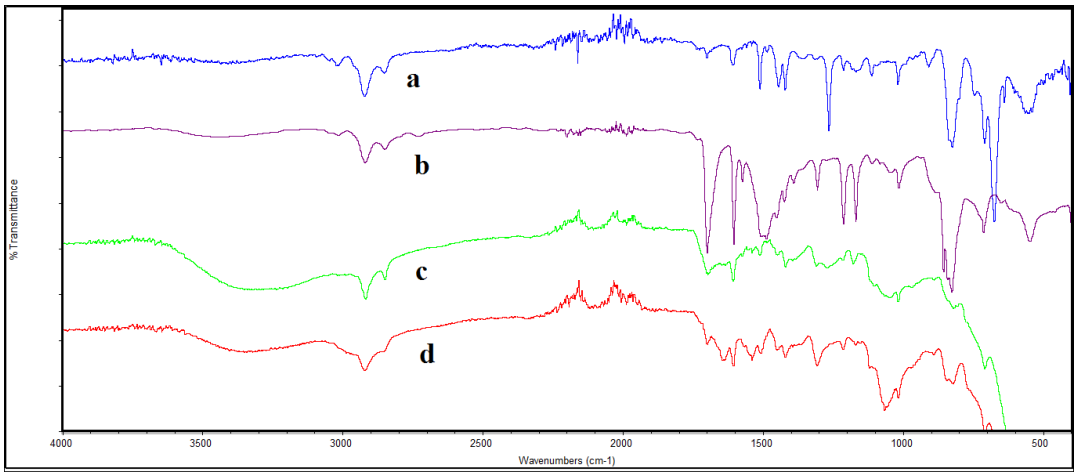

Figure 4. 8: FTIR spectra of PHP (a), aldehyde functional PHP (b), carboxylic acid functional PHP (c) and amide functional (ethanolamine).

The peak at 1485 cm^{-1} observed for all kind of polymers is the characteristic of the aromatic ring originated from the polyHIPE containing VBC and DVB. Kornblum oxidation introduced aldehyde groups which can be proved by the strong C=O stretching vibrations at 1730 cm^{-1} (Figure 4.8b). The oxidation of aldehyde groups resulted in a shift in the C=O peak from 1730 cm^{-1} to 1720 cm^{-1} and also broadening of the OH stretching vibrations between 3000-3600 cm^{-1} indicates the successfull conversion of aldehyde groups to carboxylic acid groups (Figure 4.8c). Finally, the coupling reaction formed an secondary amide groups which can be observed by the new peak appeared at 1640 cm^{-1} which belongs to the amide C=O stretching vibrations (Figure 4.8.d). And also, we can still observe the carbonyl peak of carboxylic acid group indicating that not all carboxylic acid groups were converted to amide groups. The degree of the conversion was obtained by acid-base back titration and XPS analysis. We also performed FT-IR analysis to charaterize the hypercrosslinked polyHIPE's prepared by the hypercrosslinking reaction for 30 minutes. As can be seen in Figure 4.9a C−Cl stretching vibration (685 cm^{-1}) and phenyl chloride (1260 cm^{-1}) peaks (Figure 4.8a), related to VBC pendant groups, were significantly decreased after the Friedel−Crafts reaction confirming the successful hypercrosslinking reaction. All the other peaks related to the modifications steps of HXL-30min-PHP can be observed in Figure 4.9 such as broad OH stretching vibrations between 3000-3600 cm^{-1} (Figure 4.9c) and the both amide and carboxylic acid C=O stretching vibrations in Figure 4.9d. Some FTIR peaks are not as clear as the paeks observed in Figure 4.8 propably caused by highly crosslinked structure of HXLPHP's.

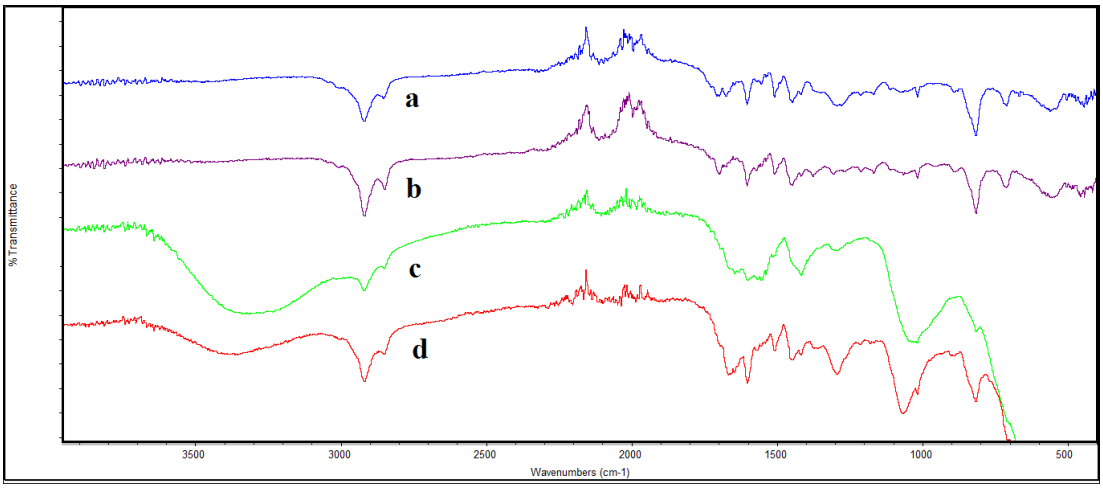

Figure 4. 9: FTIR spectra of HXL-30min-PHP (a), aldehyde functional HXL-30min-PHP (b), carboxylic acid functional HXL-30min-PHP (c) and amide functional (ethanol amine) HXL-30min-PHP.

In this study we prepared four adsorbent carrying amide groups with different side groups using aniline, diethylamine, ethanolamine and propylamine. In this way it is possible to check the effect of amide side groups on selevtivity towards mercury. Therefore the coupling reaction was carried out between HXL-30min-PHP-COOH and four amined listed above. We characterized the resulted hypercrosslinked polymers whether amide groups formed. As can be clearly observed in Figure 4.10 that the coupling reaction was successfully carried out for all four amines producing amide functionality together with carboxylic acid groups. In Figure 4.10 all FTIR spectras have the both amide and carboxylic acid C=O stretching vibrations at around 1720 and 1640 cm^{-1}, respectively.

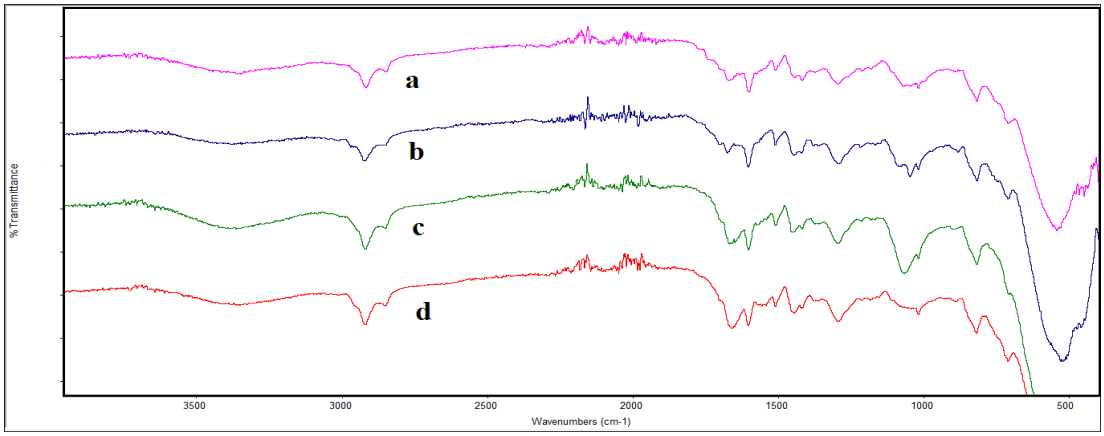

Figure 4. 10: FTIR spectra of a) HXL-30min-PHP-$CONR_2$ (aniline), b) HXL-30min-PHP-$CONR_2$ (diethylamine), c) HXL-30min-PHP-$CONR_2$ (ethanolamine) HXL-30min-PHP-$CONR_2$ (propylamine).

The hypercrosslinking reaction is a controlled reaction which consumes chlorine creating high surface area. We studied the reaction kinetically to obtain an optimum adsorbent in terms of surface area and chlorine content because together with high surface area, the unracted chlorine groups are needed for further functionalizations. The chlorine content of the polymers was measured by XPS. As can be seen in Figure 4.11 as surface area of the polymer increases the chlorine content decreases. In a just 30 minutes-reaction the surface area of polyHIPE reached around 600 m^2/g and further reaction did not changed the surface area significantly. Therefore HXL-30min-PHP was used for the futher functionalization reactions.

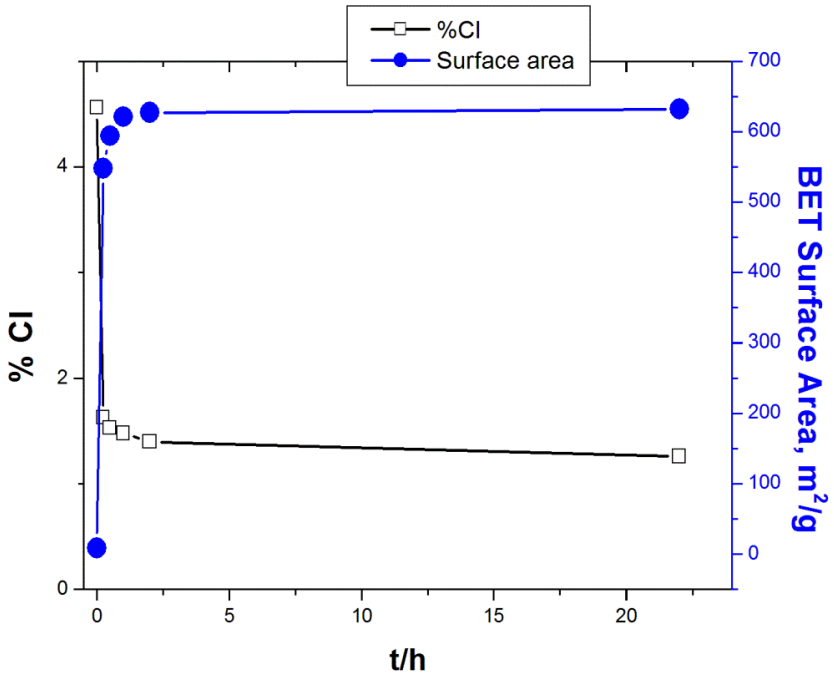

Figure 4. 11: Increase in surface area and decrease in chlorine content with the progress of hypercrosslinking reaction.

The functional groups of the polymers were found by acid-base back titration and confirmed by XPS analysis. In this way, we could follow the aldehyde conversion to carboxylic acid and carboxylic acid conversion to amide. Firstly we used DCC (dicyclohexyl carbodiimide) as a coupling agent to obtain amide groups on the polymer surface. However, because of the low solubility of the side product DCU (dicyclohexylurea), it was not possible to separate the crosslinked solid polymer from DCU. The conversions were found to be very low : trace amount for DEA and 9% (in mol) for aniline. Therefore, as an alternative coupling agent, DIC

(diisopropylcarbodiimide) being soluble in DCM was used and the higher carboxylic acid-amide conversions were obtained. Acid-base back titration results indicated a 54% acid-amide conversion for unhypercrosslinked polyHIPE for ethanol amine corresponding to 3.5 mmol/g amide content. XPS analysis also allow us to follow the conversion of functional groups. Figure 4.12 shows the XPS survevs for HXL-30min-PHP, HXL-30min-PHPCOOH and HXL-30min-PHP-$CONR_2$ (propylamine). Based on the peak areas in the surveys, the elemental compositions and the corresponding functional group capacities were calculated. As can be seen in Figure 4.12 the oxygen content increaed from 10.63% to 44.71% indicating successfull conversion of alkyl chloride groups to carboxylic acid groups. Also the chlorine peak at a binding energy of 201.08 eV (Figure 4.12a) dissaperead after 2-steps functionalzation as we can observe in Figure 4.12b. In XPS survey of amide functional (propylamine) hypercrosslinked polyHIPE N1s peak appears indicating the successfull coupling reaction between carboxylic acid groups and propyl amine.

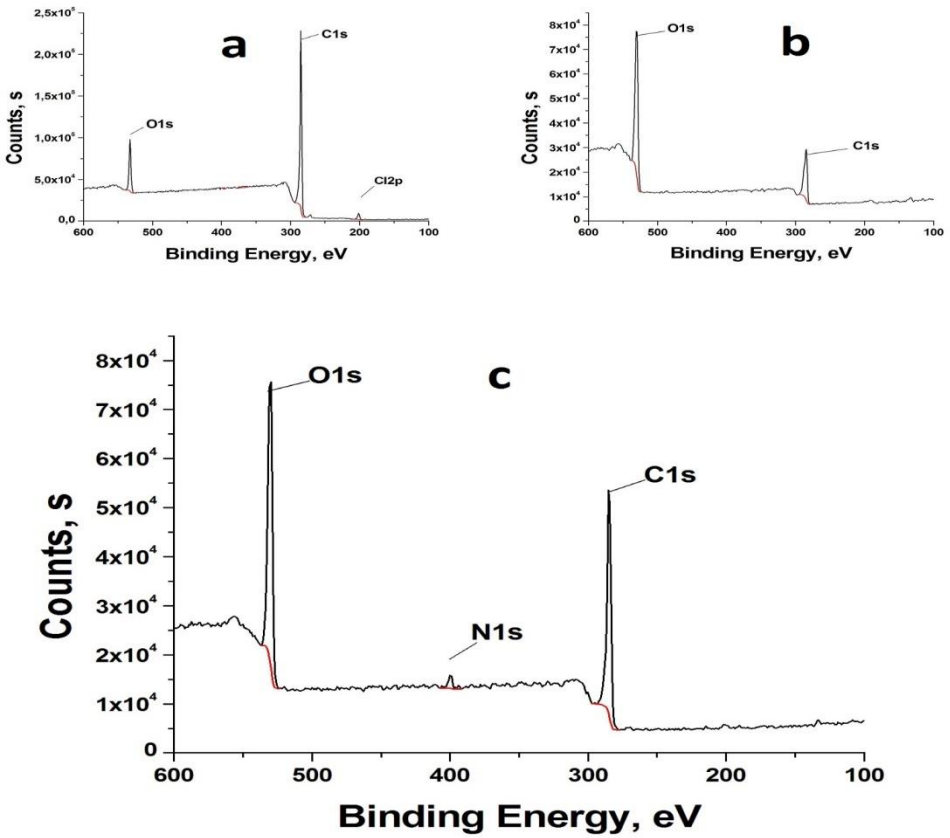

Figure 4. 12: XPS surveys of (a) HXL-30min-PHP, (b) HXL-30min-PHP-COOH and (c) HXL-30min-PHP-$CONR_2$ (propylamine).

This positive result led us to use DIC/NHS to produce amide functions using all four amines for hypercrosslinked acid functional polyHIPE.

A satisfied acid-amide conversion was obtained for all four amines using HXL-30min-PHP-COOH. The functional group contents of polymeric adsorbents can be seen in Table 4.2**.**

Table 4. 2: Functional group contents of polymeric adsorbents.

	Functional Group Content, mmol/g					
Sample ID	**Theoretical***	**XPS or Kjeldahl**		**Titration**		
PHP-COOH	5.7	**acid** 6.4	**amide** -	**acid** 6.4	**amide** -	
PHP-$CONR_2$ (Ethanolamine)	5.7	**acid** 4.2	**amide** 3.8	**acid** 6,4	**amide** 3.5	
HXL-30min-PHP-COOH	-	**acid** 4.2	**amide** -	**acid** 3.5	**amide** -	
HXL-30min-PHP-$CONR_2$ (DEA)	-	**acid** 4.5	**amide** 1.6	**acid** 3.5	**amide** 1.4	
HXL-30min-PHP-$CONR_2$ (Propylamine)	-	**acid** 2.8	**amide** 1.7	**acid** 3.5	**amide** 1.2	
HXL-30min-PHP-$NCONR_2$ (Aniline)	-	**acid**	**amide** 2.2	**acid** 3.5	**amide** 1.7	
HXL-30min-PHP-$CONR_2$ (Ethanolamine)	-	**acid**	**amide** 2.8	**acid** 3.5	**amide** 1.1	**2.4**
HXL-15min-PHP-$CONR_2$ (Ethanolamine)	-	**acid**	**amide** 2.6	**acid** 3.7	**amide** 1.2	2.5

*Based on the initial chlorine content of polymers.

Hypercrosslinked polymers shows various pore size distributions and specific surface areas. Hypercrosslinking reaction introduces micro and mesopores to polyHIPE structure possesing large void and windows. The meso/micro porosity of the materials was analyzed with the Brunauer−Emmett−Teller (BET) isotherm model. Because we aimed to obtain a high surface area poymer with unreacted benzyl chloride groups we prepared hypercrosslinked polyHIPEs for hypercrosslinking reaction time of 15 min, 30 min, 60 min, 120 min and 22 h. N_2 adsorption isotherms can be seen in Figure 4.13,

and BET and Langmuir surface areas (S_{BET} and $S_{Langmuir}$, respectively), pore volume (Vp), average pore size, micropore area, and volume are given in Tables 4.1.

Figure 4. 13: Nitrogen adsorption-desorption isotherms.

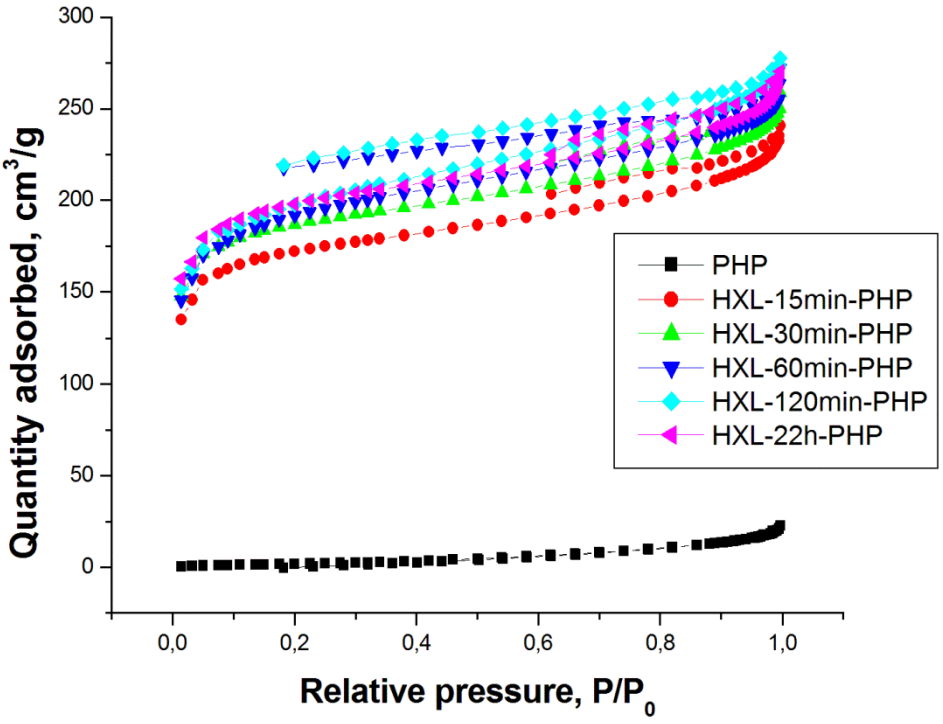

We can observe from the data presented (Table 4.1), the lowest surface area (S_{BET} = 8.96 m^2/g) was observed for the initial unhypercrosslinked polyHIPE (PHP) framework due to its macroporous structure possessing large voids and windows. However, only 15 minutes hypercrosslinking reaction enhanced an enormous surface area (S_{BET} = 549 m^2/g) of PHP precursor. The furher hypercrosslinking reaction increased the surface area around 600 m^2/g (30 minutes reaction time). We also checked wheter hypercrosslinking reaction has an effect on surface area and pore size and pore size distribution. As can be seen in Table 4.1 that aprroximitely 130 m^2/g decrease in the surface area of HXL-30min-PHP was observed after three-step surface modification to introduce the amide group (ethanol amine) to the polymer surface. This decrease could be caused either by blocking some very narrow micropores by the functional groups or some unwashed remainings from the modification steps. The higher extension of hypercrosslinking reaction did not enhance the surface area significantly. Table 4.1 indicates that 60, 120 minutes and 22h hypercrosslinking

reactions caused an increase in the surface area about 600 m^2/g. Therefore due to not significant change in surface area and also the necassary chlorine goups for the further functionalization we chose HXL-30min-PHP to prepare a mercury-selective adsorbent. We concluded that the reason why the surface area does not increase by the higher extention of hypercrosslinking reaction could be the fact that PHP precursors were prepared as 5% hypercrosslinking degree. This can cause a poor swelling and limiting the surface area of the resulting hypercrosslinked polymer. Furthermore, the pore volume was incresed ten fold only in 30 minutes by hypercrosslinking reaction. Also, the pore size distribution from the BJH method shows that hypercrosslinking reaction caused a significant increase in meso-micro porosity (Figure 4.14). These results prove that the amide functional polymers are high-surface-area micro-meso porous materials. The morphological characterization results based on the surface area and porosity analysis for all the adsorbents can be found in Table 4.1.

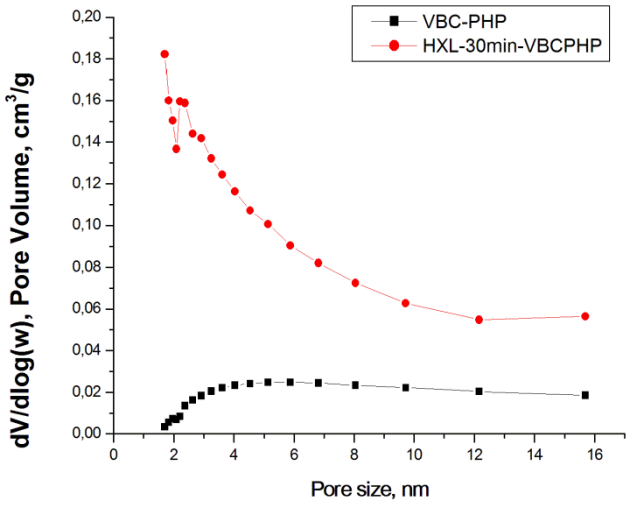

Figure 4. 14: Pore size distribution for VBC-PHP and HXL-30min-VBCPH.

4.3 Adsorption Experiments

In thesis we aimed to produce a high-surface-area, open-porous, mercury selective adsorbent. Hg(II) is a sofy acidic. In an amide function, the carbonyl group being an electron withdrawing group reduces the electron density of nitrogen and amide binds Hg(II) through soft acid-soft base specific interaction. Therefore the surface of the high-surface-area polymer was tailored with various amide. First, the selectivity of the adsorbents towards mercury (II) was tested. Once, the successful coupling reaction

between carboxylic acid groups of polyHIPE's with an amine was obtained, the effect of amide side group on the selectivity was tested by using various amines. Here, four amine were used to prepare amide functional polyHIPE's : Diethylamine, propylamine, aniline and ethanolamine. In this way, three secondary (propylamine, aniline and ethanolamine) and one tertiary amide (Diethylamine) functional porous polymers were used in mercury adsorption experiments. Initially the selectivity was tested using single metal solutions of $HgCl_2$, $CdNO_3$, $ZnSO_4$, $MgSO_4$ and $PbNO_3$. We compared the selectivity of carboxylic acid functional hypercrosslinked (30 min) polyHIPE with amide functional hypercrosslinked polyHIPE's (30 min, aniline and diethylamine). HXL-30min-PHP-COOH shows no selectivity towards mercury by having good adsorption capacities for all metals (Table 4.3). As can be seen in Table 4.3 that HXL-30min-PHP-COOH can bind all metals with a good adsorption capacity. However, amide functional polymers, HXL-30min-PHP-$CONR_2$ (aniline) and HXL-30min-PHP-$CONR_2$ (DEA) shows selectivity mercury (II) ions. HXL-30min-PHP-$CONR_2$ (aniline) has 2.5 mg/g adsorption capacity for mercury, wherase only 0.25 mmol/g for cadmium. Also, HXL-30min-PHP-$CONR_2$ (DEA) showed the similar selectivity towards mercury (II). The adsorption capacities of HXL-30min-PHP-COOH, HXL-30min-PHP-$CONR_2$ (aniline) and HXL-30min-PHP-$CONR_2$ (DEA) for Hg(II) as well as Cd(II), Zn(II), Mg(II) and Pb(II) were given in Table 4.3**.**

Table 4. 3: The comparison for adsorption capacities in single metal solutions*.

Sample ID	Adsorpiton capacity, mmol/g.				
	$HgCl_2$ $PbNO_3$	$CdNO_3$	$ZnSO_4$	$MgSO_4$	
HXL-30min-PHP-COOH	3.15	2.25	2.5	2.70	2.80
HXL-30min-PHP-$CONR_2$(Aniline)	2.5	0.25	0.25	0.40	0.50
HXL-30min-PHP-$CONR_2$(DEA)	2.2	0.2	0.65	0.70	0.75

*The concentration of metal solutions = 0.05 M

4.3.1 The selectivity measurements

Once, it was proved that amide functions shows selectivity in the single metal solutions, the selectivity of all hypercrosslinked adsorbents (prepared by coupling reactions with aniline, propylamine, DEA and ethanolamine) were tested in the ternary metal solutions. The method was based on a 2-step process. First, the excess EDTA was added to the metal solution and the remaining metals were titrated by $PbNO_3$. The secondly, 2-thiozoline thiol was added to the solution to release the selectively mercury and the released mercury was titrated by $PbNO_3$. All polymers adsorbed 0.2 mmol total metal according to $PbNO_3$ back titration. Initially the ternary metal solution contained the total of 0.6 mmol metal (Hg, Zn and Cd). After adsorption, HXL-30min-PHP-$CONR_2$ (DEA) bound 0.08 mmol Hg(II), HXL-30min-PHP-$CONR_2$ (aniline) 1.0 mmol, HXL-30min-PHP-$CONR_2$ (propylamine) 1.3 mmol corresponding to 40 to 65% of the initial amount of total metals. These results indicate that all polymers carrying amide groups showed selectivity towards Hg(II) in a ternary solution. Moreover, HXL-30min-PHP-$CONR_2$ (ethanolamine) adsorbed 0.17 mmol Hg(II) corresponding to 85% of the initial amount of total metals. Of all amide functional hypercrosslinked polyHIPE's the one with ethanolamine side group showed a very high selectivity.

4.3.2 Adsorption kinetics performance

Once we determined the hypercrosslinked polyHIPE with the highest selectivity, we wanted to see how the hypercrosslinking reaction enhances mercury adsorption kinetics. The kinetics data was obtained as explained in 3.4.1. based on the calibration curve (Figure 4.15). Mercury-diphenylcarbazide complex shows high deviations from Beer-Lambert law at high mercury concentrations so we kept the Hg(II) concentration between $5.0x10^{-5}$ and $1.0x10^{-6}$ M. As can be observed in Figure 4.16 that a very high correlation coefficient was obtained in the given Hg(II) concentration range. Therefore all mercury solutions were diluted to $1.0x10^{-5}$ M before the measurement. For comparision, an amide functional unhypercrosslinked polyHIPE (PHP-$CONR_2$, ethanolamine) and HXL-15min-PHP-$CONR_2$ (ethanolamine) were prepared and their mercury adsorption performances were compared with HXL-30min-PHP-$CONR_2$ (ethanolamine). Figure 4.16 shows that 15 min-hypercrosslinking reaction enhanced the adsorption kinetics significantly. Moreover, HXL-30min-PHP-$CONR_2$ (ethanolamine) adsorbed the half of the initial Hg(II) in just 2 minutes.

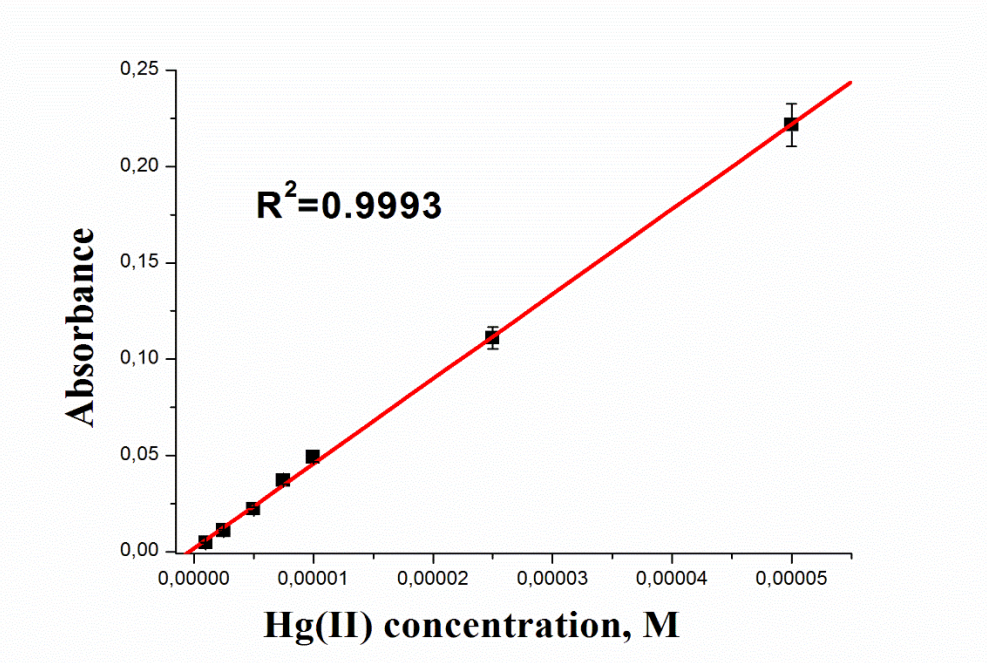

Figure 4. 15: The calibrtion curve for Hg(II)-diphenylcarbazide method.

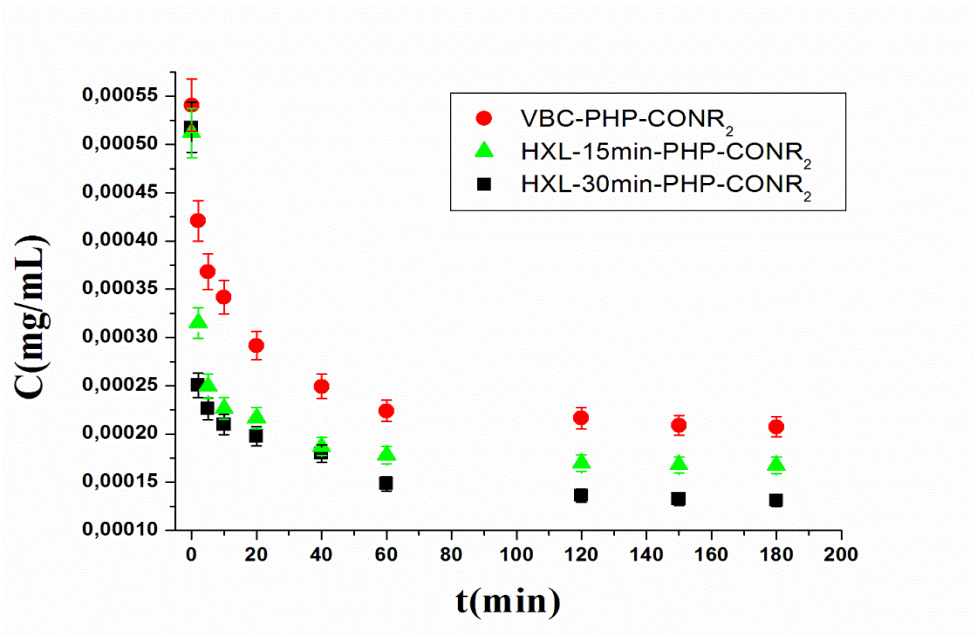

Figure 4. 16: The comparision of mercury adsorption kinetic performances for VBC-PHP-$CONR_2$ (ethanolamine), HXL-15min-PHP-$CONR_2$ (ethanolamine) and HXL-30min-PHP-$CONR_2$ (ethanolamine). The initial Hg(II) concentration = $5x10^{-4}$ M, 25 mg adsorbent, 10 mL metal solution, 25^0C.

Having proved that HXL-30min-PHP-$CONR_2$ (ethanolamine) has the best performance for Hg(II) adsorption in terms of selectivity and fast kinetics, we focused on HXL-30min-PHP-$CONR_2$ (ethanolamine) for further adsorption experiments.

4.3.3 The effect of solid/liquid ratio on mercury adsorption (Determining the optimum adsorbent amount)

The effect of solid-liquid ratio on mercury adsorption on HXL-30min-PHP-$CONR_2$ (ethanolamine) adsorbent was studied and the result is given in Figure 4.17. Adsorption capacities of the adsorbent increased up to an optimum dosage (25 mg) while $HgCl_2$ concentration was kept constant in constant mercury solutions (10 mL). This result is expected due to the fact that the higher dose of polymer in the solution, the greater availability of interaction sites for Hg(II) ions. At 0.005 M $HgCl_2$ initial concentration, the adsorption capacity of hypercrosslinked adsorbent was 1.87 mmol/g at the solid/liquid ratio of 2.5 mg/mL. The mercury amount adsorbed on polyHIPE based adsorbent from the adsorption medium lowered as adsorbent dosage increases in 10 mL adsorption medium (Figure 4.17). One can conclude that as the amount of porous polymer adsorbent so adsorption sites increases, adsorption capacity (mercury adsorption per unit weight) decreases because of constant initial solution concentration. Therefore for futher adsorption experiments 25 mg of HXL-30min-PHP-$CONR_2$ (ethanolamine) was used in 10 mL adsorption medium.

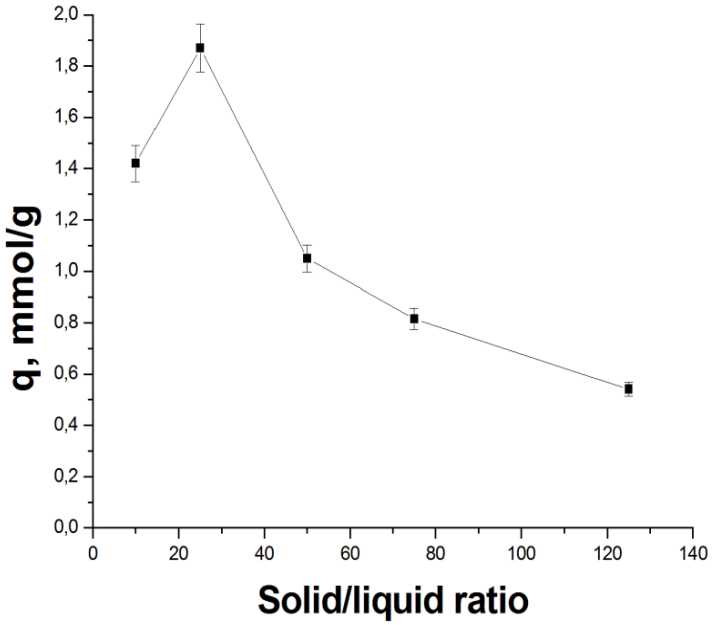

Figure 4. 17: The effect of the solid-liquid ratio on mercury adsorption for HXL-30min-PHP-$CONR_2$ (ethanolamine) adsorbent. Experimental conditions : 10 mL of mercury solution (0.005 M), 25^oC solution temperature.

4.3.4 The effect of pH on mercury adsorption

The very high surface of the hypercrosslinked adsorbent offer the opportunity for fast with aqueous Hg(II) solutions to form mercury-amide linkages. In harmony with the previous studies [107,108] mercury binding takes place through proton releasing which is affected by the pH of the adsorption medium. Hg(II) can be captured from aqueous solutions via monoamide or diamide Hg(II) structures. Therefore it was expected that the pH of the adsorption medium should have a strong effect on mercury adsorption. Also, via coupling reaction approximately 67% of carboxylic acid groups were converted to amide groups remaining some carboxylic acid groups on the surface of HXL-30min-PHP-$CONR_2$ (ethanolamine) adsorbent. The carboxylic acid groups has a pKa of 4.76 so depending on the pH of the adsorption medium the polymer surface can be charged negatively and carboxylic acid groups can contribute the mercury binding through a complex structure. Moreover, uncompleted conversion is a rather advantage. To release the adsorbed mercury and to reuse the adsorbent an acid treatment is needed. However, acid treatment can cause to hydrolyze the amide groups. Yuxin Pei and co-workers [109] showed that increasing polymer charge enhanced the stability of amide groups. Therfore, keeping some carboxylic acid groups unreacted after amide functionalization can enhance the stability of amide groups against hydrolysis during the regenaration process. Mercury adsorption on HXL-30min-PHP-$CONR_2$ (ethanolamine) was studied in a pH range between 3 to 7 and the adsorption capacities depending on pH of the adsorption medium were given in Figure 4.18. As can be seen in Figure 4.18 that HXL-30min-PHP-$CONR_2$ (ethanolamine) showed good adsorption capacites in a broad range of pH which is an advantage in real application like removal of heavy metals from waste water. The best results were observed at pH = 6 and 7 and the lowest adsorption capacity was observed at pH = 3. These results were expected due to the decreaed proton releasing at lower pH's. We did not carry out any adsorption experiment at pH higher than 7 because $HgCl_2$ precipitates in basic solutions.

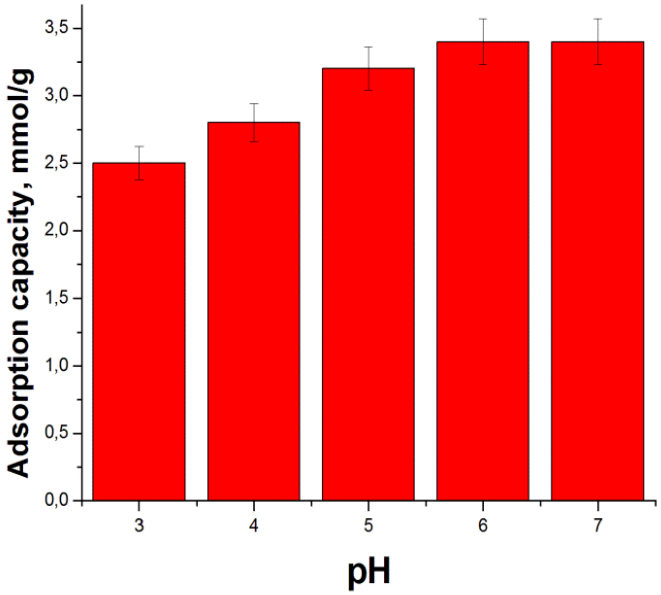

Figure 4. 18. The effect of pH on Hg(II) adsorption for HXL-30min-PHP-$CONR_2$ (ethanolamine). Adsorption conditions : 25 mg polymer, the initial $HgCl_2$ concentration = 0.05 M, the volume of metal solution = 10 mL.

4.3.5 Evaluating mercury adsorption mechanism

To evaluate the adsorption mechanism, three adsorption kinetic models were applied to the experimental data. These models are pseudo-first-order, pseudo-second-order, and intra-particle diffusion models. To apply the models, first, adsorption capacities for HXL-30min-PHP-$CONR_2$ (ethanolamine) at various time intervals were calculated at 100 ppm initial $HgCl_2$ aqueous solution (Figure 4.19). Also an adsorption capacity comparision between unhypercrosslinked and hypercrosslinked (30 min hyoercrosslinking reaction) amide functional (ethanolamine) polyHIPEs clearly indicates the faster kinetic for the hypercrosslinked polyHIPE**.** In Figure 4.19 HXL-30min-PHP-$CONR_2$ (ethanolamine) reached 70% of the max. adsorption capacity in just 2 minutes while unhypercrosslinked counterpart adsorbed 40% of its max. capcity in the same time interval. The very high surface area of the hypercrosslinked polymer enhances the external mass transfer resulting very fast adsorption kinetics.

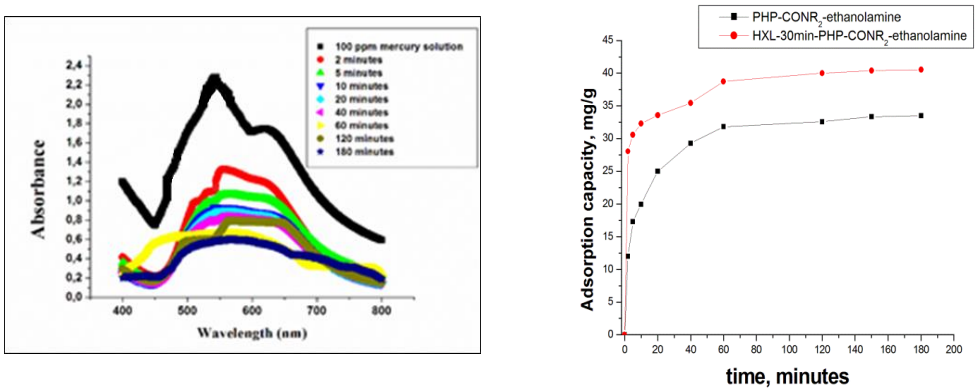

Figure 4. 19: a) UV spectrums of mercury adsorption kinetics on HXL-30min-PHP-$CONR_2$ (ethanolamine) at 100 ppm initial $HgCl_2$ concentration. b) The adsorption capacity comparision between unhypercrosslinked and hypercrosslinked (30 min hypercrosslinking reaction) amide functional (ethanolamine) polyHIPEs. Experimental conditions : 25 mg adsorbent. 10 ml adsorption medium at 25°C, 400 rpm stirring rate.

The very common equation for adsorption on solid adsorbents is the Lagergren first-order rate equation. Generally the linear form of the equation is used (Equation 4.1):

$$ln(q_e - q_t) = ln\, q_e - k_1\, t \tag{4.1}$$

Here, in this equation k_1 is the pseudo-first-order rate constant for adsorption q_{eq} and q_t indicate the amounts of adsorption (mmol g^{-1}) at equilibrium and at time t, respectively. The pseudo-first-order rate constant k_1 can be found from the slope of the plot of ln ($q_{eq} - q_t$) versus t and equilibirium capacity q_{eq} is found from the intercept of the plot. The reaction rate is proportional to k_1. The second kinetic model used in this thesis is the pseudo-second-order model. The linear form of the equation describing the adsorption kinetics is as follows (Equation 4.2):

$$\frac{t}{q_t} = \frac{1}{k_2 q_e{}^2} + \frac{1}{q_e t} \tag{4.2}$$

Here k_2 is the pseudo-second-order rate constant of sorption (g $mmol^{-1}$ min^{-1}). The rate constant k_2 and equilibrium capacity q_e can be calculated from the intercept and slope of the plot of t/q_t versus t respectively. If pseudo-second-order model fits the experimental data, the plot gives a linear relationship which allows to obtain k_2. Pseudo-first-order and pseudo-second-order kinetic plots and linear regressions for

methylene blue adsorption on HXL-15min-PHP-COOH are given in Figure 4.20 and 4.21 respectively.

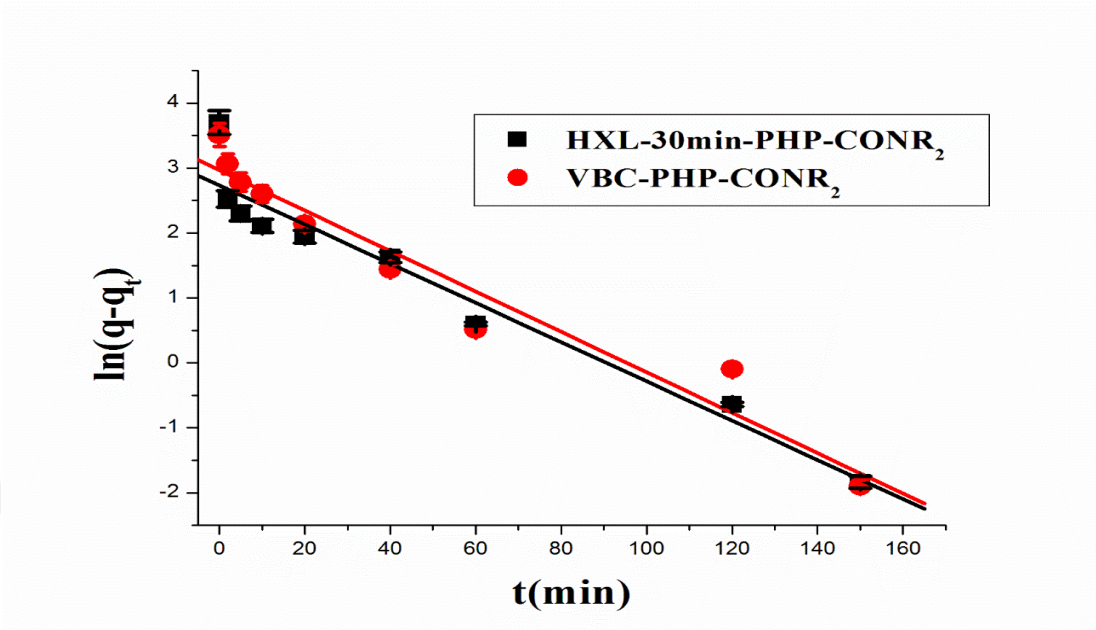

Figure 4. 20: Pseudo first order kinetic plot for Hg(II) adsorption on HXL-30min-PHP-$CONR_2$ (ethanolamine) and VBC-PHP-$CONR_2$ (ethanolamine). Adsorption conditions: 25 mg polymer, the initial $HgCl_2$ concentration = 100 ppm, the volume of metal solution = 10 mL.

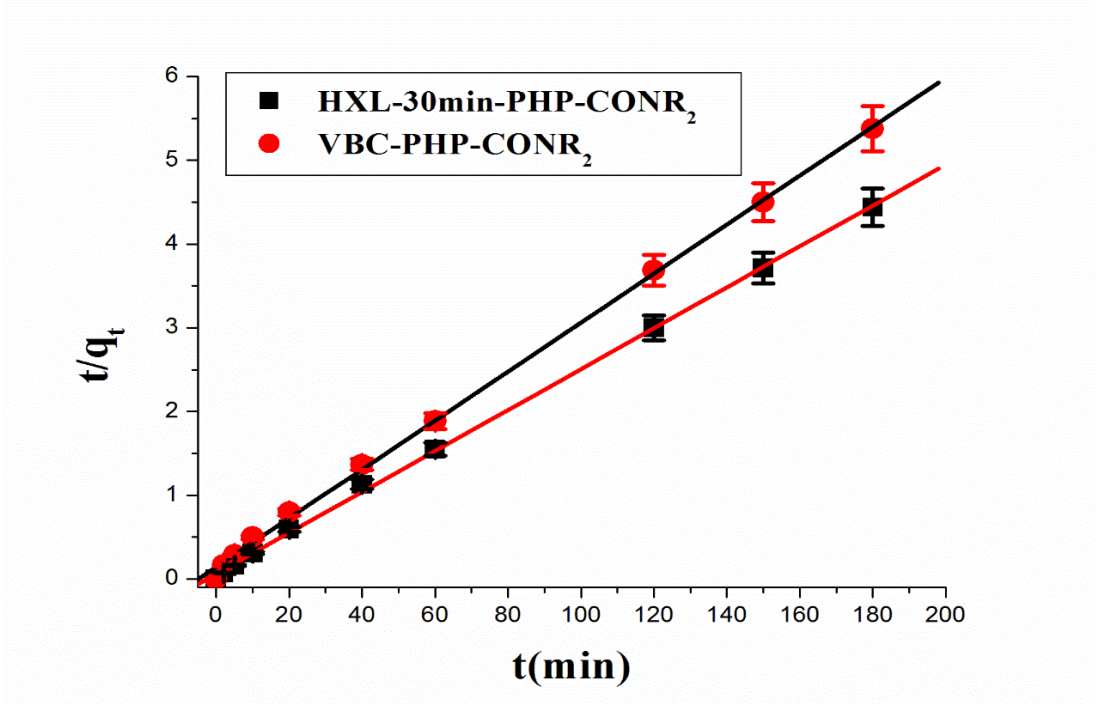

Figure 4. 21: Pseudo second order kinetic plot for Hg(II) adsorption on HXL-30min-PHP-$CONR_2$ (ethanolamine) and VBC-PHP-$CONR_2$ (ethanol amine). Adsorption conditions: 25 mg polymer, the initial $HgCl_2$ concentration = 100 ppm, the volume of metal solution = 10 mL.

It can be evaluated which model describes mercury adsorption on HXL-30min-PHP-$CONR_2$ (ethanolamine) judging by the correlation coefficients of the corresponding plots. The kinetic parameters calculated by linear regression can be seen in Table 4.4. As can be seen in Table 4.4 mercury adsorption obeys the the second-order kinetics. The high correlation coeffient and close experimental and theoretical adsorption capacity values indicate that the adsorption process can be explained by pseudo second order kinetic model. Pseudo second order kinetic model describes adsorptions where adsorbate/adsorbent ratio is low and the rate limiting step is chemical adsorption. Theoritical expectations fit well with the experimental results indicating the adsorption process via formation of amide mercury structures.

Table 4. 1: Pseudo-first-order, Pseudo-second-order, and Intra-Particle Diffusion Model Parameters for HXL-30min-PHP-$CONR_2$ (ethanolamine) and PHP-$CONR_2$ (ethanolamine).

	Pseudo first-order			**Pseudo second-order**			**Intra-particle diffusion**		
	k_1 (min^{-1})	**q_e (mg/g)**	**R^2**	**k_2 (g/mg.min)**	**q_e (mg/g)**	**R^2**	***k_d ($mg/g.min^{0.5}$)**	**C**	**R^2**
HXL-30min-PHP-$CONR_2$ (ethanolamine)	0.0311	19.504	0.948	0.004	40.98	0.989	0.257	17.73	0.957
				$q_{deneysel}$ = 40,53					
VBC-PHP-$CONR_2$ (ethanolamine)	0.0302	13.974	0.942	0.019	29.24	0.999	0.136	30.45	0.977
				$q_{deneysel}$ = 33,47					

*Calculated based on the second stage seen in Figure 4.24.

The third kinetic model used to describe the adsorption process in this study is the intraparticle diffusion (Figure 4.24). It is a transport process where subtances transfer from the bulk of the solution to the solid phase. To apply this model to the experimental data and describe the adsorption process the adsorption medium including porous adsorbent and mercury solution should be strirred well. This intraparticle diffusion model was proposed by Weber and Morris [110] and it is given as following Equation 4.3:

$$q_t = k_d t^{0.5} + C \tag{4.3}$$

In this model k_d indicates the intra-particle diffusion rate constant (g $mmol^{-1}min^{-0.5}$), C is the constant on boundary layer thickness. The plots q_t versus $t^{0.5}$ has a multilinearity character, where generally two or more steps occur. In the first step a

sudden increase in the adsorption capacity takes place and this portion of the plot is called the external surface adsorption or instantaneous adsorption stage. In the second part of the plot a slow adsorption stage takes place, where intraparticle diffusion is rate controlled. And in the final portion, because of very low concentrations in the solution, intraparticle diffusion begins to slow down and the equilibrium stage establishes. In Figure 4.22 we can clearly observe that the external surface adsorption is faster than that of its unhypercrosslinked counterpart. The active groups located in open-porous structure of polyHIPEs are accessible for mercury and the resistance to mass transfer is low. The combination of open-porous large voids together with high surface area HXL-30min-PHP-$CONR_2$ (ethanolamine) provides the enhanced external surface adsorption with respect to the unhypercrosslinked amide functional polyHIPE.

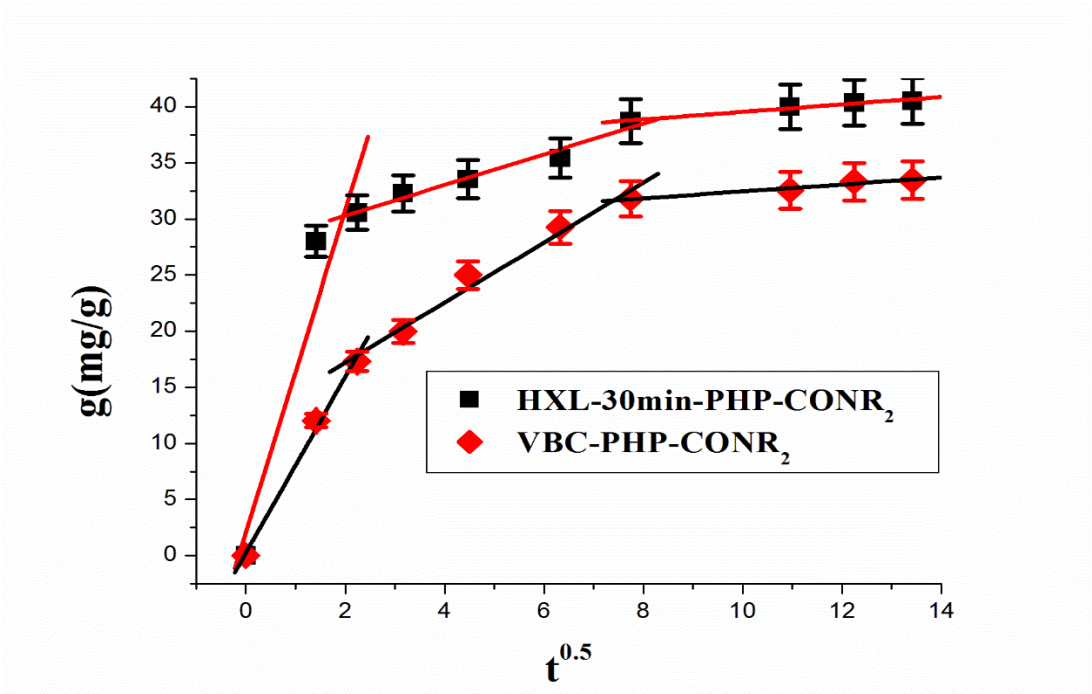

Figure 4. 22: Intra-particle diffusion plot for Hg(II) adsorption on HXL-30min-PHP-$CONR_2$ (ethanolamine) and VBC-PHP-$CONR_2$ (ethanolamine). Adsorption conditions: 25 mg polymer, the initial $HgCl_2$ concentration = 100 ppm, the volume of metal solution = 10 mL.

To find the max. Hg(II) adsorption capacity of HXL-30min-PHP-$CONR_2$ (ethanolamine), the adsorption experiments with various initial aqueous $HgCl_2$ concentrations were carried. And then, these results were tested by three adsorption isotherm models. As can be seen in Figure 4.23 as mercury concentration increases, the adsorption capacity of HXL-30min-PHP-$CONR_2$ (ethanolamine) increases and reaches a max. level at $HgCl_2$ concentration indicating a 798.58 mg/g capacity.

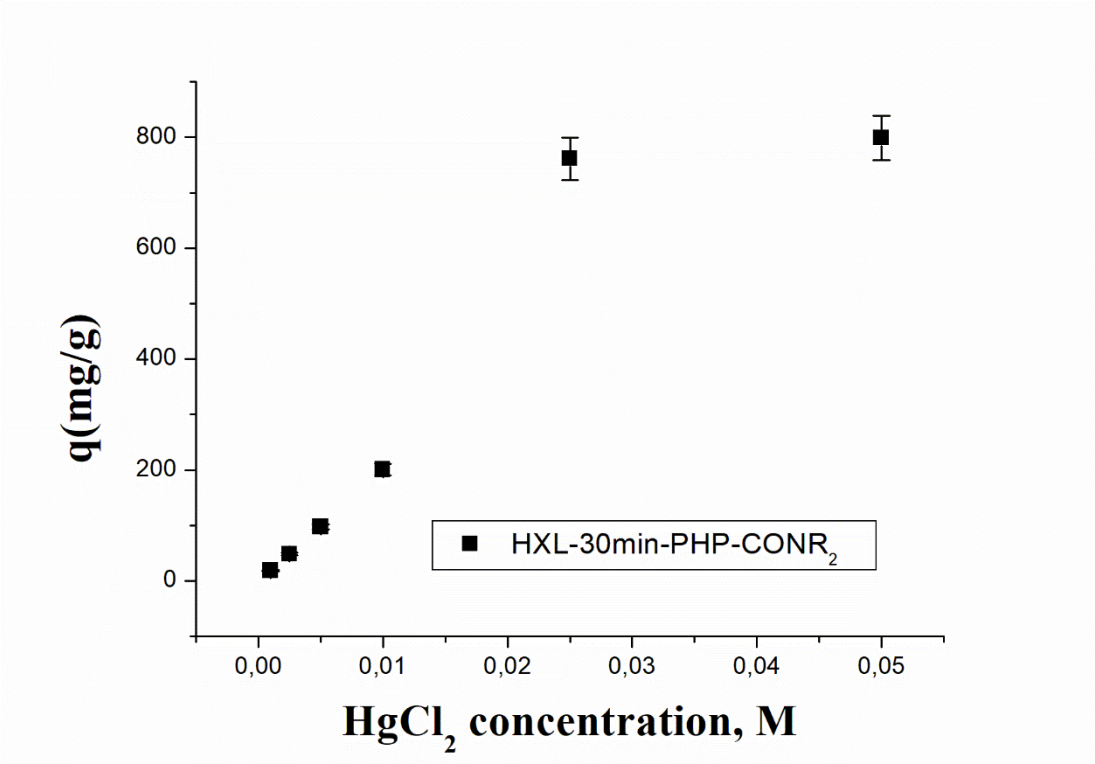

Figure 4. 23: Adsorption capacity – $HgCl_2$ concentration plot

The first adsorption model applied to the experimental adsorption results in this thesis is Langmuir isotherm model. One of the most known adsorption isotherm used to model adsorption data which may be represented as (Equation 4.4):

$$q_e = \frac{q_m b C_e}{1+bC_e} \tag{4.4}$$

To evaluate the experimental date by Langmuir isotherm a linear form of the isotherm was used (Equation 4.5):

$$\frac{C_e}{q_e} = \frac{1}{q_{max} b} + \frac{C_e}{q_{max}} \tag{4.5}$$

Here C_e shows the equilibrium concentration of dye in solution (mg/L), q_e indicates the equilibrium amount of dye adsorbed on the adsorbent at time t (mg/g). q_m is the maximum adsorption capacity of the adsorbent (mg/g) and b (i.e., the adversely of dissociation constant of the ligand/surface interaction, K_d, or equal to association constant, K_a, ($b = K_a = (1/K_d)$) is the energy of adsorption constant. When K_d is small value the dye binding is stronger. In the Figure 4.24 Langmuir isotherms of mercury adsorption on HXL-30min-PHP-$CONR_2$ (ethanolamine) and PHP-$CONR_2$ (ethanol amine) are given.

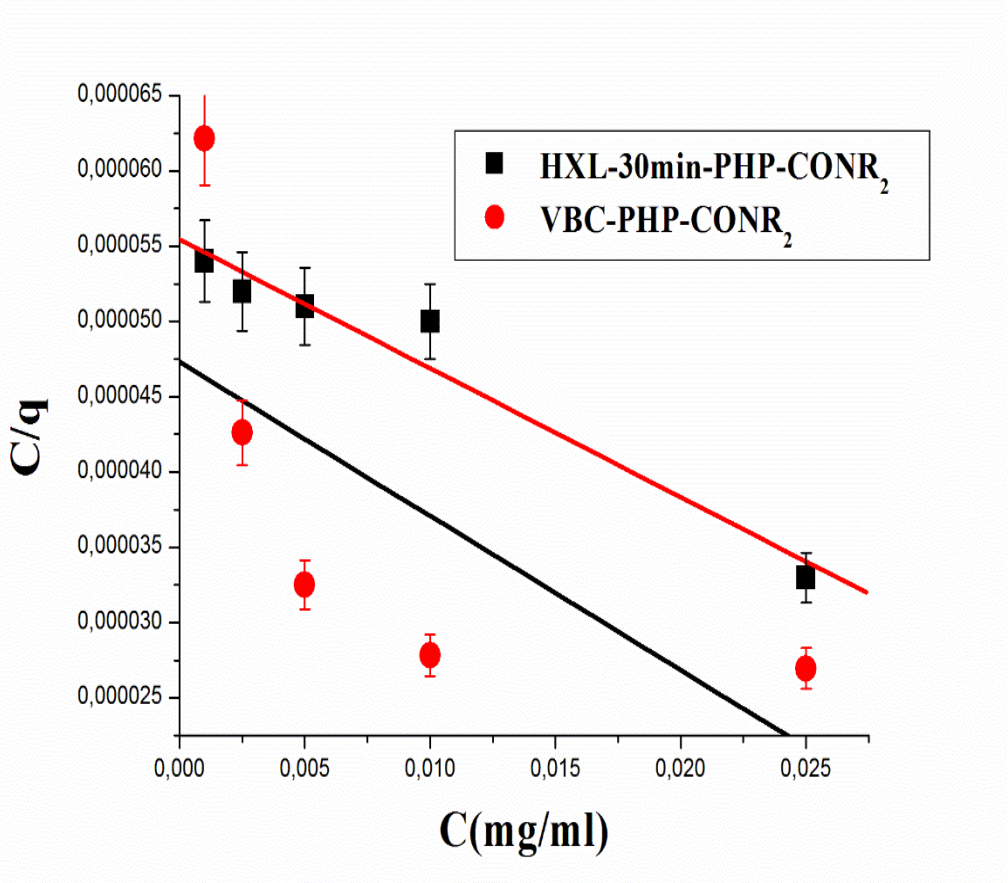

Figure 4.24: Langmuir isotherms HXL-30min-PHP-CONR$_2$ (ethanolamine) and VBC-PHP-CONR$_2$ (ethanolamine).

The second adsorption isotherm used in this study is Freundlich isotherm which is applied for the heterogeneous surface adsorption. The linear form of the Freundlich equation is represented as (Equation 4.6):

$$\ln q_e = \ln K_f + {}^{1}/_{n} \ln C_e \qquad (4.6)$$

In this equation, K_F and n are the Freundlich constants and they are indications of the characteristic of the adsorption system. K_F and n are indicates the adsorption capacity and adsorption intensity, respectively. The slope of the linear equation is 1/n and intercept of the eauation gives lnK_F. Fig. 4.25 represents Freundlich isotherms ploted using mercury adsorption data.

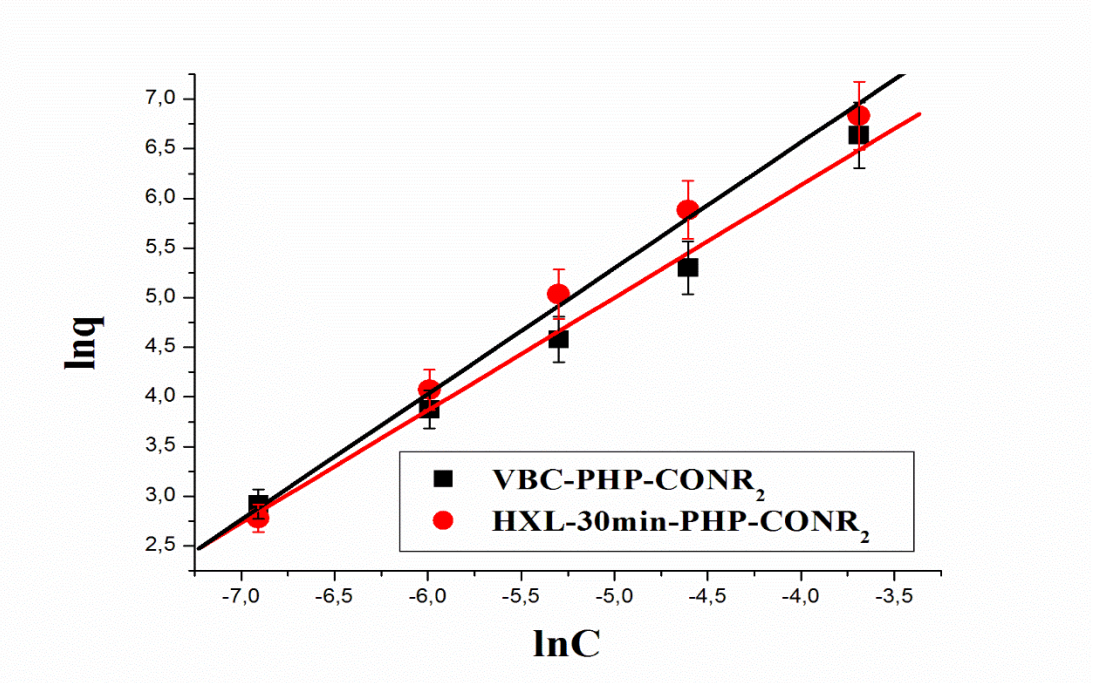

Figure 4. 25: The Freundlich isotherms for mercury adsorption on HXL-30min-PHP-CONR$_2$ (ethanolamine) and PHP-CONR$_2$ (ethanolamine).

The experimental adsorption data was applied to the Dubinin–Radushkevich (D–R) as the third adsorption isotherm model. Generally polymeric adsorbents have heteregenous surface and active groups are distributed not regularly on the polymer surface. Because D-R isotherm does not assume a homogeneous surface or constant adsorption potential [111], we also used this isotherm to evaluate the adsorption mechanism of Hg(II) on HXL-30min-PHP-CONR$_2$ (ethanolamine) and PHP-CONR$_2$ (ethanolamine). The following equation is the D–R Equation 4.7:

$$lnq_e = lnq_m - K\varepsilon^2 \quad (4.7)$$

In this equation q_e indicate the amount of the mercury adsorbed at the equilibrium, K is a constant which is related to the mean free energy of sorption, qm gives the theoretical adsorption capacity, and ε is the Polanyi potential. ε can be calculated by the equation: RT ln(1 + (1/C_e)). The plot ln q_e against ε^2 gives the values of q_m and K. The constant (K) is an indicator of the mean free energy of adsorption per mole of the adsorbate as it is transferred to the surface of the solid from infinite distance in the solution. The following equation can be used to calculae the mean free energy (E) (Equation 4.8).

$$E = (2K)^{-1/2} \quad (4.8)$$

Dubinin–Radushkevich (D–R) isotherms for mercury adsorption on polyHIPE adsorbents are given in Figure 4.26.

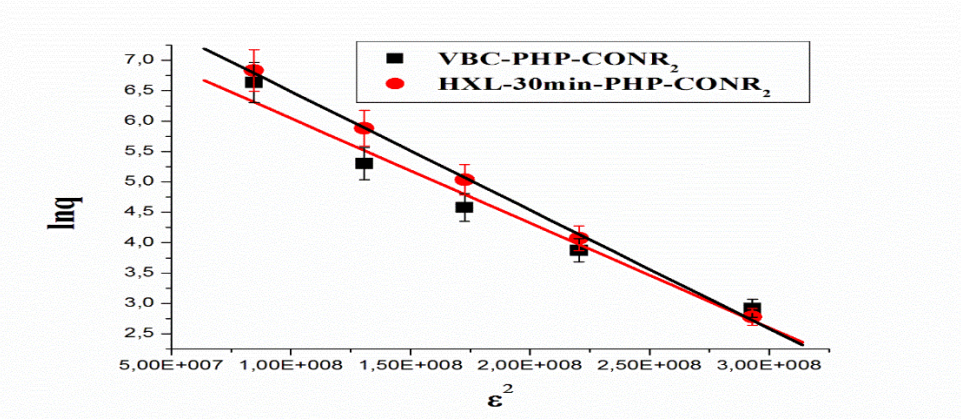

Figure 4. 26: Dubinin–Radushkevich (D–R) isotherms.

The isotherm parameters and correlation coefficients for polyHIPE based adsorbent are given in Table 4.5. According to correlation factors in Table 4.5 experimental data is fitted well with Freundlich isotherm as well as Langmuir and D-R isotherm models with high R^2 values (close value to 1). From the Langmuir model parameters, the maximum equilibrium adsorption capacities (q_m) of adsorbents were found in a good agreement with the real results which are 1160 mg/g (model) vs. 798.6 mg/g (real) for HXL-30min-PHP-$CONR_2$ (ethanolamine), and 978.5 (model) mg/g vs. 971.3 mg/g (real) for PHP-$CONR_2$ (ethanolamine).

Table 4. 5: Isotherm parameters and correlation coefficients for HXL-30min-PHP-$CONR_2$ (ethanolamine) (A) and VBC-PHP-$CONR_2$ (ethanol amine) (B).

	Langmuir			Freundlich			D-R	
	K_d (mg/L)	q_m ($mg.g^{-1}$)	R^2	K_f ($mg.g^{-1}$)	n	R^2	q_m (mg g^{-1})	E (kJ/mol)
A	0.0638	1160	0.9569	4.317	0.8815	0.9928	2366	17.05
				0.9691				
B	0.0460	978.5	0.4615	11.27	0.7894	0.9951	4623	16.01
				0.9989				

4.3.6 Thermodynamic analysis

The temperature effect of mercury adsorption on HXL-30min-PHP-$CONR_2$ (ethanolamine) was studied kinetically at various temperatures in a range between 5-45^oC. Here, we used the linear van't Hoff plot (Figure 4.29a) to calculate the values of enthalpy change (ΔH°_{ads}) and entropy change (ΔS°_{ads}). The Gibbs free energy changes of adsorption (ΔG°_{ads}) was simply calculated by using the fundamental relationship between ΔH°_{ads} , ΔS°_{ads}, and ΔG°_{ads}. In case of low adsorbate concentration (c), equilibrium constant (K) can be expressed as [112,113] (Equation 4.9):

$$K = \lim_{C \to 0} \left(\frac{q_{adsorbate}}{C_{adsorbate}} \right) \tag{4.9}$$

Then, ΔH°_{ads} and ΔS°_{ads} can be calculated from the slope and intercept of $\ln K$ vs. 1/T plot obtained by using the linear form of van't Hoff equation given in Equation 4.10 below:

$$\ln K = \frac{\Delta S^{\circ}_{ads}}{R} - \frac{\Delta H^{\circ}_{ads}}{R} \frac{1}{T} \tag{4.10}$$

ΔG°_{ads} values can be calculated by using the fundamental thermodynamic relationship of (Equation 4.11):

$$\Delta G^{\circ}_{ads} = \Delta H^{\circ}_{ads} - T\Delta S^{\circ}_{ads} \tag{4.11}$$

In order to find activation energy (E_a) for the adsorption process, linearized form of the Arrhenius equation was employed (Equation 4.12).

$$\ln k = \ln A + \frac{E_a}{R} \left(\frac{1}{T} \right) \tag{4.12}$$

Here, the rate constants (k_2) were obtained from the pseudo-second-order kinetic model at various temparatures (278 K, 288K, 298 K, 308 K, 318 K) while A is the frequency factor. E_a was simply calculated from the slope of the Arrhenius plot ($\ln k$ vs. 1/T) given in Figure 4.27b.

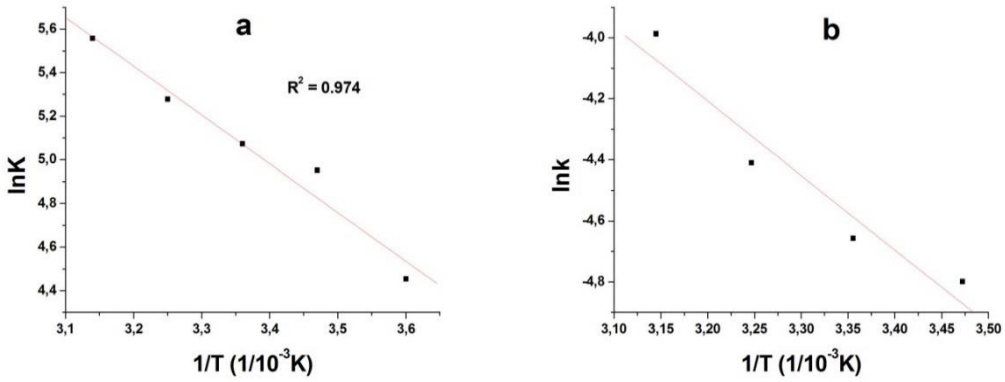

Figure 4. 27: van't Hoff (a) and Arhenius (b) plots for mercury adsorption on HXL-30min-PHP-CONR$_2$ (ethanolamine).

Figure 4.28 clearly shows that increasing temperature favored the mercury adsorption on the surface of HXL-30min-PHP-CONR$_2$ (ethanolamine) resulting a 1.35 fold increase in the adsorption capacity by 40°C temperature change. The same outcome was observed in the case of the equilibrium values which inceases as temperature increases seen in the van't Hoff plot (Figure 4.27) indicating that the adsorption process is endothermically favored [112]. As a result of the combined morphological characterics; the interconnected network dominated by macropores and the high surface area achieved by micropores through hypercrosslinking, the adsorbent showed fast adsorption rates at all temperatures.

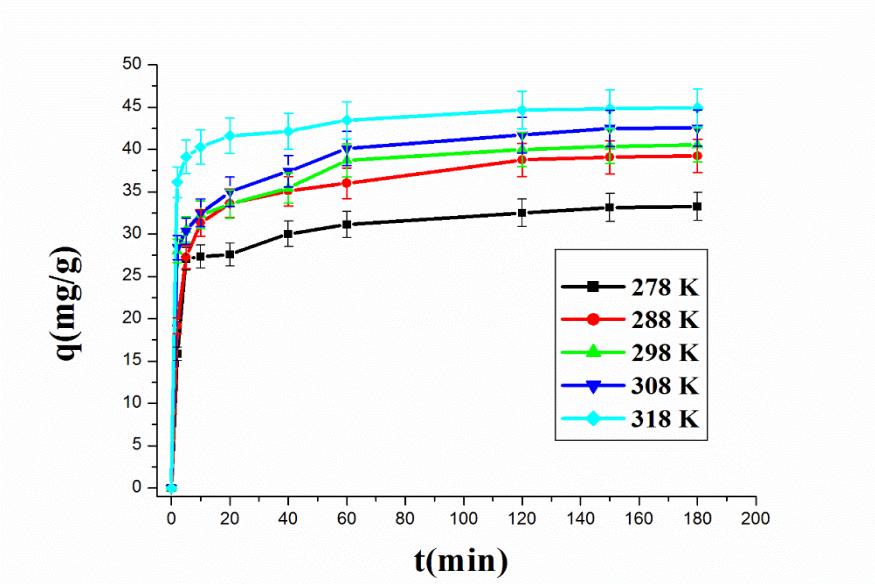

Figure 4.28: Mercury adsorption kinetics on HXL-30min-PHP-CONR$_2$ (ethanolamine) at various temperatures.

The enthalpy, entropy and Gibbs free energy changes as well as the activation energy for the mercury adsorption on the hypercrosslinked amide functional polyHIPE are given in Table 4.6**.** The nature of the adsorption process can be interpreted by analyzing the thermodynamic parameters. We can see that $\Delta G^{\circ}_{\text{ads}}$ values negative at all temperatures and become more negative as temperature increase indicating that the mercury adsorption on HXL-30min-PHP-$CONR_2$ (ethanolamine) is spontaneous. According to the thermodynamics data mercury adsorption can be defined as physisorption as the absolute values of $\Delta G^{\circ}_{\text{ads}}$ ranges from -10.49 to -14.69 kJ/mol and E_a is in the range of 5−40 kJ/mol. Positive and small (≤40 kJ mol^{-1}) ΔH°_{ads} (18.70) and ΔS°_{ads} (0.1050) values also indicates that the process is dominated by the physisorption. The signs and magnitudes of $\Delta G^{\circ}_{\text{ads}}$, ΔH°_{ads} and ΔS°_{ads} reveals that mercury adsorption is driven by the non-covalent interactions in conflict with the proposed mono or diamido mercury structures. These results show that the mercury-amide structures should be identified more clearly although many studies propose a covalent interaction between an amide and mercury in aqueous solutions.

Table 4. 6: Thermodynamic parameters for mercury adsorption on HXL-30min-PHP-$CONR_2$ (ethanolamine).

T (K)	E_a (kJ mol^{-1})	ΔH° (kJ mol^{-1})	ΔS° (kJ $mol^{-1}K^{-1}$)	ΔG° (kJ mol^{-1})
318	20.27	18.70	0.1050	-14.69
308				-13.61
298				-12.59
288				-11.54
278				-10.49

4.3.7 Adsorbent reuse

One of the most advantageous characteristic of polymer supported reagents as adsorbents, they can be reused many times without loosing the adsorbent capacity. To test the reuse ability of HXL-30min-PHP-$CONR_2$ (ethanolamine), first, the polymer loaded with mercury was treated with 0.1 M $HCl_{(aq)}$ solution (10 mL) and left constant stirring for 3 h. And then the polymer was filtered, washed with the excess water to

remove acid, ethanol (1x20 mL to ease drying) and left in a conventional oven to dry at 50^{o}C for over night. This procedure was repeated four times and the polymer did not change its adsortion capacity significantly after 5-times-use. Amide group can undergo hydrolysis in strong acids to form carboxylic acid which can also bind Hg(II). However, in this case, the selectivity of the adsorbent will be lowered because of the reduced amide content of the polymer. Therefore, we carried out an adsorption experiment in an aqueous ternary metal solution containing 0.02 M $HgCl_2$, $ZnSO_4$ and $CdNO_3$ using the polymer after 5th cycle. The polymer showed the similar selectivity towards Hg(II) after the 5th cycle indicating that regenaration in 0.1 M HCl(aq) does not cause the hydrolysis of the amide groups.

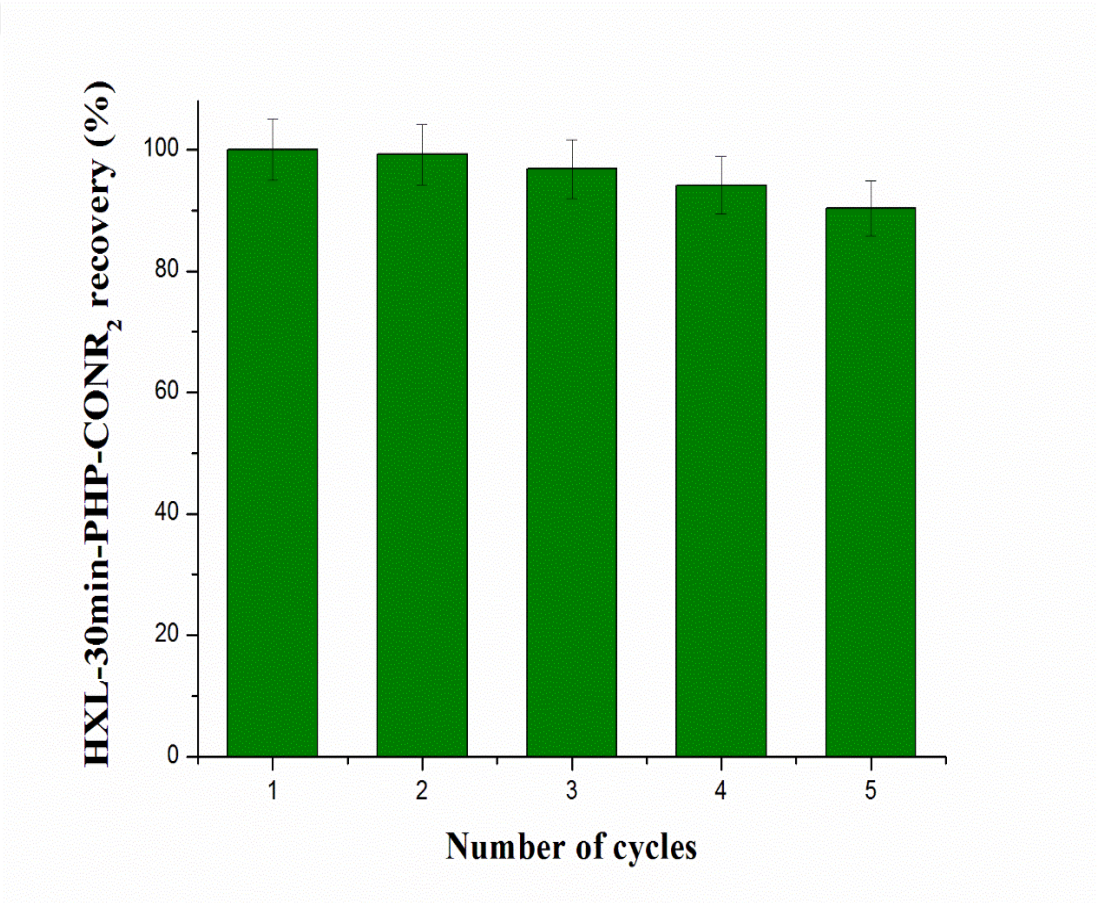

Figure 4. 29: Adsorbent Reuse.

5. CONCLUSION

In this thesis high-surface-area polymers were successfully prepared and functionalized with amide groups through a 5-steps reaction. First, high internal phase emulsions were prepared with 90% pore volume and curing monomer phase produced highly porous, interconnected polyHIPEs. The disadvantage of low-surface-area of initial polymers were overcomed by hypercrosslinking reaction. In this strategy, around 600m^2/g surface area of polyHIPEs could be obtained. PolyHIPEs and hypercrosslinked polyHIPEs surfaces were tailored with amide groups using various amines. It was shown that the hypercrosslinked polyHIPE with amide functions showed the enhanced adsorption performance compared to unhypercrosslinked polyHIPE with amide function. Moreover, it was proved that amide functions show high affinity for mercury (II) in both single and ternary metal solutions. The adsorption kinetics results were tested by three different adsorption kinetics models and it was found out that mercury (II) adsorption on polyHIPE surfaces follow pseudo second order kinetics. Also, the experimental results were tested by adsorption isotherm and Freundlich isotherm model was fitted well with experimental data. Thermodynamic parameters for mercury (II) adsorption on HXL-30min-PHP-$CONR_2$ (ethanolamine) were obtained by carrying out adsorption experiments at various temperatures. It was found out that $\Delta G^{\circ}_{\text{ads}}$ values negative at all temperatures and become more negative as temperature increase indicating that the mercury adsorption on HXL-30min-PHP-$CONR_2$ (ethanolamine) is spontaneous. According to the thermodynamics data mercury (II) adsorption can be defined as physisorption as the absolute values of $\Delta G^{\circ}_{\text{ads}}$ ranges from -10.49 to -14.69 kJ/mol and E_a is in the range of 5−40 kJ/mol. One of the most advantagous characteristic of polymer supported reagents as adsorbents, they can be reused many times without loosing the adsorbent capacity. One of the most advantagous characteristic of polymer supported reagents as adsorbents, they can be reused many times without loosing the adsorbent capacity. It was proved that HXL-30min-PHP-$CONR_2$ (ethanolamine) did not change its adsortion capacity significantly after 5-times-use.

REFERENCES

[1] **Saldivar-Guerra, E., and Vivaldo –Lima, E.,** (2013). Handbook of Polymer Synthesis, Characterization, and Processing, Introduction to Polymers And Polymer Types, First Edition, *John Wiley & Sons, Inc*.

[2] **Goodarzi, F., Zendehboudi, S.** (2019). A Comprehensive Review on Emulsions and Emulsion Stability in Chemical and Energy Industries, *The Canadian Journal of Chemical Engineering*, ***97***, 281-309.

[3] **Kale, S.N., Deore, S.L.** (2017). Emulsion Micro Emulsion and Nano Emulsion: A Review, *Systematic Reviews in Pharmacy*,***8(1)***,39-47.

[4] **Bhatia, N., Pandit, S., Agrawal, S., Gupta, D.** (2013). A Review On Multiple Emulsions, *International Journal of Pharmaceutical Erudition*, ***3(2)***, 22-30.

[5] **Rosen, M.J.** (2004). Surfactants and ınterfacial phenomena, Chapter 8, Emulsification by Surfactant, Third Edition, *A John Wiley & Sons. Inc., Publication*, New Jersey.

[6] **Rovera, F., Dziza, K., Christofolini, L., Liggieri, L.** (2021). Emulsification and emulsion stability:The role of the interfacial properties, *Advances in Colloid and Interface Science*,***288***, 102244.

[7] **Mcclements, D.J.** (2007). Critical Review of Techniques and Methodologies for Characterization of Emulsion Stability, *Critical Reviews in Food Science and Nutrition*, ***47(7)***, 611-649.

[8] **Tadros, T.F.** (2016). Emulsions: Formation, Stability, Industrial Applications, Chapter 1, Germany.

[9] **Rousseau, D.** (2000). Fat crystals and emulsion stability - a review, *Food Research International*, ***33***, 3-14.

[10] **Tadros, T.F.** (2013). Emulsion Formation and Stability, *John Wiley& Sons*, Wokingham

[11] **Van Herck, A.M.** (2013). Chemistry and Technology of Emulsion Polymerisation, Chapter 3, Emulsion Polymerization Second Edition, John Wiley& Sons, Ltd, *Institute of Chemical Engineering Sciences*, Singapore.

[12] **Thickett, S.C, Gilbert, R.G.** (2007). Emulsion polymerization: State of the art in kinetics and mechanisms, *Polymer*, ***48***, 6965-6991.

[13] **Liu, X-J., Tian, Y-H., Lu, Y-C.** (2019). A Comparative Study on Emulsion Polymerization Processes of Styrene Initiated by Water-soluble and Oil-soluble Initiators, *Chinese Journal of Polymer Science*,***37***, 142-148.

[14] **Yamak, H.B.** (2013). Emulsion Polymerization: Effects of Polymerization Variables on the Properties of Vinyl Acetate Based Emulsion Polymers, *Polymer Science*, ***2***, 35-72.

[15] **Wang, Q., Fu,S., Yu, T.** (1994). Emulsion polymerization, Progress in Polymer Science, *Department of Macromolecular Science,* Fudan University, Shanghai, China, ***19***,703- 753.

[16] **Bakr El-Hoshoudy, A.N.M.** (2018). Emulsion Polymerization Mechanism, *Recent Research in Polymerization*, ***Chapter 1***, 3-14.

[17] **Vanderhoff, J.W.** (1985). Mechanism of emulsion polymerization, Journal of Polymer Science: Polymer Symposium, *Emulsion Polymers Institute and Department of Chemistry*, Lehigh University, Bethlehem, Pennsylvania, ***72***, 161-198.

[18] **Wu, D., Xu, F., Sun, B., Fu, R., He, H., Matyjaszewski, K**.(2012). Design and preparation of porous polymer , *American Chemical Society Chemical Review*, ***112***, 3959-4015.

[19] **Silverstein, M.S**.(2014). Emulsion- templated porous polymers: A retrospective perspective, *Polymer*, ***55*** , 304-320.

[20] **Tan, L., Tan, B.** (2017). Hypercrosslinked porous polymer materials: design, synthesis, and applications, *Royal Society of Chemistry*, ***46***, 3322-3356.

[21] **Li, C., Li, Q., Kaneti, Y.V., Hou, D., Yamauchi, Y., Mai, Y**., (2020). Self-assembly of block copolymers towards mesoporous materials for energy storage and conversion systems, *Chem. Soc. Rev.*, ***49***, 4681-4736.

[22] **Altinpinar, S., Ali, W., Schuchardt, P., Yildiz, P., Zhao, H., Theato,P., Gutmann, S.J.** (2020). Porous ultra-thin film from photocleavable block copolymers: in situ degradation kinetics study pore material, *Polymers*, ***12***,781.

[23] **Qiu, S., Ben, T.** (2016). Porous polymers: design, synthesis and applications, *Royal Society of Chemistry*,19-65.

[24] **Pulko, I., Krajnc, P.** (2012). High internal phase emulsion templating- a path to hierarchically porous functional polymers, *Macromolecular Rapid Communications*, ***33***, 1731-1746.

[25] **Menner, A., Haibach, K., Powell, R., Bismarck, A**. (2006). Tough reinforced open porous polymer foams via concentrated emulsion templating, *Polymer*, ***47***, 7628-7635.

[26] **Jiao, Y.J., Yuan, F.F., Fan, P.R., Wei, Z.H., Huang, Y.P., Liu, Z, S.** (2021). Macroporous monolithic enzyme microreactor based on high internal phase emulsion functionalized with gold nanorods for enzymatic hydrolysis of protein, *Chemical Engineering Journal*, ***407***, 127061.

[27] **Thumbbarathy, D.,** (2017). Preparation of Functional PolyHIPE Polymers for Agro-process Applicatios, *School of Chemical Engineering and Advanced Materials*, New Castle University, United Kingdom, page 21.

[28] **Cameron, N.R., Sherrington, D.C.** (1996). High internal phase emulsions (HIPEs)- structure, properties and use in polymer preparation, *Advances in Polymer Science*, ***126***,163-214.

[29] **Silverstein, M.S., Cameron, N.R.** (2010). PolyHipe- Porous polymers from high internal phase emulsions, *Encylopedia of Polymer Science and Technology*.

[30] **Cameron, N.R.** (2005), High internal phase emulsion templating as a route to well-defined porous polymers, *Polymer*, ***46***, 1439-1449.

[31] **Silverstein, M.S., Cameron, N.R**. (2010), PolyHipe- Porous polymers from high internal phase emulsions, *Encylopedia of Polymer Science and Technology*.

[32] **Zhang, T., Xu, Z., Guo, Q.** (2016). Closed- cell and open- cell porous polymers from ionomer- stabilized high internal phase emulsions, The Royal Society of Chemistry, *Polymer Chemistry*, ***7***, 7469-7476.

[33] **Kravchenko, O. G., Gedler, G., Kravchenko, S. G., Feke, D., Zloczower, I.M.** (2018). Modeling compressive behavior of open – cell polymerized high internal phase emulsions: effects of density and morphology, The Royal Society of Chemistry, *Soft Matter*, ***14***, 1637- 1646.

[34] **Zhang, T., Xu, Z., Guo, Q.** (2016). Closed- cell and open- cell porous polymers from ionomer- stabilized high internal phase emulsions, The Royal Society of Chemistry, *Polymer Chemistry*, ***7***, 7469-7476

[35] **Berezovska, I., Kapilov, K., Dhavalikar, P., Cosgriff-Hernandez, E., Silverstein, M.S.** (2021). Reactive surfactants for achieving open-cell polyHipe foams from pickering emulsions, *Macromolecular Materials and Engineering*, 2000825.

[36] **Yang, H., Zhang, S., Chen, J.** (2016). Interconnected porous material prepared via high internal phase emulsion stabilized by mixture of Fe_3O_4 and Tween85, *Matec Web of Conferences*, ***67***, 06097.

[37] **Williams, J.M., Wrobleski, D.A**. (1988). Spatial distribution of the phases in water – in – oil emulsions. Open and closed microcellular foamsfrom cross-linked polystyrene,*Langmuir* , ***4***, 656-662.

[38] **Wu, Y., Zhou, Y.N., Xu, Q.J., Li, J.J., Luo, Z.H.** (2021). Porous PS- and PMMA-based poymeric monoliths prepared by PEO- PS block copolymers stabilized High internal phase emulsion templates, *Materials Today Communications*, ***26*** , 101962.

[39] **Krajnc, P., Leber, N., Stefanec, D., Kontrec, S., Podgornik, A.** (2005). Preparation and characterisation of poly(high internal phase emulsion) methacrylate monoliths and their application as separation media, *Journal of Chromatography A*, ***1065***,69-73.

[40] **Walstra, P.** (1993). Principles of emulsion formation, *Chemical Engineering Science*, ***48(2)***,333-349.

[41] **Pulko, I., Krajnc, P.** (2012). High internal phase emulsion templating- a path to hierarchically porous functional polymers, *Macromolecular Rapid Communications*, ***33(20)***, 1731-1746.

[42] **Gbadamosi, A., Junin, R., Manan, M. A., Agi, A., Yusuff, A.S.** (2019). An overview of chemical enhanced oil recovery: recent advances and prospects, *International Nano Letters*, ***9*** , 171-202.

[43] **Almalkawi, A.T., Salem, T., Hamadina, S., Darsanasiri, A.G.N.D., Soroushian, P., Balchandra, A., Al-Chaar, G.** (2018). Physio-microstructural properties of aerated cement slurry for lightweigh structures, *Materials*, ***11***, 597.

[44]**Kruglyakov, P.M.** (2000). Hydrophile – lipophile balance of surfactants and solid particles, Physicochemical Aspects and Applications, *Elsevier Science B.V.*, ***9***, Chapter 1, 4-99.

[45] **Foo, K.S., Bavoh, C.B., Lal, B., Shariff, A.M.** (2020). Rheology impact of various hydrophilic- hydrophilic balance (HLB) index non-ionic surfactants on cyclopentane hydrates, *Molecules*, ***27***, 3725.

[46] **Haibach, K., Menner, A., Powell, R., Bismarc, A.** (2006). Tailoring mechanical properties of highly porous polymer foams: Silicaparticle reinforced polymer foams via emulsion templating, *Polymer*, ***47***, 4513-4519.

[47] **Livshin, S., Silverstein, M.S.** (2008). Crystallinity and cross-linking in porous polymers synthesized from long side chain monomers through emulsion templating, *Macromolecules*, ***41***,3930-3938.

[48] **Kovačič, S., Jerabek, K., Krajnc, P., Slugovc, C.** (2012). Ring opening metathesis polymerisation of emulsion templated dicyclopentadiene giving open porous materials with excellent mechanical properties, *Polymer Chemistry*, ***3***, 325.

[49] **Tsyurupa, M.P., Davankov, V.A.** (2002). Hypercrosslinked polymers: basic principle of preparing thenew class of polymeric materials, *Reactive & Functional Polymers*, ***53***, 193-203.

[50] **Fontanals, N., Marcè, R.M., Borrull, F., Cormack, P.A.G.** (2016). Hypercrosslinked Materials, Polymer science: research advances, practical applications and educational aspects, 258-269.

[51] **Veverka, P., Jeřábek, K.** (1999). Mechanism of hypercrosslinking of chloromethylated styrene–divinylbenzene copolymers, *Reactive & Functional Polymers*, ***41***, 21-25.

[52] **Huang, J., Turner, S.R.** (2018). Hypercrosslinked Polymers: A Review, *Polymer Reviews*, ***58(1)***, 1-41

[53] **Xu, S., Luo, Y., Tan, B.** (2013). Recent Development of Hypercrosslinked Microporous Organic Polymers, *Macromolecular Rapid Communications*, ***34***, 471−484.

[54] **Ahn, J.H., Jang, J.E., Oh, C.G., Ihm, S.K., Cartez, J., Sherrington, D.C.** (2006). Rapid Generation and Control of Microporosity, Bimodal Pore Size Distribution, and Surface Area in Davankov-Type Hyper-Cross-Linked Resins, *Macromolecules*, ***39***, 627-632.

[55] **Jeřábek, K., Pulko, I., Soukupova, K., Štefanec, D., Krajnc, P.** (2008). Porogenic Solvents Influence on Morphology of 4-Vinylbenzyl Chloride Based PolyHIPEs, *Macromolecules*, ***41***, 3543-3546.

[56] **Fontanals, N., Marcè, R.M., Borrull, F., Cormack, P.A.G.** (2015). Hypercrosslinked materials: preparation, characterisation and applications, *Polymer Chemistry*, ***6***, 7231-7244.

[57] **Sing, K.S.W**. (2004). Characterization of porous materials: past, present and future, Colloids and Surfaces A: Physicochemical and Engineering Aspects, 241, 3-7.

[58] **Ambroz, F., Macdonald, T.J., Martis, V., Parkin, I.P.** (2018). Evaluation of the BET Theory for the Characterization of Meso and Microporous MOFs, *Small Methods*, ***2***, 1800173, 1-17.

[59] **Thommes, M., Kaneko, K., Neimark, A.V., Olivier, J.P., Reinoso, F.R., Rouquerol, J., Sing, K.S.W.** (2015). Physisorption of gases, with special reference to the evaluation of surface area and pore size distribution (IUPAC Technical Report), *Pure and Applied Chemistry*, ***87(9-10)***, 1051–1069.

[60] **Mohammadi, M., Shadizadeh, S.R., Manshad, A.K., Mohammadi, A.H.** (2020). Experimental study of the relationship between porosity and surface area of carbonate reservoir rocks, *Journal of Petroleum Exploration and Production Technology*, ***10***, 1817–1834.

[61] **Url-1** <*https://www.spectroscopyeurope.com/article/xps-surface-analysis-imaging-and-spectroscopy-metal-and-polymer-surfaces*>, 30.05.2021.

[62] **Wagner, J.M., Wren, A.W., Laffir, F.R., Mellot,N.P., Towler, M.R.** (2011). Chapter 1, X-ray Photoelectron Spectroscopy: Studies from Industrial & Bioactive Glass to Biomaterials, *Nova Science Publishers, Inc*.

[63] **Url-2** < *https://www.princeton.edu/~surfsci/hrxps.html* >, 14.06.2021.

[64] **Moulder, J.F., William, F.S., Sobol, P.E., Bomben, K.D.** (1992). Handbook of X-ray Photoelectron Spectroscopy,Perkin Elmer Corporation, *Physical Electronics Division*, USA.

[65] **Hawkes, P.W., Spence, J.C.H., Erdman, N., Bell, D.C., Reichelt, R.** (2019). Springer Handbook of Microscopy, *Springer International Publishing*, Chapter 5, Scanning Electron Microscopy, 229-318.

[66] **Url-3** < *https://www.biosciencenotes.com/scanning-electron-microscope-sem/*> 03.06.2021

[67] **Ul-Hamid, A**., (2018). A Beginners' Guide to Scanning Electron Microscopy, *Center for Engineering Research King Fahd University of Petroleum & Minerals Dhahran*, Saudi Arabia.

[68] **Claudia, H., De Caro, C.A.** (2015). UV/VIS Spectrophotometry - Fundamentals and Applications, *Mettler-Toledo Publication*.

[69]**Url-4**<*https://www.edinst.com/products/ds5-dual-beam-uv-vis spectrophotometer-2*>,04.06.2021.

[70] **Albert, S., Keppler Albert, K., Quack, M.** (2011). Handbook of High-resolution Spectroscopy, Chapter 26, High-resolution Fourier Transform Infrared Spectroscopy, *John Wiley & Sons, Ltd*, ***2***, 965–1019.

[71] **Url-4** <*https://www.nanogune.eu/en/equipment/ftir-spectrometer-perkinelmer-frontier-0*> , 04.06.2021.

[72] **Berthomieu, C., Hienerwade, R.**, (2009). Fourier transform infrared (FTIR) spectroscopy *Photosynthesis Research*, ***101***,157–170.

[73] **Nandiyanto, A.B.D., Oktiani, R., Ragadhita,R.** (2019). How to Read and Interpret FTIR Spectroscope of Organic Material , *Indonesian Journal of Science&Technology*, ***4(1)***, 97-118.

[74] **Ugwu, E.I., Tursunov, O., Kodirov, D., Shaker, L.M., Al-Amiery, A.A., Yangibaeva, I., Shavkarov, I.** (2020). Adsorption mechanisms for heavy metal removal using low cost adsorbents: A review, The Electrochemical Society, *IOP Conference Series: Earth and Environmental Science*, ***614***, 012166.

[75] **Afroze, S., Sen, T.K.** (2018). A Review on Heavy Metal Ions and Dye Adsorption from Water by Agricultural Solid Waste Adsorbents, *Water Air Soil Pollut*, ***229***, 225.

[76] **Li, X,G., Huang, M,R., Tao, T., Ren, Z., Zeng, J., Yu, J., Umeyama, T., Ohara, T., Imahori, H.** (2020). Highly cost-efficient sorption and desorption of mercury ions ontoregenerable poly(m-phenylenediamine) microspheres with many active groups, *Chemical Engineering Journal*, 391.

[77] **Omar, S., Muhamad, M.S., Chuan, L.T., Hadibarata, T., Teh, Z.C.** (2019). A Review on Lead Sources, Occurrences, Health Effects, and Treatment Using Hydroxyapatite (HAp) Adsorbent Made from Fish Waste , *Water Air Soil Pollut*, 230:275.

[78] **Webb, P.A.** (2003). Introduction to Chemical Adsorption Analytical Techniques and their Applications to Catalysis, *MIC Technical Publications*, Micromeritics, Norcross, Georgia.

[79] **Francis, A.G., Jane Davies, G., Balley, G.W., White, J.L.**(1970). Residue Reviews, Chapter 4, Factors influencing the adsorption, desorption, and movement of pesticides in soil, Single Pesticide Volume: The Triazine Herbicides, *Springer-Verlag New York Inc*, 29-92.

[80] **Raganati, F., Alfe, M., Gargiulo, V., Chirone, R., Ammendola, P.** (2019). Kinetic studyand breakthrough analysis of the hybrid physical/chemical CO2 adsorption/desorption behavior of a magnetite-based sorbent, *Chemical Engineering Journal*, ***372***, 526-535.

[81] **Wang, J., Guo, X.,** (2020). Adsorption kinetic models: Physical meanings, applications, and solving methods, *Journal of Hazardous Materials*, ***390***, 122156.

[82] **Wu, F-C., Tseng, R-L., Juang, R-S.** (2009). Initial behavior of intraparticle diffusion model used in the description of adsorption kinetics, *Chemical Engineering Journal*, ***153***, 1-8.

[83] **Ofomaja, A.E.**, (2010). Intraparticle diffusion process for lead(II) biosorption onto mansonia wood sawdust, *Bioresource Technology*, ***101***, 5868–5876.

[84] **Hashem, A., Al-Anwar, A., Nagy, N.M., Hussein, D.M., Eisa, S.** (2016). Isotherms and kinetic studies on adsorption of Hg(II) ions onto Ziziphus spina-christi L. from aqueous solutions, *Green Processing and Synthesis*, ***5(2)***, 213-224.

[85] **Yousef, R., Qiblawey, H., El-Naas, M.H.** (2020). Adsorption as a Process for Produced Water Treatment: A Review, *Processes*,***8***, 1657.

[86] **Gözeten, İ., Savran, A**., (2018). Metil Kırmızısının Silikajel Üzerindeki Çözeltiden Adsorpsiyonu: Denge İzotermleri Ve Kinetik İncelemeler, *Muş Alparslan Üniversitesi Fen Bilimleri Dergisi*, ***6(2)***, 581-589.

[87] **Nethaji, S., Sivasamy, A., Mandal, A.B.** (2013). Adsorption isotherms, kinetics and mechanism for the adsorption of cationic and anionic dyes onto carbonaceous particles prepared from Juglans regia shell biomass, *International Journal of Environmental Science and Technology*, ***10***, 231–242.

[88] **Khayyun, T.S., Mseer, A.H.** (2019). Comparison of the experimental results with the Langmuir and Freundlich models for copper removal on limestone adsorbent, *Applied Water Science*, 9:170.

[89] **Hu, Q., Zhang, Z.** (2019). Application of Dubinin–Radushkevich isotherm model at the solid/solution interface: A theoretical analysis, *Journal of Molecular Liquid*, ***277***, 646–648.

[90] **Wong, M.H., Ko, L.Y.Y., Qin, Y.Y.** (2012). Environmental Contamination : Health Risks and Ecological Restoration, Chapter 3, Heavy Metal Overloads and Autism in Children from Mainland China and Hong Kong: A Preliminary Study, *Taylor&Francis*.

[91] **Briffa, J., Sinagra, E., Blundell, R.** (2020). Heavy metal pollution in the environment and their toxicological effectson humans, *Heliyon*, ***6(9)***, e04691.

[92] **Wong, M.H**., (2012). Environmental Contamination : Health Risks and Ecological Restoration, Chapter 1, *Environmental Contamination : Health Risks and Ecological Restoration* , Taylor&Francis.

[93] **Yavuz, C.I.** (2020). Çevresel cıva maruz kalımı ve sağlık etkileri, *Turkish Journal of Public Health*, ***18(2)***, 204-217.

[94] **Environmental Fact Sheet**, (2019). Mercury: Sources, Transport, Deposition and Impacts, New Hampshire Department of Environmental Services, *Hazen Drive*, Concord, New Hampshire

[95] **Url-5** < *https://webcam.srs.fs.fed.us/impacts/mercury/index.shtml*> , 18.06.2021

[96] **Al-Ghout, M.A., Da'ana, D., Abu-Dieyeh, M., Khraisheh, M.** (2019). Adsorptive removal of mercury from water by adsorbents derived from date pits, *Scientific Reports*, ***9***, 15327.

[97] **Albatrni, H., Qiblawey, H., El-Naas, M.H.** (2021). Comparative study between adsorption and membrane technologies for the removal of mercury, *Separation and Purification Technology*, ***257***, 117833.

[98] **Xiong,C., Jia, Q., Chen, X., Wang, G., Yao, C.** (2013). Optimization of Polyacrylonitrile-2-aminothiazole Resin Synthesis, Characterization, and Its Adsorption Performance and Mechanism for Removal of Hg(II) from Aqueous Solutions, Industrial & Engineering Chemistry Research, *American Chemical Society*, ***52***, 4978−4986.

[99] **Bozkaya, O., Yiğitoğlu, M., Arslan, M.**, (2012). Investigation on Selective Adsorption of Hg(II) IonsUsing 4-Viny l Pyridine Grafted Poly(ethyleneterephthalate) Fiber, *Journal of Applied Polymer Science*, ***124(2)***,1256-1264.

[100] **Saad, D.M., Cukrowska, E.M., Tutu, H.** (2013). Selective removal of mercury from aqueous solutions using thiolated cross-linked polyethylenimine, *Applied Water Science*, ***3(2)***, 527-534.

[101] **Ma, F., Qu, R., Sun, C., Wang, C., Ji, C., Zhang, Y., Yin, P.** (2009). Adsorption behaviors of Hg(II) on chitosan functionalized by amino-terminated hyperbranched polyamidoamine polymers, *Journal of Hazardous Materials*, ***172(2)***, 792-801.

[102] **Laird, F. W, Smith, A.** (1938). Determination of Mercury with s – Diphenylcarbazide, *Ind. Eng. Chem. Anal. Ed*., ***10***, 576–578.

[103] **Krajnc, P., Majer, J.,** (2009). Cross-Linked Porous Poly(Acrylic Acid-co-Acrylamide) from High Internal Phase Emulsions: Preparation and Functionalisation, *Acta Chim. Slov*., ***56***, 629–634.

[104] **Barbetta, A., Cameron, N.R.** (2004). Morphology and Surface Area of Emulsion-Derived (PolyHIPE) Solid Foams Prepared with Oil-Phase Soluble Porogenic Solvents: Span 80 as Surfactant, American Chemical Society, *Macromolecules*, **37**,9, 3188-3201.

[105] **AlMarzooi, F., Bilad, F., Mansoor, B., Arafat, H.A.** (2016). Comparative Study of Image Analysis and Porometry Techniques for Characterization of Porous Membranes, *J.Mater.Sci.*, ***51***, 2017-2032.

[106] **Yang, X., Tan, L., Xia, L., Wood, C., Tan, B.** (2015). Hierarchical Porous Polystyrene Monoliths from PolyHIPE, *Macromolecules*, ***36***, 1553-1558.

[107] **Bıçak, N., Sherrington, D.C. Şenkal, B.F.** (1999). Graft copolymer of acrylamide onto cellulose as mercury selective sorbent, *Reactive & Functional Polymers*, ***41***, 69–76.

[108] **Şenkal, B.F., Yavuz, E., Bıçak, N.,** (2004). Poly(acrylamide) grafts on spherical polymetric sulfonamide based resin for selective removal of mercury ions from aqueous solutions, *Macromol. Symp.*, ***217***,169-178.

[109] **Pei, Y., Zhao, L., Du, G., Li, N., Xu, K., Yang, H.** (2016). Investigation Of The Degradation And Stability of Acrylamide-Based Polymers in Acid Solution: Functional Monomer Modified Polyacrylamide, *Petroleum*, ***2***, 4, 399-407.

[110] **Weber, W. J.; Morris, C. J.** (1963). Kinetics of Adsorption on Carbon from Solution, *Journal of the Sanitary Engineering Division*, ***89***, 31-60.

[111] **Mahadik, D.B., Lee, K., Ghorpade, R.V. et al.** (2018). Superhydrophobic and Compressible Silica-polyHIPE Covalently Bonded Porous Networks via Emulsion Templating for Oil Spill Cleanup and Recovery. *Sci Rep* ***8***, 16783

[112] **Lima, E. C., Gomes, A. A., & Tran, H. N.** (2020). Comparison of the nonlinear and linear forms of the van't Hoff equation for calculation of adsorption thermodynamic parameters (ΔS° and ΔH°). *Journal of Molecular Liquids*, ***311***, 113315.

[113] **Gerstner, J. A., Bell, J. A., & Cramer, S. M.** (1994). Gibbs free energy of adsorption for biomolecules in ion-exchange systems, *Biophysical Chemistry*, ***52***, 97–106.

APPENDICES

APPENDIX A: SEM image analysis results; Morphology characterization of VBC-PHP, HXL-30min-PHP, HXL-30min-PHP-$CONR_2$.

APPENDIX A

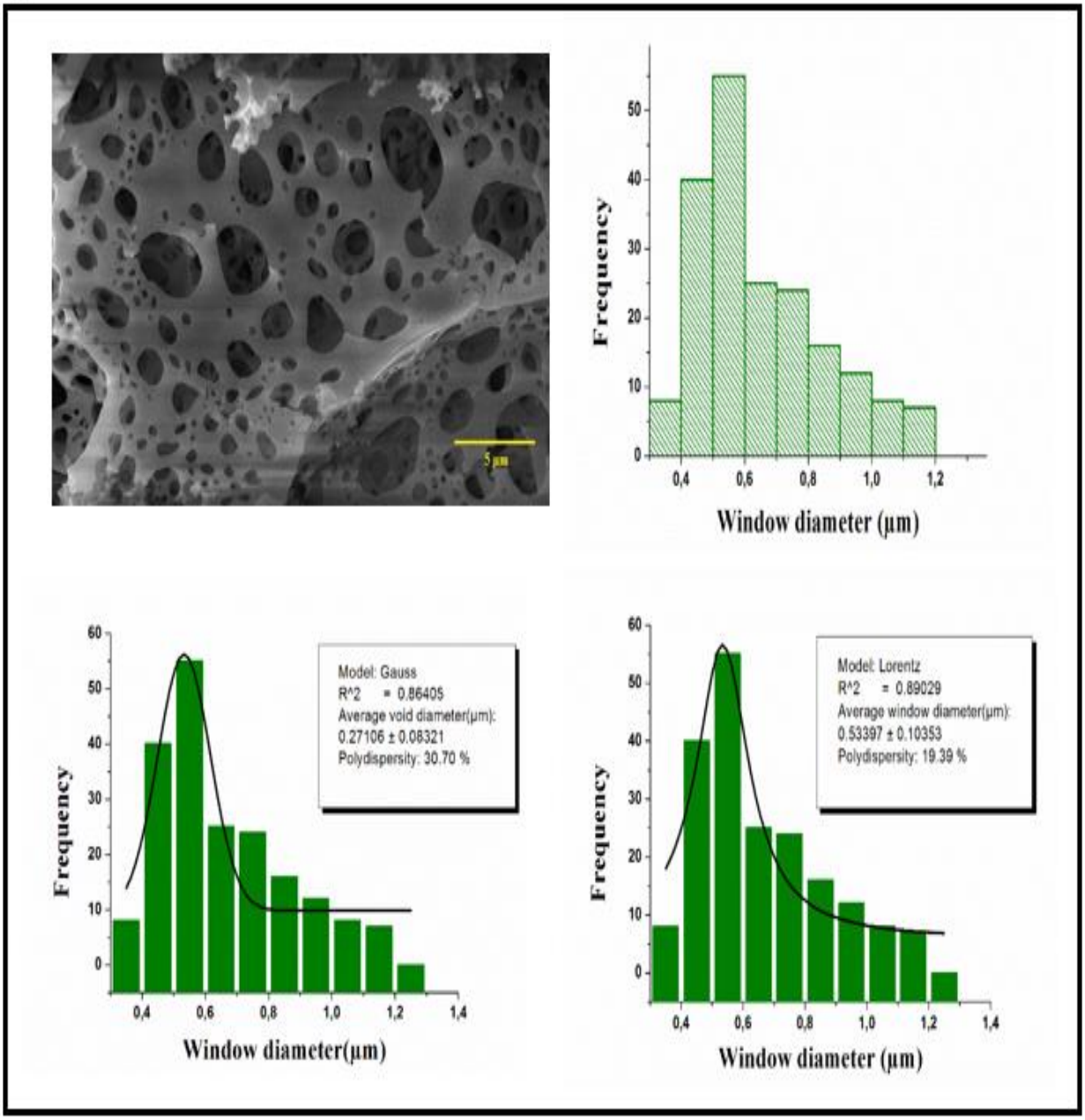

Figure A.1: SEM image analysis for average window diameter of VBC-PHP.

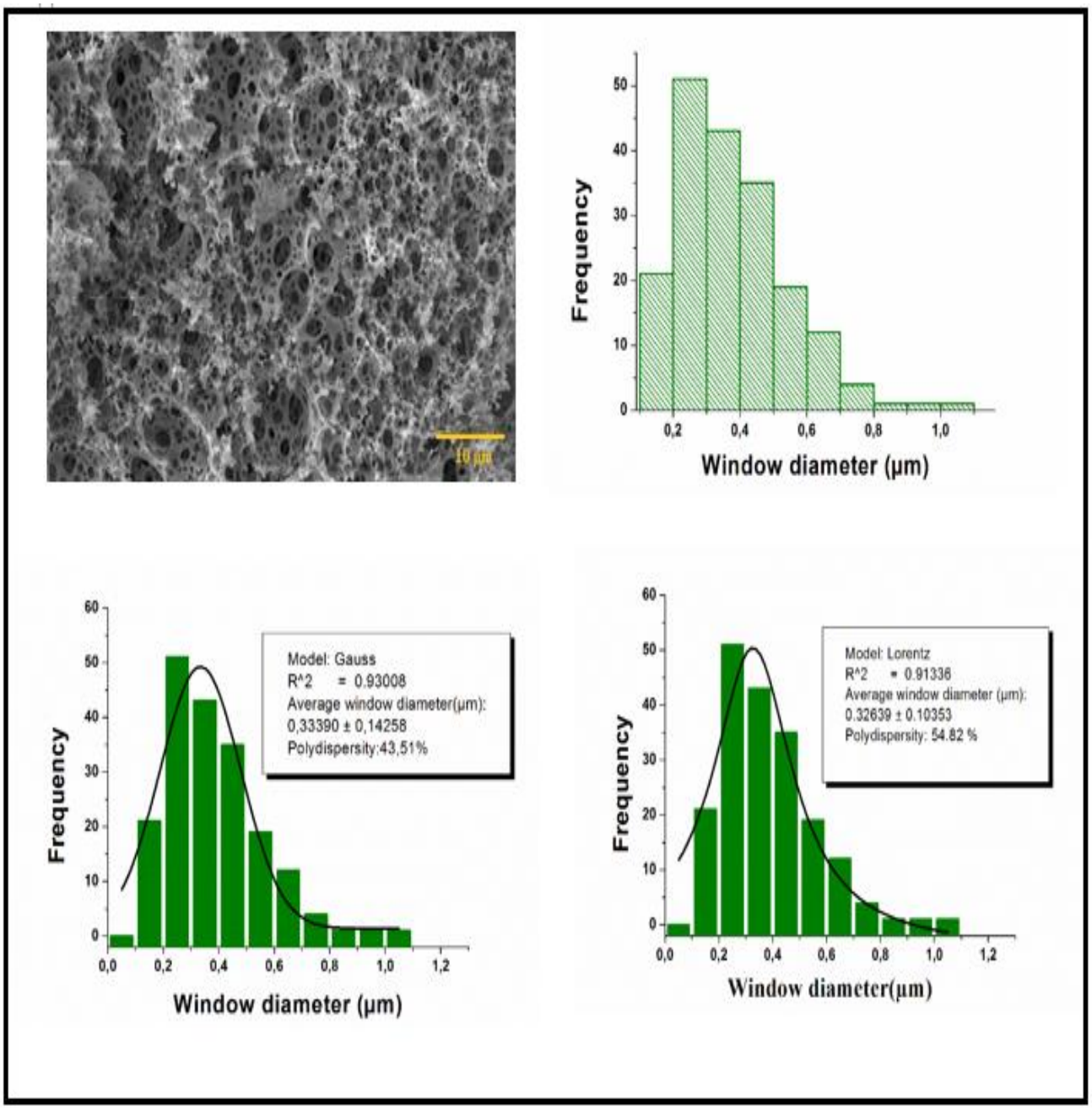

Figure A.2: SEM image analysis for average window diameter of HXL-30min-PHP.

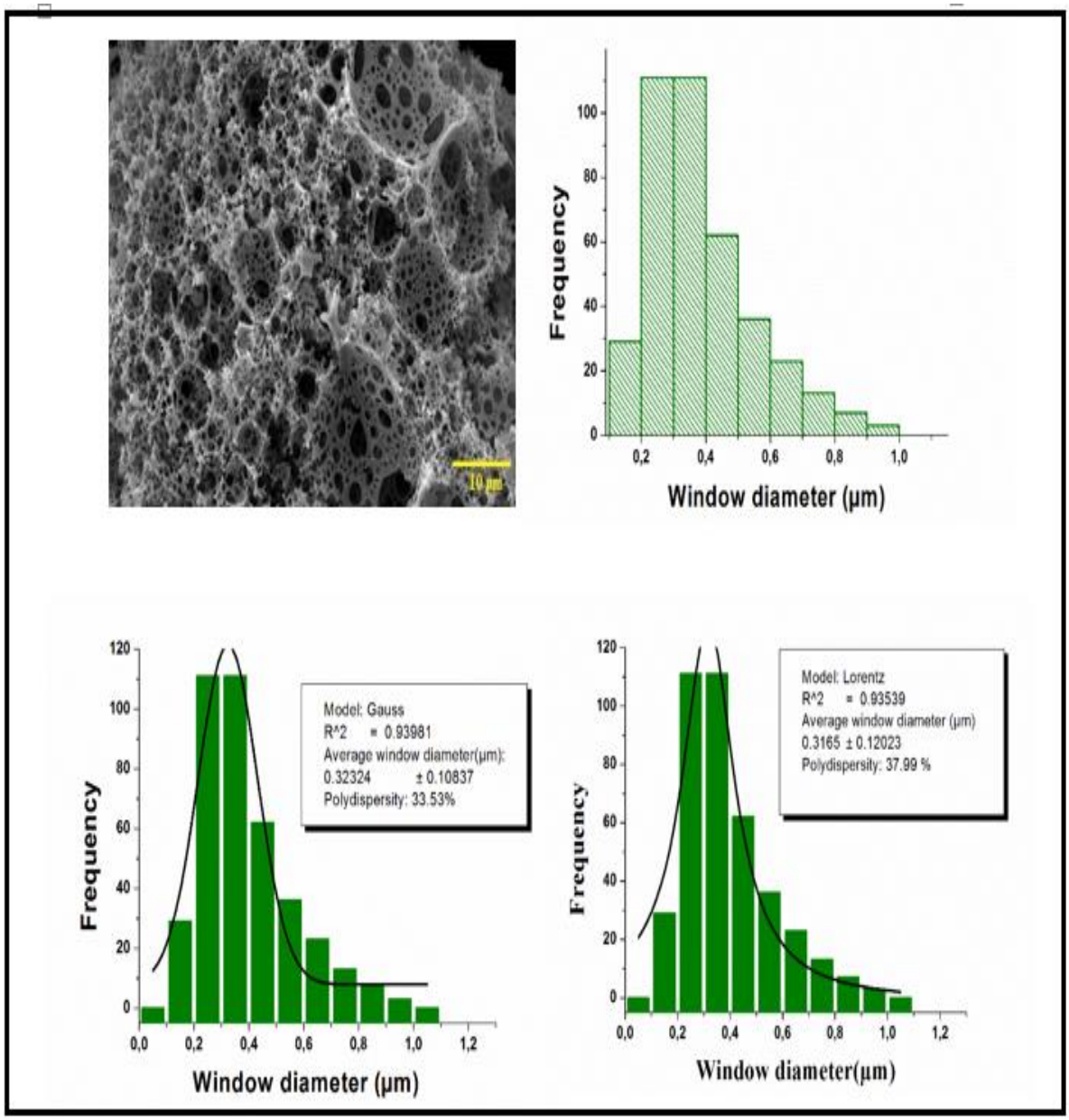

Figure A.3: SEM image analysis for average window diameter of HXL-30min-PHP-$CONR_2$.

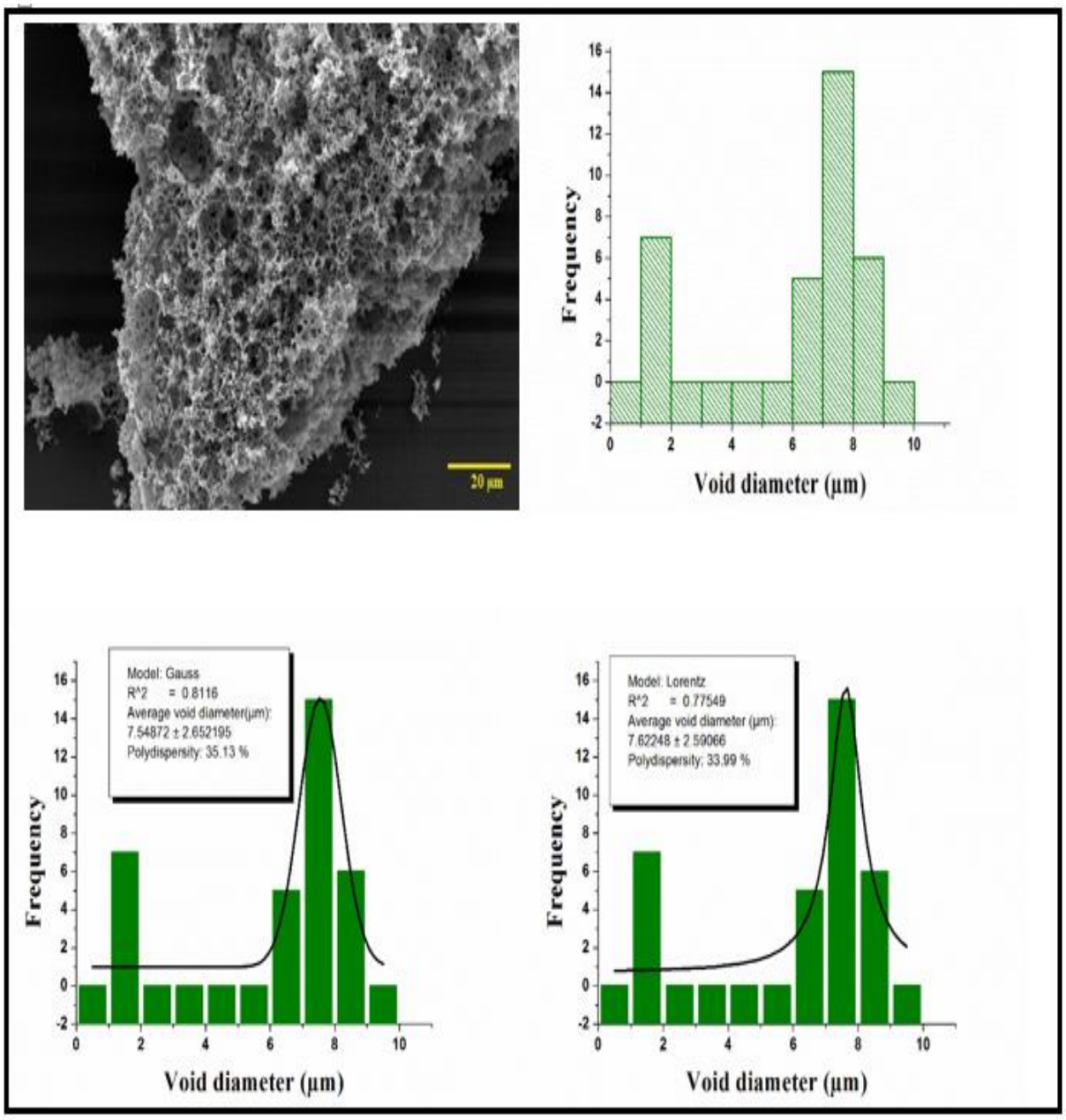

Figure A.4: SEM image analysis for average void diameter of VBC-PHP.

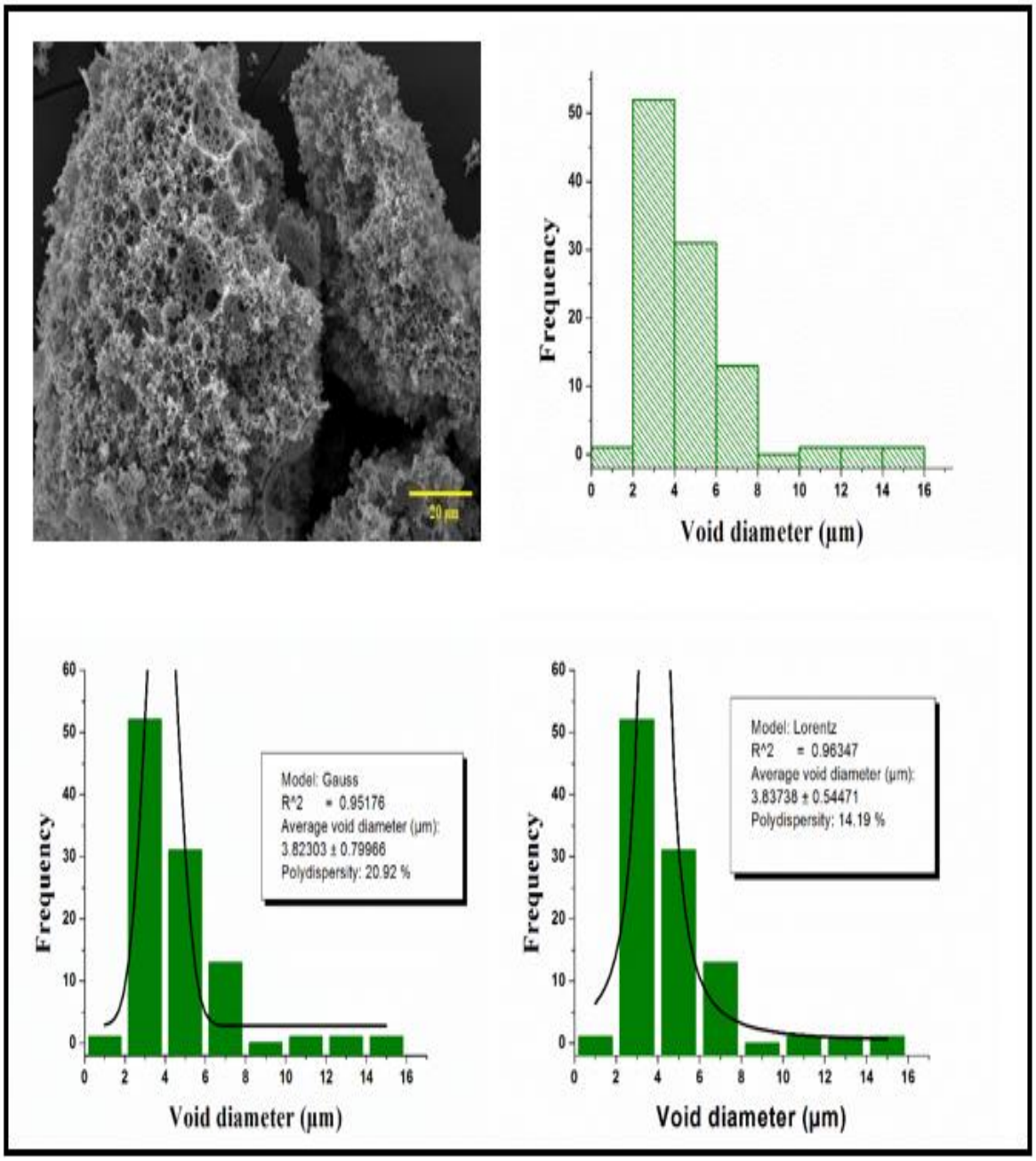

Figure A.5: SEM image analysis for average void diameter of HXL-30min-PHP.

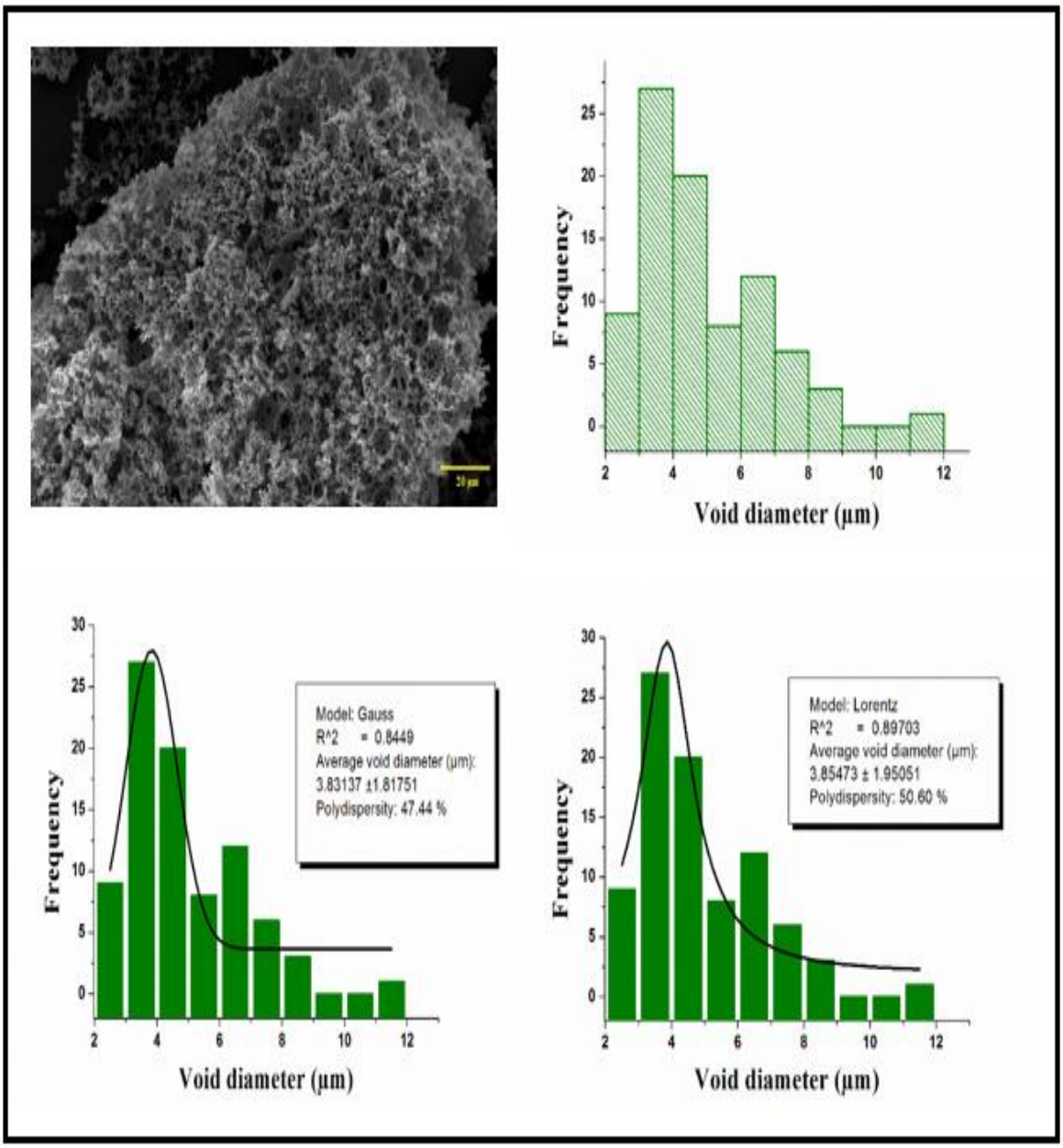

Figure A.6: SEM image analysis for average void diameter of HXL-30min-PHP-$CONR_2$.

CURRICULUM VITAE

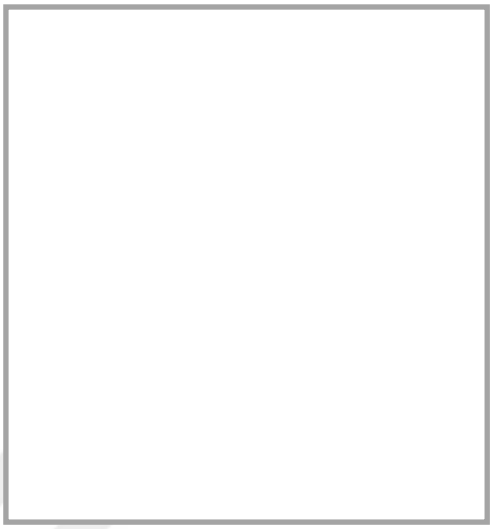

Name Surname : Melis Seval Yıldırım

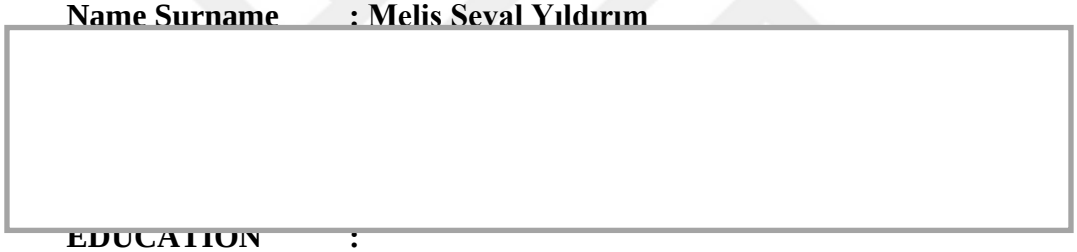

EDUCATION :

- **B.Sc. :** 2016, Eskişehir Osmangazi University, Faculty of Chemical and Metallurgical Engineering, Chemical Engineering Department